



**University of
Nottingham**

UK | CHINA | MALAYSIA

Human Factors Research Group

Faculty of Engineering

Assessment of Mitral Valve Geometry for Personalised Annuloplasty
Ring Development

By

Chirattikan Srisook

Supervisors: Prof. Donal McNally, Prof. Ruth Goodridge

Thesis submitted to the University of Nottingham for the degree of
Doctor of Philosophy

Abstract

Heart valve disease can occur when one valve or a combination of the heart valves is not working properly. Heart valve disease is found in more than one million people in the UK (Malhotra, 2012) and more than five million people in the USA each year (Nkomo et al., 2006). In terms of all types of heart valve disease, mitral regurgitation is the most common (Malhotra, 2012; Moore et al., 2016). Mitral valve repair, the preferred method for treating mitral regurgitation, typically requires surgical intervention. While mitral valve replacement is available, mitral valve repair is claimed to have better outcomes (Magne et al., 2008; Fattouch et al., 2009). Previous papers have shown that valve repair with the use of an annuloplasty ring is able to restore the valve functions and overcome the mitral regurgitation by reducing the mitral valve size to completely coapt the mitral orifice area.

The aim of this study is to assess the geometry of the healthy mitral valve to determine the relationship between the mitral valve dimensions and to develop a method of isolating and 3D reconstructing the mitral valve in order to develop a personalised annuloplasty ring which is the ring that specifically designed and manufactured for an individual patient based on their unique cardiac anatomy.

This study makes a substantial contribution by improving the selection process for existing commercial rings, offering guidance on personalised ring considerations, evaluating opportunities for enhancing commercial ring designs, and providing a systematic approach to design personalised annuloplasty rings.

The research enhanced selection of current commercial rings through an examination of healthy mitral valve dimensions and their comparison with commercially available rings, the study identifies which existing rings closely align with the mitral valve's healthy dimensions. This information aids surgeons in making more informed choices

during mitral valve repair surgeries. The research also emphasizes specific sizing strategies that better accommodate the anatomical variations observed in mitral valves.

The study emphasizes the considerable variability in individual mitral valve dimensions, highlighting the necessity of considering personalised annuloplasty rings. It provides a rationale for choosing personalised rings, especially in cases where standard-sized commercial rings may not precisely replicate a patient's unique mitral valve geometry. The insights gained into the limitations of commercial rings in accommodating diverse anatomies assist in deciding when to opt for personalised solutions.

The research also evaluates the accuracy of current commercial rings in mimicking healthy mitral valve dimensions, offering a foundation for assessing the efficacy of their designs. Identified areas for potential improvement in commercial ring designs provide valuable feedback for manufacturers. The study's findings may contribute to optimizing existing commercial ring designs to better align with the diverse anatomical characteristics of mitral valves.

For personalised ring design, the study outlines a comprehensive methodology for the design of bespoke annuloplasty rings tailored to individual patients. It emphasizes the importance of considering both shape and size in the design process, utilizing advanced tools and software such as ITK-SNAP and Blender for accurate 3D modelling and customization. The proposed workflow, including gap filling through statistical analysis in R Studio, provides a clear guide for researchers.

In conclusion, this study acts as a resource, refining the choice of existing commercial rings and advocating for thoughtful consideration of personalized and bespoke solutions. The gained insights have the potential to influence future improvements in the design of commercial annuloplasty rings.

Declaration

I, Chirattikan Srisook, hereby declare that this thesis titled "Assessment of Mitral Valve Geometry for Personalised Annuloplasty Ring Development" is my work during my PhD at the University of Nottingham under the supervision of Professor Donal McNally and Professor Ruth Goodridge. The information derived from the literature has been acknowledged in the text, and a list of references has been provided. No part of this thesis has been previously presented for an award of another degree at this or any other University.

This work has been funded by the Ministry of Science and Technology of Thailand.

Acknowledgement

Firstly, I would like to express my sincere gratitude to my supervisors, Professor Donal McNally and Professor Ruth Goodridge for all their expertise, guidance, and support throughout my PhD journey at the University of Nottingham. I am really grateful that my supervisors always gave me valuable comments and feedback that guided me through my research experiment and during my thesis writing. Moreover, I would like to thank Professor Ian Dryden and Dr. Rudolf Billeter-Clark for their support and advice. I would like to thank my internal assessor, Professor Ian Ashcroft for his comments and feedback on the progress of my research. I would like to thank Charlotte Blake for the collaborative work during the research experiment and for the resources. Many thanks to all the staff and technicians from the Faculty of Engineering at the University of Nottingham for all their advice and support.

I also would like to thank all my friends in the research group and my friends in Nottingham and Thailand for their advice and experience and for helping me throughout the PhD period in Nottingham.

Finally, and most importantly, I would like to thank my family, who always support me. I could feel the encouragement all the time, and I am forever grateful.

Table of Contents

<i>Abstract</i>	2
<i>Declaration</i>	4
<i>Acknowledgement</i>	5
<i>Table of Contents</i>	6
<i>List of Tables</i>	11
<i>List of Figures</i>	12
Chapter 1 Introduction	21
1.1 Background to the project.....	21
1.2 Thesis aims and objectives	25
1.3 Contributions to Knowledge.....	27
1.4 Thesis outline.....	29
Chapter 2 Literature review	32
2.1 Anatomy and function of the mitral valve.....	32
2.1.1 The Mitral leaflets.....	34
2.1.2 The chordae tendineae	37
2.1.3 The Mitral annulus.....	39
2.2 Experimental study of geometry of the mitral valve and controversy	41
2.3 Pathology of the mitral valve.....	44
2.4 The treatment for mitral regurgitation	47

2.4.1 Mitral valve treatment with annuloplasty ring.....	47
2.4.1.1 Flexibility of an Annuloplasty Rings.....	49
2.4.1.2 Annuloplasty ring sizing.....	51
2.5 Personalised annuloplasty ring development	52
2.6 Imaging the mitral valve.....	56
2.6.1 Magnetic resonance imaging (MRI).....	56
2.6.2 Echocardiograms	58
2.6.3 Computed Tomography scan (CT scan).....	62
2.7 The mitral annulus segmentation.....	64
2.8 Statistical shape analysis	65
2.8.1 Procrustes analysis.....	66
2.8.1.1 Generalized Procrustes analysis.....	66
2.8.2 Principal component analysis	67
Chapter 3 Assessment of the mitral valve geometry	68
Methodology.....	68
Study 1 Interobserver and inter-method differences	70
3.1.1 Method	70
3.1.2 Results.....	71
3.1.3 Discussion	73
Study 2 Relationships of mitral valve dimensions from cadaver dissection	75
3.2.1 Method	75
3.2.2 Results.....	78

3.2.3 Discussion.....	81
Study 3 Prediction of healthy mitral valve geometry from intertrigonal distance	83
3.3.1 Method.....	84
3.3.2 Results.....	85
3.3.3 Discussion.....	87
Conclusion.....	89
Chapter 4 Annuloplasty ring sizing from intertrigonal distance	91
Methodology.....	91
Study 1 The correlation between the healthy mitral valve dimensions and ring geometry sizing from intertrigonal distance strategy	92
4.1.1 Method	92
4.1.2 Results.....	96
4.1.3 Discussion.....	101
Study 2 How much undersized annuloplasty ring would fit the mitral valve?.....	101
4.2.1 Method	102
4.2.2 Results.....	102
4.2.3 Discussion	106
Conclusion.....	108
Chapter 5 Personalised annuloplasty ring design to fit individuals	110
Methodology.....	110
Study 1 Development of the methods of isolating and 3D reconstructing the mitral annulus ..	113
5.1.1 Method.....	113

5.1.1.1 The point-based method for isolating and 3D reconstructing the mitral annulus	113
5.1.1.2 Method for developing of imaging, isolating and 3D reconstructing the mitral annulus using a thresholding method	114
5.1.2 Results	116
5.1.2.1 Point-based method	116
5.1.2.2 Thresholding method	118
5.1.3 Discussion	119
5.1.4 Repeatability of the Point-based Method in the Mitral Annular 3D Modelling	120
5.1.4.1 Method	120
5.1.4.2 Results	121
5.1.4.3 Discussion	123
5.1.5 The Application of the Point-based Method with MRI	124
5.1.5.1 Method	124
5.1.5.2 Results	127
5.1.5.3 Discussion	128
Study 2 Completing the missing posterior annulus of the mitral annulus model	129
5.2.1 Method	130
5.2.2 Results	132
5.2.3 Discussion	135
Study 3 Personalised annuloplasty ring size selection from patients' pre-operation medical scan image	136
5.3.1 Method	136
5.3.2 Results	140

5.3.2.1 Results from the 1 st MRI	140
5.3.2.2 Results from the 2 nd MRI	145
5.3.3 Discussion.....	151
Conclusion.....	153
Chapter 6 Discussion	155
6.1 General discussion and major findings.....	155
6.1.1 Assessment of the mitral valve geometry	156
6.1.2 Annuloplasty ring sizing with intertrigonal distance	157
6.1.3 Personalised annuloplasty ring design to fit individuals	158
6.2 Revising aim and objectives	160
6.3 Limitations.....	161
Chapter 7 Conclusion and Future Directions	162
7.1 Conclusion	162
7.2 Future work	164
<i>References</i>.....	<i>165</i>
<i>Appendix</i>.....	<i>183</i>

List of Tables

Table 2 Statistics for relative biases for intermethod of measuring the mitral valve dimensions by manual and computer measurement. Negative bias indicates larger value by manual measurement versus computer measurement.	80
Table 3: Size label and the true dimensions of the annuloplasty rings and sizers: the Carpentier-Edwards Physio annuloplasty ring, the St. Jude Medical (SJM) rigid-saddle shape ring (RSA) and the Medtronic 3D Profile (Bothe, Miller and Doenst, 2013).	95
Table 4 Size label and the true dimensions of the annuloplasty rings and sizers: the Carpentier-Edwards Physio annuloplasty ring, the Carpentier-Edwards Physio II annuloplasty ring the St.Jude Medical (SJM) rigid- saddle shape ring (RSA) and the Medtronic 3D Profile.	139
Table 5: Ring size selection for the first data. Note, AML is the anterior mitral leaflet, CC is the intercommissural distance or the transverse diameter.....	141
Table 6: shows the ring size selection for the second data. The Carpentier-Edward Physio ring (size 24-40), the Carpentier-Edward Physio II ring (size 26-38), St.Jude Medical (SJM) rigid- saddle shape (RSA))(size 24-34), and Medtronic 3D Profile.	147

List of Figures

Figure 1.1: The atrioventricular opens during the diastolic phase and closes during the systolic phase of the cardiac cycle to control blood flow (Samuel, 2018).....	21
Figure 1.2: An annuloplasty ring is sutured around the mitral valve to facilitate the leaflets coaptation (Carpentier, 2010).....	22
Figure 1.3: The main steps taken in this thesis.	26
Figure 1.4: The thesis outline.....	31
Figure 2.1: The mitral valve opens during the diastolic phase and closes during the systolic phase of the cardiac cycle to control blood flow (Samuel, 2018).....	33
Figure 2.2: Components of the mitral valve leaflets and the chordae tendineae insertion area (Kanjanauthai, 2015).	34
Figure 2.3: The mitral valve with three scallops of the anterior leaflet (A1, A2, A3) and three scallops of posterior leaflet (P1, P2, P3) connecting at anterior commissure (AC) and posterior commissure (PC) (Carpentier, Adams and Filsoufi, 2010).....	35
Figure 2.4: Stress-strain curve of the anterior mitral leaflet (AML) and posterior mitral leaflet(PML) in the circumferential and radial directions (Pham et al., 2017).	36
Figure 2.5: Anatomy of the mitral valve showing the chordae tendineae connecting leaflets to ventricular muscle (Fontes and Glower, 2018).	37
Figure 2.6: Three types of chordae tendineae in the left panel attached to the mitral valve (Carpentier, Adams and Filsoufi, 2010).	38
Figure 2.7: Function of the chordae tendineae during diastole and systole (Human body anatomy system, 2017).....	39

Figure 2.8: Diagram showing the anterior and posterior mitral annuli that surround the mitral leaflets (Pick, 2008).	40
Figure 2.9: The saddle-shaped mitral annulus with the highest point at the mid anterior annulus and the lowest to the trigones (Castillo et al., 2011).	40
Figure 2.10: The changes of the mitral annulus during early, mid and late systole studied by Kwan et al.,(2009).	42
Figure 2.11: The anterior-posterior plane (AP) and the commissure-commissure plane (CC) of the mitral annulus (Tsang et al., 2011).	43
Figure 2.12: Images showing mitral regurgitation occurring as the mitral valve dysfunction as a result of annular dilation (left), papillary muscle rupture (middle) and leaflet tethering excessive valve motion (right) (Mahmood and Matyal, 2015). 44	
Figure 2.13: An annuloplasty ring is sutured around the mitral valve to facilitate the leaflets coaptation (Carpentier, 2010).	48
Figure 2.14: (A) The Carpentier-Edwards rigid annuloplasty ring (Reul and Cohn, 1997), (B) The Duran flexible annuloplasty ring (Reul and Cohn, 1997), (C)The semi-rigid Carpentier-Edwards Physio annuloplasty ring (Kurosawa et al., 1999)...51	
Figure 2.15: Comparison of personalised ring designs (left) with Cosgrove-Edwards flexible rings (A), Carpentier-Edwards rigid rings(B) and Medtronic’s semi-rigid Future Band (C) (Díaz Lantada et al., 2009).	53
Figure 2.16: The MRI images showing the three chamber view of the human heart and demonstrating the measurement of mitral annulus diameter and coaptation height (left), and mitral tenting area (right) (Srichai et al., 2005).	57
Figure 2.17: 2D and 3D echocardiography allows the visualisation of the structure of the mitral valve. While 2D Echocardiography shows the mitral valve from the ventricular perspective, 3D echocardiography shows the mitral valve from the ventricular and the atrial views.	59
Figure 2.18: Generalised Procrustes analysis steps.....	67

Figure 3.1: The pig heart was dissected to show the mitral annulus and the landmarks.	70
Figure 3.2: The comparison of the anteroposterior diameter performed by two observers with three measurement methods with the error bars show the standard error of the mean, measuring the variability between sample means.	72
Figure 3.3: The comparison of the transverse diameter performed by two observers with three measurement methods.	73
Figure 3.4: The heart with the cut directions shown as the dash lines (Phase of the cardiac cycle, 2019).	75
Figure 3.5: The mitral valves were excluded from the experiment because one was squeezed from storage (left) and another one had a total valve replacement ring (right) which alter the natural shape of the mitral annulus.	76
Figure 3.6: The 3D model of a cadaveric heart clearly showed the mitral valve dimension.	76
Figure 3.7: The comparison between the 2D image (left) taken with a digital camera and the 3D image reconstructed using the Meshlab software.	77
Figure 3.8: The landmarks of the mitral valve showing the anteroposterior and transverse diameters (Carpentier et al., 2010).	77
Figure 3.9: In one heart, the mitral valve was stained (left), then, the 3D model that was created in the Meshlab (right) was too dark to see the annulus.	78
Figure 3.10: Mitral valve dimensions by manual measurement with the average ratio between the anteroposterior and transverse diameters = 3:3.9.	79
Figure 3.11: Mitral valve dimensions by computer measurement with the average ratio between the anteroposterior and transverse diameters = 3:4.0.	80

Figure 3.12: The residuals plot of the error between the predicted dimension from 3:4 ratio and the measurement dimensions of transverse diameter found from manual measurement.	81
Figure 3.13: The residuals plot of the error between the predicted dimension from 3:4 ratio and the measurement dimensions of transverse diameter found from computer measurement.	82
Figure 3.14: Diagram showing the mitral valve and the fibrous trigones (Pick, 2020).	83
Figure 3.15: The mitral valve shows the intertrigonal distance (ITG) where the anterior leaflet attached to the fibrous skeleton between trigones (Carpentier et al., 2010, Oliveira et al., 2020).....	84
Figure 3.16: Plot of the intertrigonal distance and anteroposterior diameters of thirty-four cadavers. The solid line represents a line of fit to the data presented ($y=0.8824x$, $R^2 = 0.9876$).....	86
Figure 3.17: Plot of the intertrigonal distance and transverse diameters of thirty-four cadavers. The solid line represents a line of fit to the data presented ($y=1.1739x$, $R^2 = 0.9971$).	87
Figure 3.18: The residuals plot of the error between the predicted dimensions and the measurement dimensions of the anteroposterior and transverse diameters.	88
Figure 4.1: (A) Medtronic 3D Profile ring(Medtronic, 2021) (B) St.Jude Medical (SJM) rigid-saddle shape (RSA) (SJM™ RigidSaddle Ring, 2013) (C) Carpentier-Edwards Physio annuloplasty ring (Edwards Lifesciences, 2021).	93
Figure 4.2: The assessment of anteroposterior (A-P), transverse diameter, and intertrigonal distance(N-N) dimensions for intertrigonal distance in (A) annuloplasty rings (B) sizers. (Bothe, Miller and Doenst, 2013).	95
Figure 4.3: The graph of transverse diameter versus intertrigonal distance of the healthy mitral valves and the Carpentier-Edwards Physio ring.	96

Figure 4.4: The graph of transverse diameter versus intertrigonal distance of the healthy mitral valves and the St.Jude Medical ring.	97
Figure 4.5: The graph of transverse diameter versus intertrigonal distance of the healthy mitral valves and the Medtronic 3D Profile ring.....	97
Figure 4.6: The bars present the transverse diameter difference between the commercial rings and the healthy mitral valve.	98
Figure 4.7: The graph of anteroposterior diameter versus intertrigonal distance of the healthy mitral valves and the Carpentier-Edward Physio ring.....	99
Figure 4.8: The graph of anteroposterior diameter versus intertrigonal distance of the healthy mitral valves and the St.Jude Medical ring.	99
Figure 4.9: The graph of anteroposterior diameter versus intertrigonal distance of the healthy mitral valves and the Medtronic 3D Profile.	100
Figure 4.10: The bar presents the anteroposterior diameter absolute error difference between the commercial rings and the healthy mitral valves.	100
Figure 4.11: The bar presents the transverse diameter mean error (mm) between the three sizes of the commercial rings and the healthy mitral valves.....	103
Figure 4.12: The bar presents the transverse diameter mean percent error between the three sizes of the commercial rings and the healthy mitral valves.....	104
Figure 4.13: The bar presents anteroposterior diameter error (mm) between the three sizes of the commercial rings and the healthy mitral valves.....	105
Figure 4.14: The bar presents anteroposterior diameter percent error between the three sizes of the commercial rings and the healthy mitral valves.....	105
Figure 5.1 The workflow of the studies in Chapter 5	112
Figure 5.2: The echocardiographs of the mitral valve were displayed in Materialise Mimics in the three views and one 3D image during point-based method.....	114

Figure 5.3: The echocardiographs of the mitral valve were displayed in Materialised Mimics in the three views and one 3D image, showing the mitral valve and surrounding tissue.....	115
Figure 5.4: The mitral annulus was shown as the red line drawn attached inside of the extracted 3D object(blue) which included both the mitral valve and surrounding tissue.....	116
Figure 5.5: Point based method with the red landmarks showing the mitral annulus shape.....	117
Figure 5.6: Top view (left) and side view (right) of the 3D shape of the mitral annulus created with the point based method.	117
Figure 5.7: Two half-rings produced with the same data and point-based method showing the shape similarities and differences: first produced (blue), second produced (grey).	118
Figure 5.8: Top view (left) and side view (middle) of the complete 3D shape of the mitral annulus. The 3D annulus shape in the thresholded mitral valve from Mimics (right).....	118
Figure 5.9: The comparison of the 3D reconstruction of the mitral annulus using the thresholding method twice. The pink ring shows the first result while the grey ring shows the second result obtained.	119
Figure 5.10: Comparison between the annular lengths of the five 3D models of the mitral annulus produced from the same data with mean equal to 54.1 mm.....	121
Figure 5.11: Comparison between the anterior annular lengths of the five 3D models of the mitral annulus produced from the same data with mean equal to 38.9 mm. .	122
Figure 5.12: Comparison between the commissural diameter of the five 3D models of the mitral annulus produced from the same data with mean equal to 26.8 mm. .	122

Figure 5.13: Comparison between the distance from the starting to ending points of the five 3D models of the mitral annulus produced from the same data with mean equal to 27.7 mm.....	123
Figure 5.14: The MRI of the heart that shows the mitral annulus was shown in four windows display the image views in horizontal axial (1), sagittal plane (2), coronal plane (3), and 3D model view (4).	125
Figure 5.15: ITK-SNAP image for locating the annulus area (marked with red landmarks) using the point-based method process.....	126
Figure 5.16: The four windows present the medical image after the Edge attraction adjustment and a red model represents the segmented mitral annulus.	127
Figure 5.17: The model of the extracted mitral annulus.	128
Figure 5.18: The mean shape of the mitral annulus determined from the thirty-four sample cadaveric hearts.....	132
Figure 5.19 The incomplete model shows as black landmarks while the red landmarks are the predicted data from the regression model.....	133
Figure 5.20: The new filled mitral annulus model from the predicted data.....	134
Figure 5.21: Figure 5.20 The filled mitral annulus model (red) and the observed annulus model (blue) were analysed with the Procrustes analysis to analyse the distribution of the models and to provide the minimum sum of squared distance of the models at each landmark (1) the Procrustes rotated shapes of x-y coordinates only, (2) the Procrustes rotated shapes of x-z coordinates only, (3) the Procrustes rotated shapes of y-z coordinates only.	134
Figure 5.22: Workflow of the Personalised annuloplasty ring size selection from patients' pre-operation medical scan image.	138
Figure 5.23: The graph presents the height of the rings selected based on the height of the anterior mitral leaflet (AML) and the intercommissural distance (CC). The intercommissural distance (CC) is the measurement between the two commissures,	

which are the points where the valve leaflets meet and coapt within the mitral valve.
.....142

Figure 5.24: The residual charts show the anteroposterior diameter of the mitral valve minus the ring height when the rings were selected based on the height of the anterior mitral leaflet (AML) and the intercommissural distance (CC).143

Figure 5.25 The residual charts show the ring anteroposterior minus the height of anterior mitral leaflet of the mitral valve when the rings were selected based on the height of the anterior mitral leaflet (AML) and the intercommissural distance (CC).
.....143

Figure 5.26: The graph presents the intercommissural distance of the rings selected based on the height of the anterior mitral leaflet (AML) and the intercommissural distance (CC).144

Figure 5.27: The residual chart shows the intercommissural of the mitral valve minus the ring width when the rings were selected based on the height of the anterior mitral leaflet (AML) and the intercommissural distance (CC).145

Figure 5.28: The graph presents the anteroposterior diameter of the rings selected based on the height of the anterior mitral leaflet (AML) and the intercommissural distance (CC).148

Figure 5.29: The residual charts show the anteroposterior diameter of the mitral valve minus the ring height when the rings were selected based on the height of the anterior mitral leaflet (AML) and the intercommissural distance (CC).149

Figure 5.30 The residual charts show the ring height minus the height of anterior mitral leaflet of the mitral valve when the rings were selected based on the height of the anterior mitral leaflet (AML) and the intercommissural distance (CC).149

Figure 5.31: The graph presents the intercommissural distance (mm) of the rings selected based on the height of the anterior mitral leaflet (AML) and the intercommissural distance (CC).150

Figure 5.32: The residual chart shows the comparison between the transver diameter of the rings and the mitral valve selected based on the height of the anterior mitral leaflet (AML) and the intercommissural distance (CC).....151

Chapter 1 Introduction

The thesis is about the assessment of the mitral valve geometry in order to better understand the geometry correlation of the mitral valve. Moreover, this thesis is moving towards the development of a personalised annuloplasty ring, the ring that specifically designed and manufactured for an individual patient based on their unique cardiac anatomy, used for treating regurgitant mitral valves to serve individual differences.

1.1 Background to the project

The human heart can be divided into left and right, with the upper chamber called the atrium and the lower chamber called the ventricle. The heart contains four valves. The tricuspid valve and pulmonary valve are known as the semilunar valves, while the mitral valve and aortic valve are also known as the atrioventricular valves. These valves open and close to control the blood flow into the heart and out to the body [Figure1.1]. The mitral valve is located between the left atrium and the left ventricle and is made of the mitral leaflets, the chordae tendineae, the mitral annulus, and the papillary muscles. The mitral valve's physiological function is to ensure unidirectional blood flow from the left atrium to the left ventricle during the cardiac cycle.

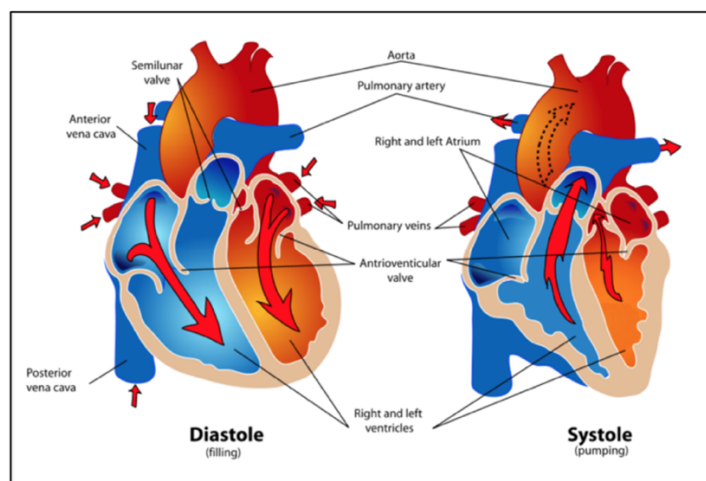


Figure 1.1: The atrioventricular opens during the diastolic phase and closes during the systolic phase of the cardiac cycle to control blood flow (Samuel, 2018).

Mitral valve regurgitation is one of the heart valve diseases. It occurs when the mitral valve does not function properly. Mitral regurgitation occurs when the mitral valve does not close completely, allowing the blood to flow backward from the left ventricle to the left atrium instead of passing through the aorta. The leading causes of mitral regurgitation include rheumatic fever, Barlow's disease, endocarditis, and congenital defects.

Over the last decade, mitral valve repair has become the most common method for treating mitral valve diseases and abnormalities such as mitral stenosis, mitral regurgitation, annular dilatation, and calcification of the mitral leaflets (Stevanella et al., 2011; Rausch et al., 2011). Mitral valve repair is preferred over mitral valve replacement because of its long-term durability and survival rate (Accola et al., 2005; Spiegelstein et al., 2007; Magne et al., 2008; Eckert et al., 2009; Fattouch et al., 2009; Rausch et al., 2011).

Annuloplasty is one of the repair techniques used to treat mitral valve dysfunction with the concept of reconstructing the mitral annulus, which is a fibrous ring located around the mitral opening. Annuloplasty is used to treat patients who have mitral regurgitation by the implantation of an annuloplasty ring around the mitral annulus [Figure 1.2], leading to a reduced mitral orifice size, reinforcing the annulus, and restoring the mitral leaflets coaptation during the systolic stage.

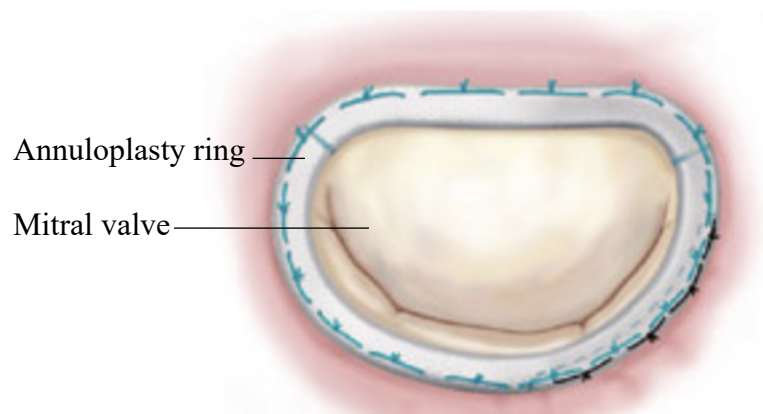


Figure 1.2: An annuloplasty ring is sutured around the mitral valve to facilitate the leaflets coaptation (Carpentier, 2010).

The first annuloplasty ring was developed in the rigid form in the late 1960s by Dr. Alain Carpentier (Carpentier, 1969). The procedure was to implant the ring permanently to stabilise the annulus. Subsequent studies have shown that the mitral annulus keeps moving, changing its size and shape during the cardiac cycle (Flachskampf et al., 2000; Kaplan et al., 2000). Annuloplasty rings have therefore been designed, and manufactured, and further developed into flexible and semi-rigid rings that could support the movement of the mitral annulus. Thus, these ring developments have begun to introduce controversy as to the optimal annuloplasty ring. Whilst there are various commercial annuloplasty rings available with different materials, sizes, and shapes, there is no evidence to suggest that one is significantly better than another (Bothe et al., 2010). The majority of commercial rings are designed based on a 3:4 ratio of the anteroposterior and transverse diameters of the mitral annulus. This ratio has been cited by many journals to represent the ratio of healthy mitral valves. However, there is limited evidence found to support the ratio, whether the 3:4 ratio should be used to optimise an annuloplasty ring design or whether a personalised annuloplasty ring should be developed using this ratio.

The reasons why a personalised annuloplasty ring is needed rather than the existing commercial annuloplasty rings are as follows. First, the shapes and sizes of the commercial annuloplasty rings do not cover all the variations in mitral valve anatomy to serve individual differences (Al-Maisary et al., 2017). In addition, the major drawback of using commercial annuloplasty rings is that when the ring does not have the appropriate geometry to match the mitral valve, it results in changing the geometry of the mitral valve, which affects and changes the mitral annular dynamics (Jensen et al., 2008). That is the main reason why this thesis concerns with using commercial annuloplasty rings to implant into patients' heart valves that have unique shapes among individuals. Therefore, the concept of using personalised annuloplasty ring is proposed.

Moreover, an annuloplasty ring is selected based on the surgeons' preference and experience by making a visual decision during surgery. Not only does this method increase the time spent on decision making during operation, but sometimes, the annuloplasty rings available do not fit the individual (Al-Maisary et al., 2017; Bothe, Miller and Doenst, 2013; Shiota et al., 2011). Further, there are repair failures with

recurrence of mitral regurgitation after the ring annuloplasty. This requires reoperation, that carries a high risk, especially in elderly people (Descoutures et al., 2013). Therefore, the use of a personalised annuloplasty ring for each patient is proposed for greater sufficiency and durability of the treatment.

Recent studies have focused on personalised annuloplasty ring development to optimise mitral valve repair. These developments aim to design an annuloplasty ring that can replicate the native mitral valve to correct its pathology and functions. Although the personalised annuloplasty ring might be better in terms of suitable size and complex valve morphology, nonetheless, the time and cost of designing and manufacturing difficulties are the reasons why the bespoke ring has been limited (Díaz Lantada et al., 2009; Sundermann et al., 2013). Designing a personalised annuloplasty ring is challenging and time consuming because the soft tissue of the annulus is not easily identified in medical images, such as an MRI, CT scan, or echocardiography, as the density of the mitral annulus is very similar to that of the leaflets and surrounding muscular tissue. However, recent technologies have improved the medical imaging with the use of CT scan and echocardiographic data to identify the mitral leaflet insertion zone to the mitral annulus. Therefore, to reduce the design time and cost, it is necessary to study and improve the method of using the medical data combined with the use of a CAD-CAM programme to identify the shape of the mitral valve.

Choosing the suitable annuloplasty ring size is another controversy found when using an annuloplasty ring. Annuloplasty ring sizing remains critical since the implantation of an improperly downsized ring affects long-term outcomes and repair durability (Ohno et al., 2019). In addition, there is no sufficient scientific justification for the optimal ring choice to fit patients with different anatomies and pathologies. Also, there is not enough scientific justification to show the correlation between the strategies and to prove which one should be the standard to optimise the degrees of undersized rings. Normally, surgeons play an important role in choosing the ring size during the operation with direct vision based on their experience, preference, and background training (Ferraó de Oliveira, 2006). There is no research to compare and make a conclusion about which sizing strategy works best to overcome mitral regurgitation

and restore the mitral valve function prior to dilation. Also, there is no study to investigate if ring sizing can be done preoperatively with patient data.

1.2 Thesis aims and objectives

This research aims are to evaluate the geometry of the healthy mitral valve and to develop a method for isolating and creating a 3D model of the mitral annulus, leading to designing a personalised annuloplasty ring that accommodates individual variations and ensuring a more precise fit compared to standard commercial annuloplasty rings. To achieve the aims of this research, this thesis followed the steps shown in Figure 1.3.

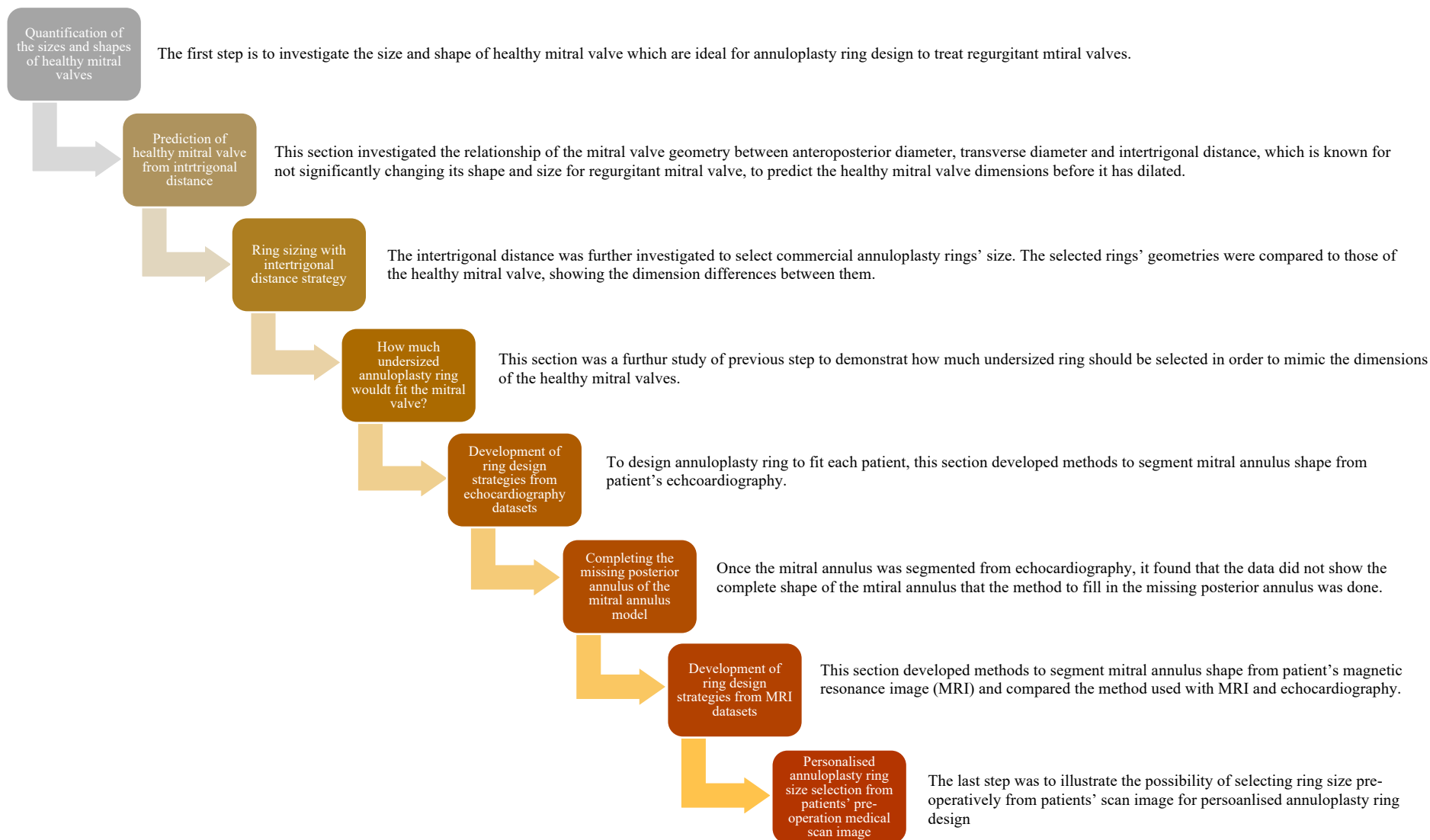


Figure 1.3: The main steps taken in this thesis.

The objectives of this research are

- To investigate the geometry of the healthy mitral valve and whether it conforms to a general pattern of dimensions and ratios
- To determine the relationship between the healthy mitral valve dimensions to investigate whether intertrigonal distance can be used to predict the true anteroposterior and transverse diameters of the mitral annulus before dilation, leading to developing the annuloplasty ring sizing with intertrigonal distance strategy
- To investigate whether commercial annuloplasty rings could mimic the dimensions of the healthy mitral valves and determine the necessity of using personalised annuloplasty ring
- To develop different methods of designing a personalised annuloplasty ring from medical scan images pre-operatively that closely aligns with the dimensions of the patient's mitral valve to enhance valve function, potentially improving long-term outcomes and lowering the risk of complications.

1.3 Contributions to Knowledge

The contributions to knowledge of this thesis are focused on the assessment the mitral valve geometry of the healthy mitral valve and the correlation between its geometry in order to move towards designing a personalised annuloplasty ring to serve individual differences.

First, assessing mitral valve geometry is a complex process that integrates various techniques and methods to gain comprehensive insights. Nowadays, medical imaging plays an important role, with echocardiography and MRI providing detailed visualizations of the mitral valve, including its structure and function. Normally, anatomical measurements, both physical, utilizing callipers during surgeries or post-mortem examinations, and dimensional, such as intertrigonal distance assessments, contribute to understanding mitral valve dimensions. In additions, computational analysis, involving 3D reconstruction from imaging data and digital modelling

through CAD tools, enhances the precision of geometric assessments which could be found in previous studies. These processes help identify mitral valve geometry variations, while functional assessments consider dynamic valve behaviour. Recognizing individual variability in mitral valve geometry is important, making it a collaborative effort among clinicians, imaging specialists, engineers, and researchers in varied clinical and research contexts. To contribute to the existing knowledge in this field, this thesis introduces a methodology for evaluating the mitral valve geometry in healthy hearts obtained from donated cadavers. The focus is on exploring dimension correlations and relationships, providing valuable insights into the dimensions of a healthy mitral valve. This understanding is pivotal for the design of annuloplasty rings that mimic the optimal shape of a healthy mitral valve. Furthermore, the thesis addresses potential errors that may arise during the measurement processes associated with mitral valve geometry.

Annuloplasty ring sizing stands as a crucial phase in mitral valve repair procedures, wherein considerations encompass the transverse diameter, anteroposterior diameter, and intertrigonal distance—the measurement between specific points on the valve annulus. Medical professionals employ diverse methods, including imaging, anatomical measurements, and computational analysis, to determine the appropriate annuloplasty ring size. Nevertheless, the selection of ring size often varies based on surgical preferences and individual experiences, leading to potential discrepancies in sizing choices. Attaining the optimal fit is paramount for enhancing the success of mitral valve repair surgeries and ultimately improving patient outcomes. However, the existing evidence is insufficient to definitively establish which factors should be prioritized to optimize annuloplasty outcomes. To contribute to this field's knowledge, this thesis explores the connections between the dimensions of a healthy mitral valve and the commercial annuloplasty rings employed in this investigation, particularly when the ring selection is based on the distance between the trigones which is known to not significantly dilate in disease mitral valve. Additionally, it discusses the feasibility of utilizing an undersized annuloplasty ring rather than a true-size ring to more accurately replicate the dimensions of a healthy mitral annulus.

The process of constructing a three-dimensional representation of the mitral valve involves utilizing imaging data to create a digital model of the valve. This commonly

employs techniques such as medical imaging, computational analysis, and digital modelling. While advanced imaging modalities like echocardiography and MRI offer detailed visualizations of the mitral valve's structure, computational tools, often utilizing 3D reconstruction algorithms, then process this imaging data to produce a digital model of the mitral valve. This model can be further refined and analyzed using computer-aided design (CAD) tools, resulting in a comprehensive and accurate three-dimensional of the mitral valve's geometry. This 3D reconstruction proves valuable for comprehending the valve's dimensions, shape, and overall structure, especially in medical applications like personalised annuloplasty ring design and mitral valve repair. Nevertheless, the 3D reconstruction of the mitral valve comes with its challenges. The intricate three-dimensional structure, encompassing components like leaflets, annulus, chordae tendineae, and papillary muscles, presents a significant challenge in accurately capturing and reconstructing each element. Furthermore, the dynamic movement of the mitral valve throughout the cardiac cycle demands precise representation in the 3D reconstruction for a realistic portrayal. Challenges also arise from imaging artifacts, computational complexity, and the potential need for manual intervention to refine the reconstructed model. Despite these challenges, continuous advancements in imaging technology, computational algorithms, and software tools contribute to improving the accuracy and efficiency of 3D reconstruction of the mitral valve, broadening its applications in various medical contexts. Hence, this thesis introduces and compares methods for visualizing, segmenting, and constructing the 3D model of the mitral annulus using sequential images from echocardiography and MRI. The optimal shape for a personalised annuloplasty ring corresponds to the mitral annulus shape. However, when patient data lacks a complete representation of the mitral annulus, the study provides a technique to fill in the missing posterior annulus.

1.4 Thesis outline

Over the course of this thesis, the overall research aims to explore the development of a personalised annuloplasty ring design through an investigation of the mitral valve geometry and how to generate the design of a personalised annuloplasty ring using 3D modelling software. The thesis outline is shown in Figure 1.4 and as followed

- Chapter 2 begins with a thorough literature review of the anatomy of the mitral valve, its pathology and treatment, and the method to visualise and segment the mitral annulus for 3D shape analysis and modelling.
- Chapter 3 describes the research methodology, the research method, and the results found from the assessment of the mitral valve geometry of healthy hearts from cadaveric dissection and identifies the errors found between observers and inter-method during the mitral valve assessment in this study.
- Chapter 4 describes the research methodology, the research method, and the results found from the study about annuloplasty ring sizing. This chapter presents the correlation between the healthy mitral valve dimensions and the ring selected from an intertrigonal distance strategy. Undersized rings and true-size rings were also investigated to better imitate the size of healthy mitral valves.
- Chapter 5 describes the research methodology, the research method, and the results found from the development of techniques to segment and 3D reconstruct the mitral annulus out of the patient's scan data. In addition, a method to complete the missing data is also explained. This chapter also illustrates the possibility of annuloplasty ring sizing pre-operatively from the patients' data set.
- Chapter 6 describes the general discussion and major findings of the research with revised aims and objectives.
- Chapter 7 presents the conclusions of this research in addition to possible areas of future research towards personalised annuloplasty ring development

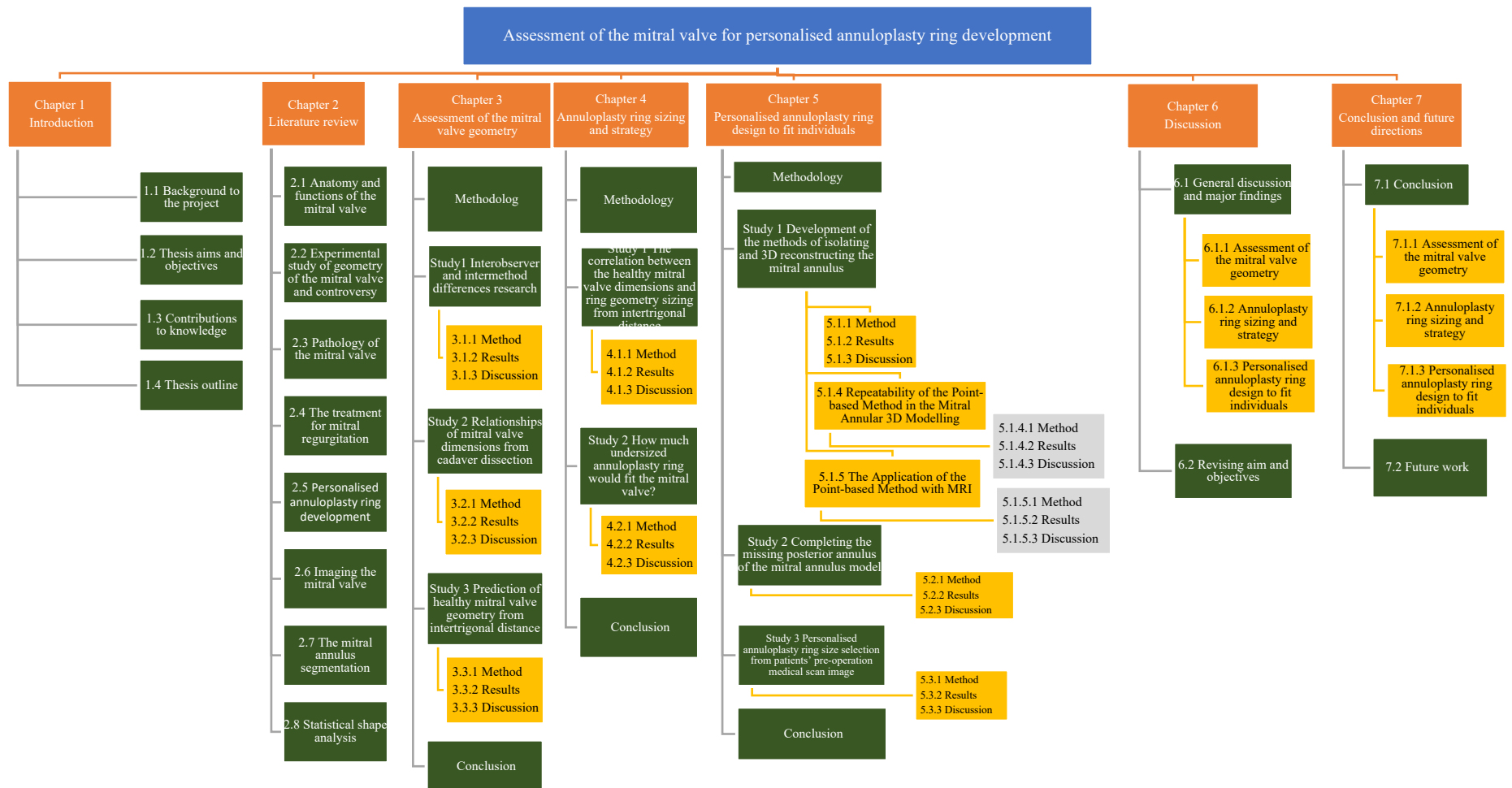


Figure 1.4: The thesis outline.

Chapter 2 Literature review

This chapter describes the background of the project, especially the mitral valve anatomy, function, pathology, and treatment for mitral regurgitation.

2.1 Anatomy and function of the mitral valve

The human heart can be divided into the left and right sides of the heart. While the right side of the heart collects the blood with low oxygen from the body and pumps it to the lungs, the left side of the heart collects blood with high oxygen from the lungs and pumps it to the body. The right side has two chambers, which are the right atrium and the right ventricle. The right atrium is the upper part of the heart that receives blood from the body. As the right atrium contracts, it increases the pressure within the chamber, which forces blood flow through the open tricuspid valve. The tricuspid valve is located between the right atrium and the right ventricle. The valve allows blood to flow from the right atrium to the right ventricle. The right ventricle is the lower right part of the heart that has the pulmonary valve. Once the right ventricle contracts, the pressure inside the chamber increases. This causes the tricuspid valve to close and allow blood to travel through the open pulmonary valve to the lung. The left heart is also made of two chambers: the left atrium and the left ventricle. The left atrium is the upper posterior part of the heart and is behind the aortic root, while the left ventricle is the lower chamber in the posterior heart with a thicker wall. The human heart consists of four valves: the tricuspid valve, the pulmonary valve, the mitral valve, and the aortic valve. Over an average human lifetime, which spans several decades, the intricate and vital heart valves perform several actions. Specifically, each heart valve will open and close at least 3 billion times over a person's lifetime to facilitate the flow of blood through the heart. (Sacks and Yoganathan, 2007). The mitral valve is located between the left atrium and the left ventricle. The mitral valve is also known as the left atrioventricular valve. It is made up of the mitral leaflets, the chordae tendinea, the mitral annulus, and the papillary muscles. The mitral valve's physiological function is to control unidirectional blood flow from the left atrium to the left ventricle during the cardiac cycle. There are two phases of the cardiac cycle that occur during heart beats: diastole and systole [Figure 2.1]. In the diastole phase,

the heart muscle relaxes, and the pressure in the left atrium is higher than that in the left ventricle, causing the mitral valve leaflets to open. Blood from pulmonary veins then flows through the left atrium to the left ventricle. The initial relaxation of the left ventricle during early diastole causes the blood filling velocity to start from a peak of 50–80 cm/s and begin to decelerate as the mitral leaflets partially close (Sacks and Yoganathan, 2007). In the systole stage, the atria contract and pump blood into the ventricle, followed by the ventricles, which contract and pump blood out of the heart to the arteries. During this stage, the mitral valve leaflets close to achieve maximal coaptation in order to prevent blood from flowing backward from the left ventricle to the left atrium and then to prevent mitral regurgitation. Therefore, one cardiac cycle is complete when these two stages have been completed. During the cardiac cycle, the mitral valve is affected by three loading states. Shear stress happens when blood is passing from the left atrium to the left ventricle through an open valve. Tension stress occurs when the mitral valve reduces the annular circumference to form a closed valve. Flexure is formed when the mitral valve is moving to form an opened or closed valve (Hinton and Yutzey, 2011).

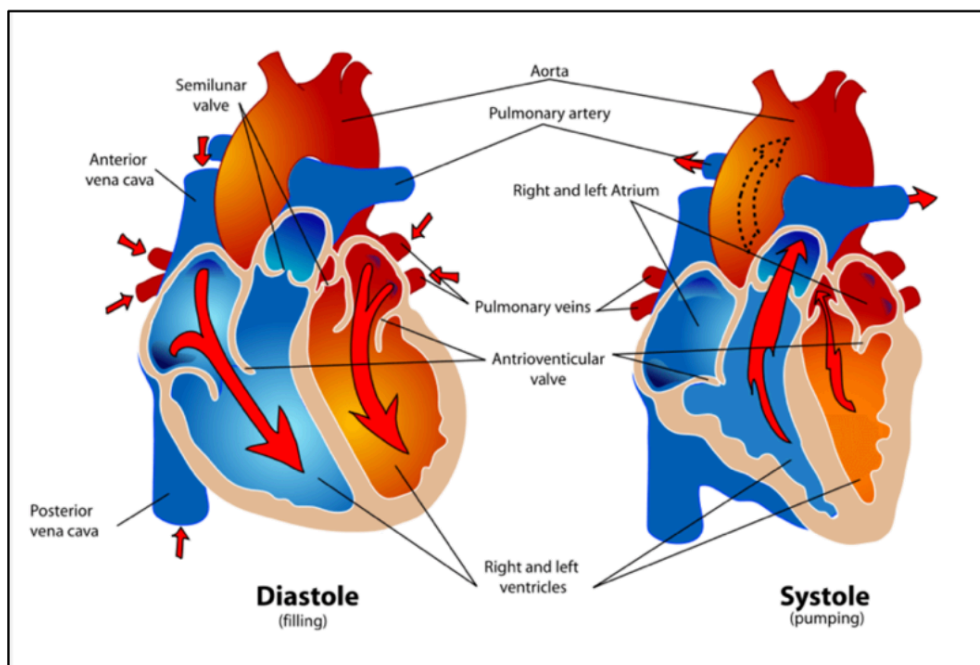


Figure 2.1: The mitral valve opens during the diastolic phase and closes during the systolic phase of the cardiac cycle to control blood flow (Samuel, 2018).

2.1.1 The Mitral leaflets

The mitral valve is also known as the bicuspid valve, as it consists of two thin, pliable, and soft leaflets that join at the commissure points and are surrounded by the mitral annulus. A 1.5:2 ratio between the leaflet area and the mitral annulus area has been claimed by Dal-Bianco and Levine (2013) to be sufficient to prevent mitral regurgitation. Each leaflet has an atrial and a ventricular surface. The anterior leaflet comprises one third of the mitral annular circumference and has clear and rough zones according to the chordae tendineae insertion [Figure 2.2]. The ventricular surface has a thick, rough zone that has a curve shape with chordae tendineae insertions, while the atrial surface has a clear zone that has few or no chordae tendineae insertions (Kanjanauthai, 2015). The anterior leaflet is continuous and semicircular in shape with a free edge. It has no indentations, but it can be divided into three scallops, A1, A2, and A3, as shown in Figure 2.3. Compared to the posterior leaflet, the anterior leaflet has a higher modulus of elasticity in uniaxial and biaxial tensile tests, allowing it to return to its original shape after deformation (Richards et al., 2012).

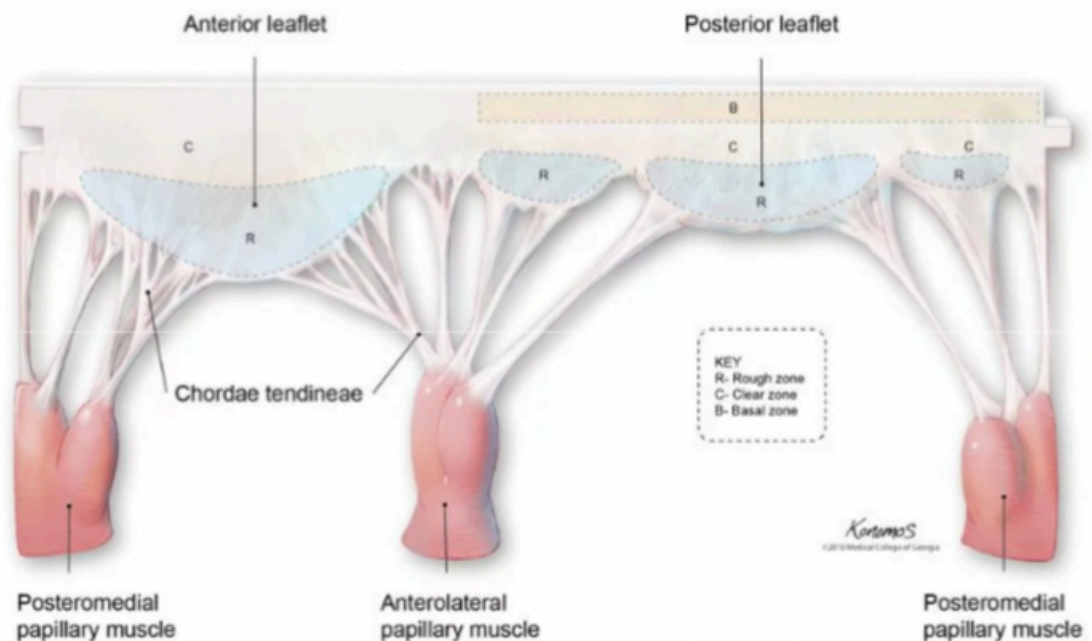


Figure 2.2: Components of the mitral valve leaflets and the chordae tendineae insertion area (Kanjanauthai, 2015).

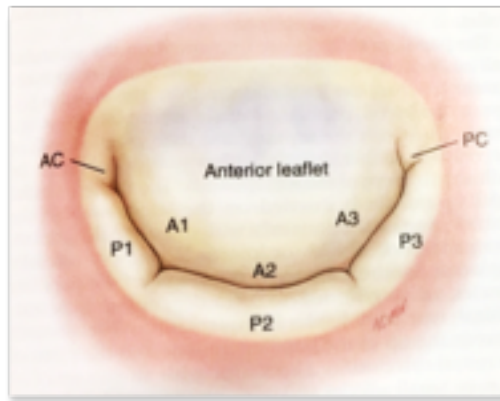


Figure 2.3: The mitral valve with three scallops of the anterior leaflet (A1, A2, A3) and three scallops of posterior leaflet (P1, P2, P3) connecting at anterior commissure (AC) and posterior commissure (PC) (Carpentier, Adams and Filsoufi, 2010).

The mitral valve has three scallops on the anterior leaflet (A1, A2, and A3). The posterior leaflet is thinner and smaller than the anterior leaflet. The posterior leaflet has two indentations that help distinguish the leaflet into three scallops, P1, P2 and P3, whereas the middle scallop (P2) is bigger than the others [Figure 2.3]. The posterior leaflet has a higher number of chordal insertions to increase mechanical support (Richards et al., 2012). The posterior leaflet can be divided into three zones, which are the rough, clear, and basal zones. Similar to those found in the anterior leaflet, the posterior leaflet clear zone is smooth and has few or no chordae tendineae insertion. Moreover, the clear zone is located in the middle, in between the basal zone and the rough zone. The rough zone of the posterior leaflet is on the ventricular side, at the free edge of the leaflet. It is thicker than the clear zone as it is the region of coaptation where there are several chordae tendineae insertions (Kanjanauthai, 2015). The basal zone is the region in between the clear zone and the mitral annulus. It has basal chordae tendineae insertion, which connects the leaflet base and the annulus to the papillary muscle in order to limit the movement of the posterior leaflet. The presence of the chordae tendineae also influences the stiffness of the leaflets. Hence, the leaflets are found to be stiffer in the area that has more chordae insertions. That is why the annular area is stiffer than the free edge. The combined area of the anterior and posterior leaflets is more than twice the area of the mitral orifice. This allows the

leaflets to completely coapt during systole with lower mechanical stress (Ferrao de Oliveira, 2006). The differences between the anterior and the posterior leaflets are that the anterior leaflet is longer than the posterior leaflet, while the posterior leaflet is narrower but has more length attached to the mitral annulus, which covers two thirds of the overall annular circumference (Mahmood and Matyal, 2015). Those two leaflets are connected at the anterior and posterior commissures at both ends, which form a coaptation line and provide coaptation during systole.

Pham et al. (2017) used biaxial testing to study the stress and strain of the anterior mitral leaflet and the posterior mitral leaflet. They found that the AML was stiffer and more isotropic than the PML because the collagen network in the AML was aligned circumferentially. Also, the central part of the AML was found to anisotropically stretch with little shear exerted during the systolic stage. Its peak stretch was found to reach up to 1000% per second (Sacks et al., 2002).

The circumferential direction (CIRC), the direction parallel to the annulus, is stiffer than the radial direction, the direction from the free edge to the annulus, for both leaflets [Figure 2.4]. The stiff circumferential direction supports the leaflets so they can resist load and pressure. In contrast, the radial direction is more flexible and compliant, supporting the leaflets coaptation. Pham et al. (2017) also found evidence showing a correlation between age and the valve mechanical data, where the leaflets were stiffer with less extensibility in both circumferential and radial directions with increasing age.

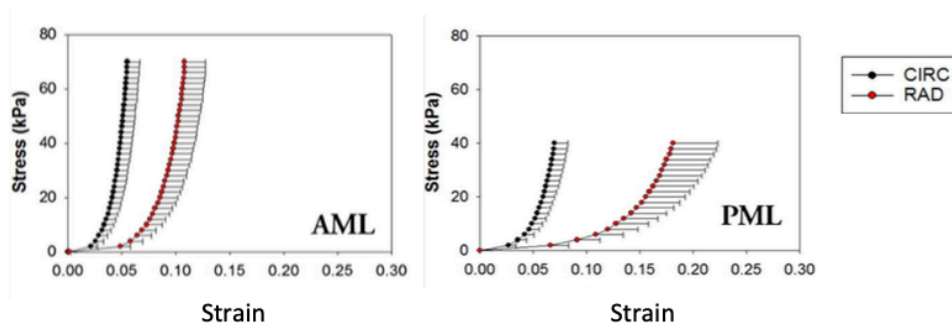


Figure 2.4: Stress-strain curve of the anterior mitral leaflet (AML) and posterior mitral leaflet (PML) in the circumferential and radial directions (Pham et al., 2017).

2.1.2 The chordae tendineae

Figure 2.5 shows the left side of the heart, where the mitral valve lies between the left atrium and the left ventricle. The white tendons connecting the mitral leaflets to the papillary muscle attached to the left ventricle are called the chordae tendineae. The chordae tendineae, or heart strings, are a group of string-like, tendinous strands found in both the left and right ventricles. Normally, there are 8–12 chordae tendineae, 15–20 mm long and around 0.45 mm in diameter, that link the papillary muscle and the mitral valve leaflets. They are made up of around 75% water, 14% collagen, and proteoglycans, with the remaining being elastin and endothelial cells (Liao and Vesely, 2004). The collagen found in the chordae is highly cross-linked and has minimal creep characteristics. It helps to reduce the deformation of the chordae tendineae during valve closure, such that mitral regurgitation does not occur. On the other hand, if the chordae tendineae elongate during valve closure, coaptation will malfunction and lead to mitral regurgitation (Ritchie, Warnock and Yoganathan, 2005). The chordae tendineae originate at the tip of the papillary muscles and split into thinner branches before insertion into the mitral leaflets to balance the mechanical force distribution among the chordae tendineae and to help hold the mitral valve in place (Faletra and Narula, 2018). Also, collagen provides a significant amount of stress relaxation to the chordae (Liao and Vesely, 2004).

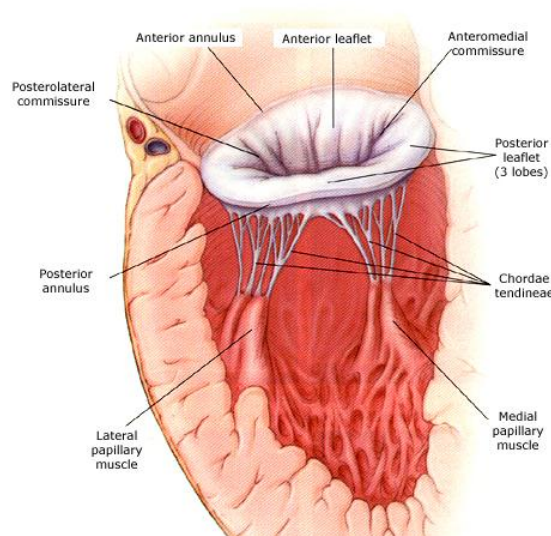


Figure 2.5: Anatomy of the mitral valve showing the chordae tendineae connecting leaflets to ventricular muscle (Fontes and Glower, 2018).

The chordae tendineae can be classified into three types according to the insertion area of the leaflets [Figure 2.6]. The marginal chordae tendineae insert into the free edge of the rough zone of the leaflets to ensure coaptation. The intermediate chordae tendineae insert at the junction of the rough and clear zones on the ventricular surface of the leaflets to balance tension distribution throughout the leaflets. The basal or tertiary chordae tendineae are found only in the posterior leaflet. They insert into the basal zone of the posterior leaflet to connect the leaflet base and the mitral annulus to the papillary muscle (Kanjanauthai, 2015).

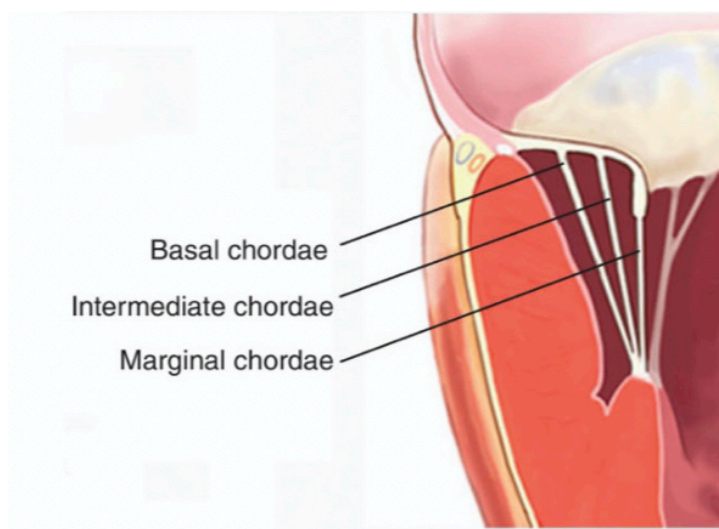


Figure 2.6: Three types of chordae tendineae in the left panel attached to the mitral valve (Carpentier, Adams and Filsoufi, 2010).

During diastole, the papillary muscle relaxes as a result of increased pressure in the left atrium, which forces the mitral valve to open to allow blood flow from the left atrium to the left ventricle. When the ventricle contracts during systole, blood pressure in the left ventricle increases to a higher level than in the left atrium. This forces the mitral valve to close and prevents blood backflow into the atrium. Hence, the chordae tendineae tighten up to hold the leaflets in the closed position [Figure 2.7] (Karas and Elkins, 1970). The chordae tendineae can stretch, tear, and rupture. Failure of the chordae tendineae can cause valve dysfunction and lead to leaflet prolapse and mitral regurgitation (Castillo et al., 2011; Díaz Lantada et al., 2009).

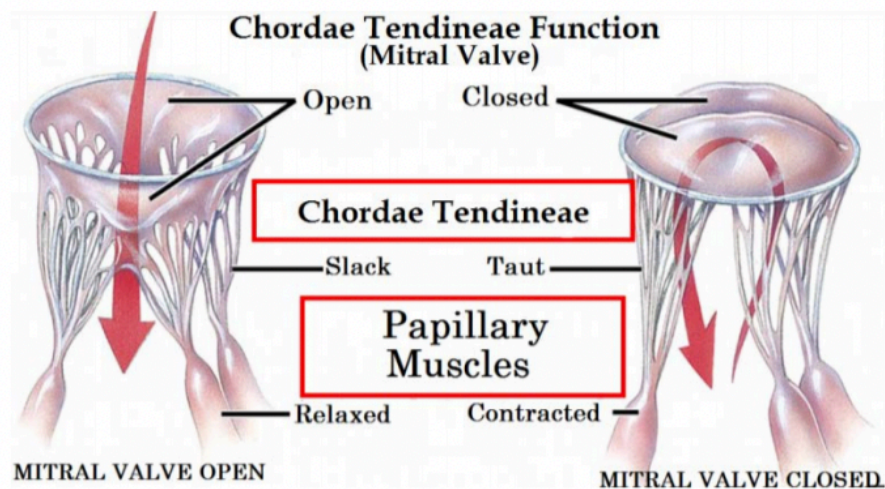


Figure 2.7: Function of the chordae tendineae during diastole and systole (Human body anatomy system, 2017).

2.1.3 The Mitral annulus

The mitral annulus is the region between the atrial myocardium and the mitral leaflet tissue (Rausch et al., 2011). It is a flexible, nonplanar, saddle-shaped, fibrous ring that surrounds the leaflets [Figure 2.8]. The normal mitral annulus circumference is approximately 10 cm with a 5cm^2 to 11cm^2 annular area that is modified during the cardiac cycle (Castillo et al., 2011). The annulus has the highest point in the middle of the anterior annulus (Mahmood et al., 2008), whereas the two lower points, known as trigones, are points to separate the annulus into anterior and posterior parts [Figure 2.9]. These anterior and posterior parts elevate upward to form a saddle-shaped annulus. The function of the mitral annulus is to restrict and reduce the mitral valve surface area during systole to ensure that the leaflets are completely coapted. During systole, when the annulus contracts and the commissural area moves apically, the three-dimensional saddle shape is exaggerated to narrow down the circumference. In contrast, during diastole, the annulus relaxes, its circumference increases, and the annular area also increases by 20% up to 40% compared to that in the systolic stage (Dal-Bianco and Levine, 2013). The nonplanar shape of the mitral annulus and the shape of the leaflets are believed to help reduce mitral leaflet stress (Mahmood et al., 2010) because the nonplanar saddle annulus increases more leaflet curvature and area

compared to a flat annulus, this supports stress distribution and further reduces leaflet stress (Salgo et al., 2002).

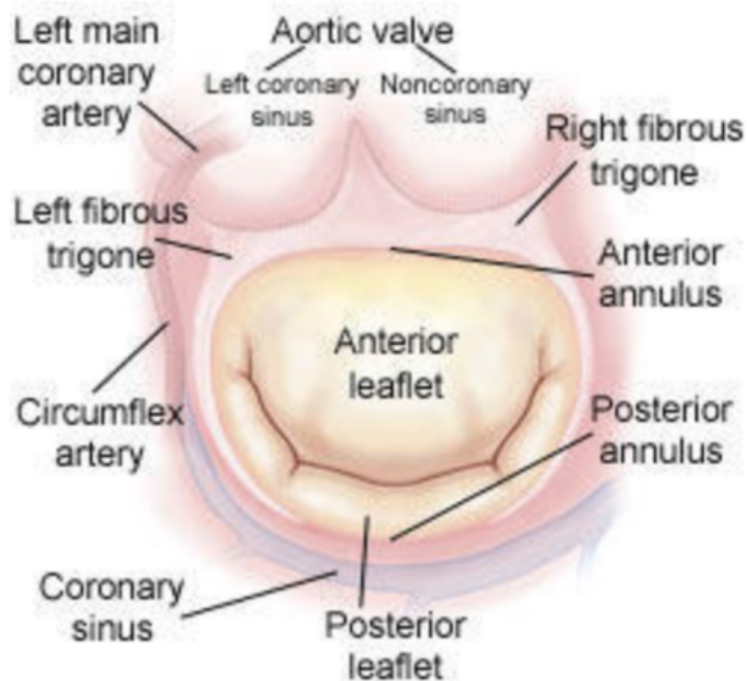


Figure 2.8: Diagram showing the anterior and posterior mitral annuli that surround the mitral leaflets (Pick, 2008).

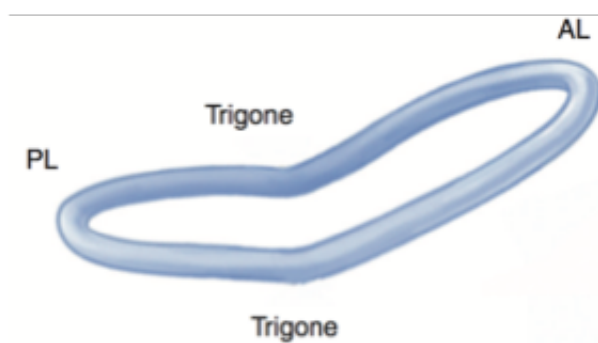


Figure 2.9: The saddle-shaped mitral annulus with the highest point at the mid anterior annulus and the lowest to the trigones (Castillo et al., 2011).

The anterior annulus is part of the fibrous skeleton of the heart, between the left and right fibrous trigones, which restricts the portion of the anterior annulus from increasing in circumference. The medial portion of the anterior annulus is continuous with the aortic annulus. In contrast, the posterior annulus is mainly muscular and is less static compared to the anterior annulus because it does not attach to any fibrous

structures and the fibrous skeleton is discontinuous, allowing it to move freely with myocardial contraction and relaxation. Moreover, it bends along the commissure-commissure axis and increases saddle height to support mitral orifice area reduction and leaflet coaptation during the systolic stage.

The processes of achieving leaflet coaptation can be affected by annular calcification and annular dilatation. In patients with a dilated left atrium or left ventricle, the mitral annulus increases its circumference, decreases its saddle shape, and becomes flat. These changes lead to mitral leaflet remodelling, leaflet stress alteration, and mitral regurgitation (Dal-Bianco and Levine, 2013). Since the posterior annulus is able to enlarge and shrink its circumference, it is prone to dilation (Carpentier, Adams and Filsoufi, 2010; Ferrao de Oliveira, 2006). However, even when the anterior annulus is less prone to increasing its circumference, some studies have shown that the anterior annulus is active and able to deform and can cause mitral regurgitation as well (Hueb et al., 2002; Ahmad et al., 2004; Topilsky et al., 2013). Calcification of the mitral annulus is very common. Ten percent of patients age over 50 suffer from mitral annular calcification, which can weaken and restrict the mobility of the leaflets, resulting in mitral regurgitation. On the other hand, a loss of annular relaxation during diastole can be the cause of mitral valve stenosis (Dal-Bianco and Levine, 2013).

2.2 Experimental study of geometry of the mitral valve and controversy

Many researchers have studied mitral valve geometry, but the majority of them have only focused on a specific stage of the cardiac cycle, mostly the systolic stage. This is because the systolic stage plays an important role in showing the mitral annular shape that promotes mitral valve coaptation. A few papers have studied the difference in geometry between patients with primary and secondary mitral regurgitation, but none of them have compared the dilation of the mitral valve and its transformation in patients with different degrees of mitral regurgitation. Delgado et al. (2009) studied mitral valve geometry by comparing patients with heart failure (HF) to patients with moderate to severe mitral regurgitation during the systolic phase using multi-slice computerised tomography (MSCT), as they claimed that the MSCT gave more insight into the mechanical function of mitral regurgitation. Naoum et al. (2016) used a 64-

slice CT scan, mitral annulus segmentation software (3mensio Structural Heart Software), and volume analysis software (Aquarius iNtuitin) to determine the mitral annulus dimension, projected area, perimeter, and distances comparing between patients with and without cardiac disease. They concluded that patients with mitral regurgitation or mitral valve prolapse had larger mitral dimensions at all points compared to those without cardiac disease. As well as CT scanning and 3D echocardiography, some studies use 2D echocardiography in investigating the valve geometry, but they cannot be used to create 3D models (Dal-Bianco and Levine, 2013).

Although technologies and 3D scans can improve the methods of understanding mitral valve geometry, there is still controversy about the changes in shape of the mitral annulus during the cardiac cycle. Real-time 3D echocardiography and 3D computer software have been applied to reconstruct and automatically measure the geometry of the 3D annulus (Mahmood et al., 2010; Kwan et al., 2009). There are many claims about the transformation of the mitral annulus during systole. Kwan et al. (2009) studied the changes of the mitral annulus during three phases of systole, early systole (the phase after the mitral valve closure and before the aortic valve opening), mid systole (the middle phase in between the other systoles), and late systole (the phase after the aortic valve closure and before the mitral valve opening). They claimed that from early systole to late systole, the saddle-shaped annulus consistently increased its circumference and became flat. The expansion of the annulus was significantly changed in the anterior-posterior plane (AP), while they reported not much change in the commissure-commissure plane as shown in Figure 2.10 and Figure 2.11.

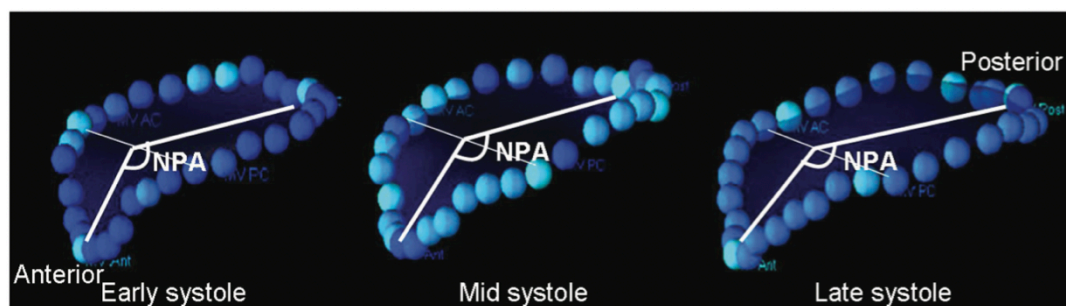


Figure 2.10: The changes of the mitral annulus during early, mid, and late systole studied by Kwan et al., (2009).

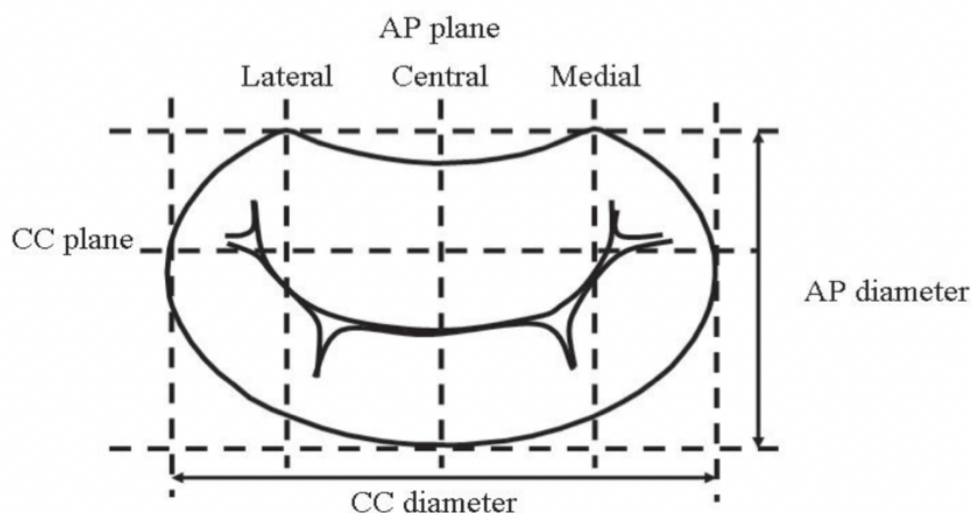


Figure 2.11: The anterior-posterior plane (AP) and the commissure-commissure plane (CC) of the mitral annulus (Tsang et al., 2011).

Conversely, Rausch et al., 2011 claimed the opposite results. Their study showed that throughout the cardiac cycle, the curving of the mitral annulus remained unchanged. The controversy continues as previous studies claimed that during early systole, the annulus reduced its size, then enlarged at the later stages of systole and diastole (Timek et al., 2000). These claims go along with Ormiston et al. (1981), who pointed out that there was the presystolic stage in which the annular area started to decrease its size by 26.3% and reduce its circumference by 13.3% to reach the minimum in the mid-systole and then started increasing at the late systole. The increase in the circumference of the mitral annulus during the late systole was probably caused by the left atrium filling with blood, which expanded the left atrium size and increased the annular size accordingly. The controversies can be caused by some limitations found in determining mitral valve geometry in previous papers. Some studies have only studied annular geometry at one phase, which is either diastole or systole, therefore, those studies cannot compare the size of the mitral annulus in the systole and diastole phases. Next, some other studies have used an animal model, whose results might not be applicable to humans. Moreover, the studies with an abnormal heart valve could produce abnormal annular behaviour and motion that do not represent the state of the mitral annular geometry in general humans. Another limitation is that the reliability of the reconstruction shape depends on the number of points used in tracing the annular

shape. The more points used in reconstruction, the more reliable the results are (Kwan et al. 2009).

2.3 Pathology of the mitral valve

Heart valve disease can occur when one valve or a combination of the heart valves is not working properly. For mitral valves, common pathologies include mitral stenosis and mitral regurgitation. Mitral stenosis is a narrowing of the mitral valve, or when the mitral valve does not open properly, the orifice area is reduced, blocking the blood flow from the left atrium to the left ventricle. The main cause of mitral stenosis is when a rheumatic fever infection scars the mitral valve. This causes it to narrow and develop symptoms including shortness of breath, fatigue, coughing up blood, and chest pain. In terms of all types of heart valve disease, mitral regurgitation is the most common (Malhotra, 2012; Moore et al., 2016). There is a 2% chance of having mitral regurgitation in the normal population, especially in the elderly (Nkomo et al., 2006). Mitral regurgitation is a leakage of the mitral valve, allowing blood to flow backward through the mitral valve to the left atrium. The blood leakage increases the blood pressure in the left atrium, and the person may also feel tired and out of breath. There are many pathologies and mechanisms that can alter the mitral valve function and lead to changes in annular shape and mitral regurgitation [Figure 2.12].

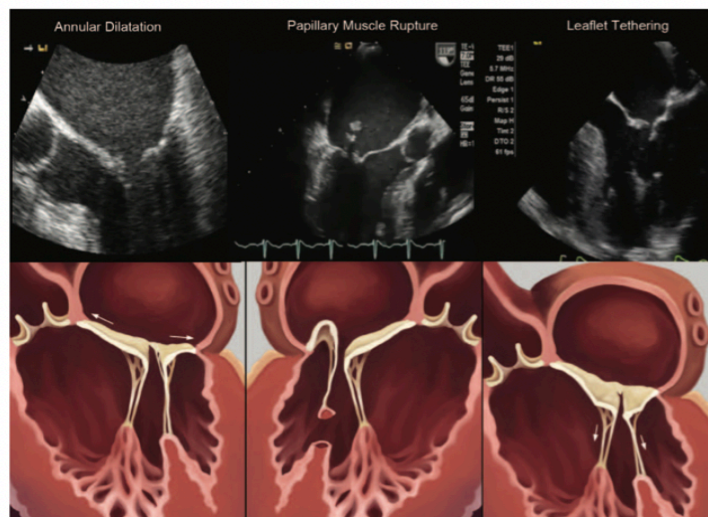


Figure 2.12: Images showing mitral regurgitation occurring as the mitral valve dysfunction as a result of annular dilation (left), papillary muscle rupture (middle) and leaflet tethering excessive valve motion (right) (Mahmood and Matyal, 2015).

There are two types of mitral regurgitation. The primary (degenerative) mitral regurgitation results from primary diseases and degeneration of the leaflets and chords. Rheumatic disease is one of the primary diseases as it thickens the mitral leaflets, especially at their free edge, and causes them to become rigid. This change represents inflammation of the mitral valve, which normally progresses over time (Lancellotti et al., 2013). Additionally, fibrous-elastic degeneration, which reduces leaflet motion, and infective endocarditis, caused by bacteria on the valve, are known to be primary diseases as well. The primary diseases are intrinsic to the mitral valve tissue (Stevanella et al., 2011) which leads to the alteration of the mitral apparatus, causing incompetence in the closing of the mitral valve and allowing blood to leak and flow back through the orifices into the left atrium as the leaflets cannot completely coapt during valve closure (Rausch et al., 2011; Díaz Lantada et al., 2009). The secondary (functional) mitral regurgitation occurs as a result of the annulus and left ventricular dysfunction that stretch out the valve and prevent it from closing properly while the mitral valve itself remains normal. Secondary mitral regurgitation can occur when there is dilation of the mitral annulus, ventricular wall abnormalities and dilation, and a functional alteration in the papillary muscles that prevents the valves from coaptation.

Mitral regurgitation is regarded as mild, moderate, or severe (Akdemir et al., 2005). In the mild phase, the change is the enlargement of the left ventricle, but the amount of mitral regurgitation is so small that the backward blood leak has no significant consequences and does not cause symptoms. In the moderate phase, surgical treatment is recommended as the mitral regurgitation progresses to the point that the left ventricle can no longer compensate for the regurgitation and the myocardium becomes weakened. Some people have experienced fatigue with less active ability, while other people have no symptoms at all. The last phase is the severe phase. It is the phase that develops into heart failure as the left ventricle and left atrium enlarge and function less efficiently with abnormal heart rhythms, causing a greater volume of regurgitated blood. These changes require the left ventricle, the myocardium, and the circulatory system to perform even harder to supply oxygenated blood to the body. Over time, heart failure eventually develops (Gaasch, 2018). The severity of the mitral regurgitation can be graded by angiography, Doppler echocardiography, or magnetic

resonance imaging (MRI). Angiography is a medical imaging technique that is used for regurgitant severity evaluation. This method inserts a catheter through blood vessels to the heart. Then, contrast media or dye is delivered to the left atrium through the mitral valve before images are taken. It evaluates regurgitant severity by looking at the quantity and density of contrast media ejected into the left atrium. Then, the regurgitant volume is calculated and graded. This is an invasive method with a risk of complications. Also, the grading can be affected by rhythm disturbance, catheter position, and the amount of dye delivered. Doppler echocardiography has been claimed to give a better regurgitant assessment compared to angiography because of its non-invasive method and lower cost (Apostolakis and Baikoussis, 2009). Doppler echocardiography, or doppler colour flow imaging, is a technique that uses ultrasound to capture blood flow and display it as colour-coded pixels. It is used to grade mitral regurgitation by evaluating the amount of regurgitant jet and blood backflow direction in the left atrium (blue is moving away and red is moving towards the transducer), the width of the vena contracta, the point where the diameter of the blood stream is the least, to show the narrowest diameter of the regurgitant orifice area, and calculating blood flow velocities and proximal iso-velocity surface area (PISA). These components are considered to fully describe the severity of mitral regurgitation. However, the position of the jet affects the regurgitant grading. A peripheral jet, or other jets that are not central, have been claimed to lead to underestimations of the severity of regurgitation of up to 40% (Sugeng et al., 2003). The other limitations of this technique are that Doppler echocardiography relies on the operator's experience and might present errors because of variations in ultrasound image quality. Another method for the estimation of mitral regurgitation is magnetic resonance imaging (MRI). MRI is beneficial because it does not need to consider regurgitant jets or contrast in patients. Regurgitant volume is determined by calculating the difference between left ventricular stroke volume and right ventricle stroke volume (forward stroke volume). Normally, the stroke volume of the ventricles is equivalent. Hence, the difference in stroke volume shows the amount of regurgitation. The method is valid only with no tricuspid valve regurgitation and aortic valve regurgitation, or else the volume difference represents the sum of the regurgitation of both the aortic and mitral valves.

2.4 The treatment for mitral regurgitation

There are no medications proven to help the mitral leaflets close completely, but some medications can help reduce the symptoms of mitral regurgitation. Therefore, patients with moderate to severe mitral regurgitation typically require surgical intervention to restore mitral valve function. There are two surgical treatments: mitral valve replacement and repair. Mitral valve replacement is a surgery that replaces the mitral valve in the human heart with a mechanical valve or a bioprosthetic valve; the latter is a valve made from animal tissue. However, mitral valve repair, which is the operation to restore the valve coaptation, is preferred over valve replacement, and it is claimed to have better outcomes as the heart functions more efficiently with fewer complications and results in higher survival rates (Magne et al., 2008; Fattouch et al., 2009; Rausch et al., 2011; Eckert et al., 2009; Accola et al., 2005). The mortality rate for mitral valve repair is about 1 percent with 2.7 percent reoperation, compared with 4-5 percent mortality rate with 5.8 percent reoperation for mitral valve replacement (D'Agostino et al., 2016). There are many techniques that can be used alone or in combination during mitral valve repair (Díaz Lantada et al., 2009): the edge-to-edge technique (which is a procedure that anchors portions of the free edge of the leaflets together), chordal replacement and transposition, leaflet resection (to remodel the leaflet by cutting and suturing some portion), and annuloplasty (to narrow down the mitral valve and orifice area by implanting a ring around the mitral valve). Previous papers have shown that mitral valve repair with the annuloplasty technique is able to restore the valve function and overcome mitral regurgitation, and this technique has been considered the gold standard for mitral regurgitation treatment over the last decade (Ferraó de Oliveira, 2006; Stevanella et al., 2011; Rausch et al., 2011).

2.4.1 Mitral valve treatment with annuloplasty ring

Mitral valve annuloplasty is a technique that implants an annuloplasty ring to a patient's dilated mitral annulus. As the annuloplasty ring is smaller in size than the dilated mitral valve, it helps to restore the mitral valve shape, narrows down the mitral valve orifice and pulls the leaflets to improve coaptation [Figure 2.13] (Díaz Lantada et al., 2009). This technique has more stable outcomes compared to other forms of

mitral valve surgery. So, many researchers have focused on developing the mitral annuloplasty ring and the repair durability to lower the probability of reoperation (Díaz Lantada et al., 2009). Nowadays, there are a variety of annuloplasty rings for cardiac surgeons to choose from because annuloplasty rings are manufactured in different shapes, sizes, and materials but they all seek to support mitral leaflet coaptation.

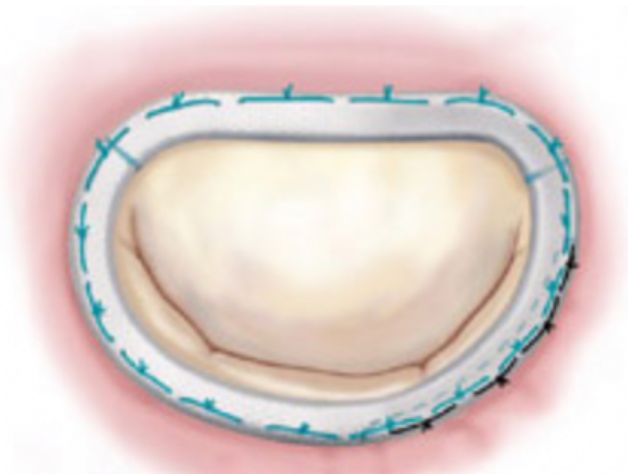


Figure 2.13: An annuloplasty ring is sutured around the mitral valve to facilitate the leaflets coaptation (Carpentier, 2010).

Some of the annuloplasty rings, such as the Carpentier-Edward physio ring, are designed based on the concept of a 3:4 ratio. The 3:4 ratio is the ratio of mitral valve transverse and anteroposterior diameters, proposed by Alain Carpentier and cited by many researchers. (Carpentier et al., 1995; Medtronic.com, 2019). In patients with mitral regurgitation, the ratio alters, resulting in valve leakage as the leaflets cannot completely coapt. However, there is no evidence to support the claim of the ratio nor the ratio after valve alteration.

Various studies have reported favourable results after mitral valve repair. Nevertheless, for long-term outcomes, the implantation of an undersized annuloplasty ring can probably induce forces in the surrounding tissue. Attaching an annuloplasty ring to the annulus can restrict the annular shape and impact the stress distribution. This can produce overload tissue stress, resulting in tissue damage (Eckert et al., 2009) and trigger ventricular remodelling (Baillargeon et al., 2015). These are signs of operation failure and the signs of recurrence of mitral regurgitation. Therefore,

reoperation is needed (Himbert et al., 2018). Moreover, the use of annuloplasty rings has raised some concerns in young patients who need mitral valve repair because the annuloplasty ring can restrict their native mitral valve from growing. It can even cause mitral stenosis when the implanted ring becomes too small as the native mitral valve keeps growing over time (Zacà, Ballo and Mondillo, 2007).

2.4.1.1 Flexibility of an Annuloplasty Rings

The annuloplasty ring was first introduced as a rigid flat ring. However, as the aim is to preserve and replicate the natural mitral annulus functions and movements throughout the cardiac cycle, the concept of creating flexible and semi-rigid annuloplasty rings was introduced (Sundermann et al., 2013). Carpentier (1969) introduced the rigid ring, which was made of a metal core, to protect the mitral annulus from further progression, and has been shown to restrict natural annulus motion [Figure 2.13] (Jensen et al., 2011). A rigid ring succeeds in reducing dynamic motions of the mitral annulus at all times. Its shape is designed with its non-physiological geometry to reform the annulus shape with strain profiles close to zero throughout the cardiac cycle, which means that there is no deformation, and the mitral annulus is fixed in all directions (Rausch et al., 2011).

Duran and Ubago (1976) first proposed replacing a rigid ring with a fully flexible ring to reduce the risk of ring dehiscence, a post-operative situation of mitral valve repair in which the sutures attaching the annuloplasty ring to the mitral annulus pulled out of the tissue. A flexible ring follows the physiological nature and dynamic motion of the mitral annulus and demonstrates continuous changes in the mitral orifice area during systolic and diastolic phases (Borghetti, 2000). It is claimed to be the closest to mimicking three-dimensional shape, preserves changes in saddle shape and height, preserves strain of the native mitral annulus, and supports the posterior annulus against dilation (Rausch et al., 2011). Thus, the flexible ring was developed to replace the rigid ring; however, there are controversial results. The short-term follow-up proved that the flexible annuloplasty was beneficial and was later claimed to be better at preserving left ventricular function than a rigid ring (Borghetti, 2000). In addition, a flexible ring [Figure 2.14] was found to preserve the mitral valve area better and

produce less interference with valvular function in a porcine model (Shahin et al., 2006). In contrast, Izutani, Nakamura and Kawachi (2010) proposed that the rate of reoperation and recurrent mitral regurgitation was significantly higher in patients with flexible rings for mid-term outcomes because the rigid ring was more effective at controlling mitral regurgitation.

The semi-rigid ring, which has a rigid anterior region and a flexible posterior region, is a hybrid between a saddle shape and a flat ring to remodel the mitral annulus. The semi-rigid Physio ring is designed with a kidney shape and a 3:4 ratio between the anteroposterior and transverse diameters. The posterior flexibility allows the annulus to change shape and undergo physiological contraction during valve closure. This region is made of Elgiloy, a cobalt-chromium-nickel-molybdenum alloy that is corrosion resistant, has high strength, fatigue resistance, and ductility, and is separated by plastic bands. This ring type has been found to produce better outcomes in reducing valvular stress, ring dehiscence, and increasing durability compared with the others (Skov et al., 2017) since it allows physiological movements in three dimensions to preserve a saddle shape during systole and a planar shape during diastole of the mitral annulus. (Ryan et al., 2008; Jensen et al., 2008). One study reported that after 8 years of having an annuloplasty with a Carpentier semi-rigid ring or a Duran flexible ring, 62% and 55% of patients, respectively, do not have significant mitral regurgitation (Chang et al., 2007). Furthermore, the semi-rigid Carpentier-Edwards ring is comparable with the Duran flexible ring in terms of survival rate and reoperation rate, but the flexible ring has a higher tendency to develop mitral stenosis because of the formation of pannus, an abnormal tissue growth around a prosthetic heart valve or an annuloplasty ring that lowers the mitral valve orifice area and blocks blood flow (Chee et al., 2008 ; Ha et al., 2018).

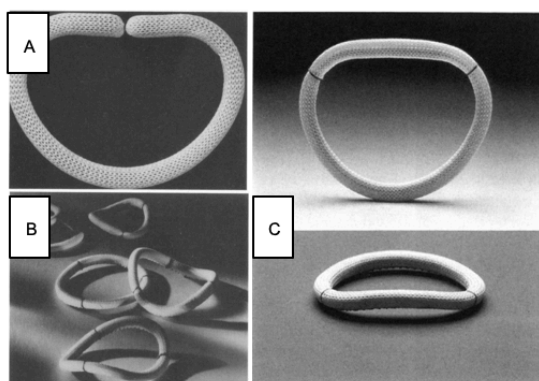


Figure 2.14: (A) The Carpentier-Edwards rigid annuloplasty ring (Reul and Cohn, 1997), (B) The Duran flexible annuloplasty ring (Reul and Cohn, 1997), (C) The semi-rigid Carpentier-Edwards Physio annuloplasty ring (Kurosawa et al., 1999).

2.4.1.2 Annuloplasty ring sizing

Available commercial rings made by manufacturers come in various shapes, materials, and sizes to serve individual anatomy variations. However, choosing the suitable ring size remains critical since the implantation of an improperly downsized ring affects long-term outcomes and repair durability (Ohno et al., 2019). Too aggressive downsized ring can cause ring dehiscence, mitral stenosis, and reoperation. On the other hand, not enough degree of a downsized ring can affect the sufficiency of supporting leaflet coaptation and the reoccurrence of mitral regurgitation (Al-Maisary et al, 2017). In addition, there is no sufficient scientific justification for the optimal ring choice to fit patients with different anatomies and pathologies.

Normally, surgeons play an important role in choosing the ring size during the operation with direct vision based on their experience, preference, and background training, which strategies they rely on, and which degree of a downsized ring they consider to work best in that case (Ferrao de Oliveira, 2006). Besides being time consuming, these factors lead to non-standardized decisions being made by surgeons, which directly affect the operation outcome and repair durability.

Various ring sizing strategies have been developed with the use of a “Sizer”. Sizers are ring templates that have similar shapes and sizes to commercial rings. These sizers

are placed onto the mitral valve one at a time intraoperatively to find the suitable ring size according to different anatomical relations based on different ring sizing strategies, such as the height of the anterior mitral leaflet, the intercommissural distance, and the intertrigonal distance (Ohno et al., 2019). However, in some cases, the available annuloplasty rings do not represent an accurate shape and size to fit the individual (Al-Maisary et al., 2017; Bothe, Miller and Doenst, 2013; Shiota et al., 2011).

Recently, the use of pre- operation medical images such as echocardiography and MRI has shown the mitral valve anatomy, which is important for surgery planning and pre-selecting the annuloplasty ring. The images allow CAD software to create three-dimensional models of the patient's heart, the mitral valve, and the mitral annulus, as well as a ring model and size that fit with the specific anatomy (Al-Maisary et al, 2017). This technique can be applied to predict the operation outcomes and the annular deformation after implantation with different undersized rings based on the variation in ring sizing strategies.

2.5 Personalised annuloplasty ring development

Since there are limited sizes and shapes of manufactured annuloplasty rings, the idea of generating a personalised mitral annuloplasty ring has emerged not only to serve anatomic variation but also to get rid of intraoperative decision making and to reduce the time of the operation as well. Studies of personalised annuloplasty rings have undergone significant examination and inquiry in recent times. Researchers and healthcare professionals have extensively explored various facets, including the methodologies employed in the design, sizing, and evaluation of these specialized rings for mitral valve repair. Investigations have searched into comprehending the geometry of healthy mitral valves, refining techniques for the 3D reconstruction of the mitral annulus, and examining the connections between mitral valve dimensions and annuloplasty ring sizing. Additionally, research endeavors have sought to enhance the precision of personalised ring design, taking into account variables such as intertrigonal distance and individual anatomical differences. Ongoing studies continue to probe the potential advantages of personalised annuloplasty rings in improving

surgical outcomes and tailoring care to individual patients. These collective endeavors contribute to the advancement of knowledge and the refinement of strategies in the development and application of personalised annuloplasty rings.

Díaz Lantada et al. (2009) proposed the concept of a personalised annuloplasty ring and designed a ring based on 3D images obtained from a computed tomography scan (CT). The ring was manufactured using epoxy resin material with rapid prototyping techniques called laser stereolithography technology, a type of 3D printing that uses a laser beam controlled by CAD/CAM software to produce 3D models. Since epoxy resin is not biocompatible, the ring cannot be implanted, and no suture can be placed through a solid ring. The research showed that the personalised rings designed for each patient were unique and different from Cosgrove-Edwards flexible rings, Carpentier-Edwards rigid rings, and Medtronic's semi-rigid Future Band [Figure 2.15]. This finding shows the differences between the personalised ring and the commercial rings and proposes that the personalised one could be beneficial for treating mitral insufficiency.



Figure 2.15: Comparison of personalised ring designs (left) with Cosgrove-Edwards flexible rings (A), Carpentier-Edwards rigid rings(B) and Medtronic's semi-rigid Future Band (C) (Díaz Lantada et al., 2009).

Later, Sundermann et al., (2013) developed a personalised annuloplasty ring using biocompatible titanium alloy and pierced holes along the ring so that sutures could be placed through the holes. The study was also performed using computed tomography images (CT) of pig hearts and claimed that the CT images were good enough to segment the mitral annulus. The ring was manufactured by selective laser melting and then implanted in pigs.

Although a personalised annuloplasty ring might be better in terms of its more suitable size and morphology, nonetheless, the time-consuming, cost of designing and manufacturing difficulties are the reasons why the bespoke ring has to date been limited (Díaz Lantada et al., 2009; Sundermann et al., 2013) and does not compete with existing commercially sized rings. Another difficulty in designing a personalised annuloplasty ring is to design the ring's dimensions. The custom dimensions of the ring are not the dimensions of the pathological heart. In contrast, it needs to be further changed in the dimensions that it is capable of bringing back the mitral valve function and to support the leaflet coaptation.

In a study conducted by Owais et al. in 2014, the researchers explored the feasibility of creating an annulus shape based on patient scan data for potential application in a clinical setting. The assessment utilized 3D transoesophageal echocardiographic (TOE) scan data obtained during routine procedures to closely mimic typical inpatient treatment scenarios. Mitral valve analysis was performed using TomTec's Image Arena software, enabling the automatic segmentation of the mitral valve and identification of the annulus amidst surrounding structures. Subsequently, Cartesian coordinates of the annulus were extracted and transferred to SolidWorks to generate a 3D curve based on the scan data, resulting in the creation of a cylindrical surface. Although the 3D model was physically printed using an "inflexible bioderived plastic" with a MakerBot Replicator 2, it was not employed for further analysis or the production of a supportive implant. The authors acknowledged the model's potential for personalised implants in the future but emphasized its primary utility in surgical planning and visual confirmation of repair procedures.

Subsequently, (Graser et al. 2014) enhanced this process by introducing a technique that not only adjusted the CAD file to create a supportive implant but also utilized a biologically safe material for the final ring. The primary data source for the model remained 3D echocardiography, with measurements averaged across the cardiac cycle to provide a representative representation. While the specific software used is not mentioned, the authors described a semi-automatic method for identifying areas for measurement, claiming it took only 74 seconds to generate the shape based on the input scan (Graser et al. 2014). The resulting ring could be resized overall, modified following the 3:4 ratio of the natural annulus, or adjusted to account for deformation stresses. Additionally, the file could be modified to reduce the risk of dehiscence or fracture. Following the creation of a suitably adjusted ring file, the design was manufactured in titanium, a material commonly used for medical implants with a proven safety record and employed as the core material in many commercially available annuloplasty rings.

Pitsis et al., 2019 studied a personalised ring for mitral valve repair surgery that was created in the operating room, tailored to each patient's mitral annulus shape and size using a Dacron sheet and titanium ligating clips. The research included 127 patients with severe mitral regurgitation (MR). Among them, 58 patients received the personalised annuloplasty ring, and 69 patients received a commercial Carpentier-Edwards Physio II ring. Key findings revealed that the personalised annuloplasty ring group had a greater mitral valve area, significant changes in mitral annular area from systole to diastole, and no occurrences of systolic anterior motion (SAM) compared to the Physio II ring group. There were no surgical deaths, and both groups showed positive outcomes during up to 8 years of follow-up, with all patients alive and experiencing mild or less MR symptoms. The study concludes that the personalised annuloplasty ring is suitable for all patients requiring mitral valve repair, offering precise fit, better preservation of valve area and sphincter function, prevention of SAM, and excellent short- and long-term results.

One of the main limitations in designing a personalised annuloplasty ring is that the soft tissue is not easily recognised in medical images as the density of the mitral annulus is very similar to the leaflets and surrounding muscular tissue. However,

recent technologies have improved the medical image capture system with the use of CT scans and echocardiographic data to identify the mitral leaflet insertion zone in the mitral annulus. The medical data combined with the use of a CAD-CAM programme is able to identify the shape of the mitral annulus. The 3D information of the geometric structure from CAD-CAM programmes such as Materialise Mimics is directly passed to 3D printing technologies for manufacturing. These results in a less time-consuming and less expensive manufacturing process for a personalised device. Moreover, a CAD-CAM programme can be applied to determine stress and deformation between different ring designs and materials.

2.6 Imaging the mitral valve

The mitral valve has a complex structure that interacts with blood flow and ventricular motion. Its structure is not easily identified in medical images as there is little contrast between the mitral annulus, the leaflets, and surrounding tissue. However, recent medical imaging techniques provide data that can capture the mitral leaflets insertion zone to the mitral annulus, allowing the annulus to be identified. The main imaging techniques that represent the data for the mitral valve assessment are magnetic resonance imaging (MRI), computed tomography scan (CT scan) and echocardiography. These techniques are imaging processes that are capable of assessing the mitral valve anatomy and pathology. The geometric details required for patient anatomy modelling can be obtained from the imaging data.

2.6.1 Magnetic resonance imaging (MRI)

MRI is a technique that generates images based on the interaction of hydrogen nuclei with magnetic fields. The contrast between tissues is the result of small changes in the concentration of the nuclei and their chemical environment. A strong primary field (normally between 1.5 and 7T) is used to align the spin of the protons, while field gradients are applied to allow spatial localisation in three dimensions. The protons are interrogated using radiofrequency pulses. MRI can be used throughout the body, including the brain, bones, internal organs, blood vessels, and heart. A cardiac MRI is

a painless test that uses an MRI machine with radio waves and magnets to create images of the heart in two or three dimensions, showing detailed images of the heart. It provides anatomic and functional information about the heart that shows how well the heart is functioning, including how the blood is moving inside it. It is capable of showing the detailed damage to a specific area of the heart to determine heart disease, and to assess the severity of the heart condition. Furthermore, because it is non-ionising with 1–2 mm spatial resolution (Lin & Alessio, 2009) and there is no restriction in the position of the plane or orientation without contrast agent, MRI is frequently used for a comprehensive assessment of the heart and mitral valve structure. It has been proven safe and even claimed to be the most precise method for determining ventricular volumes and function (Marcu, Beek and van Rossum, 2006). For imaging the mitral valve, normal valves are difficult to visualise because of their fast movement and thin structure, but when the valves are thickened and move less, it is easier to identify the mitral leaflets (Bogaert, Dymarkowski and Taylor, 2012). However, the process of MRI acquisition is relatively short due to the nature of the physics of the imaging process; typical spin-lattice (T1) and spin-spin (T2) relaxation times for muscles are 900 and 50 ms, respectively. This leads to motion blurring. A way around this problem is to exploit the regularity of the motion of the heart during its cycle by using a technique called ECG or cardiac gating. Cardiac gating or synchronising image acquisition with the ECG allows images of different time points within a cycle to be built up over several cycles. With recent technology and technique, the data is sufficient to provide good detail of the valve structure [Figure 2.16], motion, and velocity of the blood flow (Lau, Diaz, Scambler and Burriesci, 2010) and to determine patient-specific treatment and surgical strategies to treat heart valve diseases.

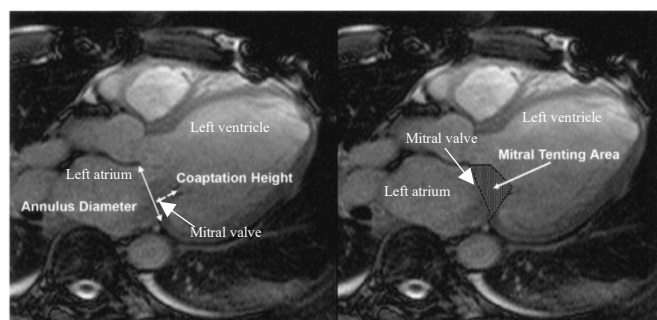


Figure 2.16: The MRI images showing the three chamber view of the human heart and demonstrating the measurement of mitral annulus diameter and coaptation height (left), and mitral tenting area (right) (Srichai et al., 2005).

The heart's motion during the cardiac cycle or during respiration has an impact on the MRI pictures' quality. Thus, the electrocardiogram (ECG) gating is used to synchronising image acquisition with the cardiac-cycle phases while the images are captured while holding one's breath for 10 to 20 seconds (Marcu, Beek and van Rossum, 2006).

2.6.2 Echocardiograms

For a few decades, echocardiography has been preferred for cardiac assessment and diagnostics because it is non-invasive, accurate, and inexpensive (Kamp and Valocik, 2005). An echocardiogram is a type of ultrasound scan that is used to look at the heart and blood vessels and identify heart disease. The process starts by sending out sound waves. Some sound waves are reflected, and some are transmitted when they come into contact with an interface between two tissues with varying acoustic impedances, a measure of the resistance of a substance to the transmission of sound waves that is based on the material's density and sound speed. To create contrast between various tissues and help physicians discriminate between healthy and diseased tissues, this phenomenon is exploited in medical imaging. For instance, there is a sizable differential in the acoustic impedance of the two tissues when an ultrasonic wave contacts the interface between a bone and soft tissue. Compared to soft tissue, bone has a higher acoustic impedance, which causes more of the sound wave to be reflected back towards the transducer. As a result, the bone appears as a bright reflection on the ultrasound image. On the other hand, less sound travels through bone and into soft tissue, causing a darker area to appear on the ultrasound image. The core idea underpinning ultrasonic imaging is the capacity of sound waves to reflect off surfaces between tissues with variable acoustic impedance. Ultrasound technology may produce images of internal organs, blood vessels, and other bodily structures by adjusting the frequency and direction of sound waves. For diagnosing disorders in the abdomen, pelvis, and cardiovascular system, ultrasound scans are especially helpful. There are many types of echocardiograms that are used to get a closer look at the mitral valve. A transoesophageal echocardiogram is an ideal type where a transducer is inserted down into the oesophagus for a closer distance than a regular echocardiogram and to avoid the obstructions of the ribs and lungs that do not transmit ultrasound.

Nevertheless, with several limitations, including the lack of 3D coordinates and geometric assumptions, the evolution of 3D echocardiography has emerged [Figure2.17].

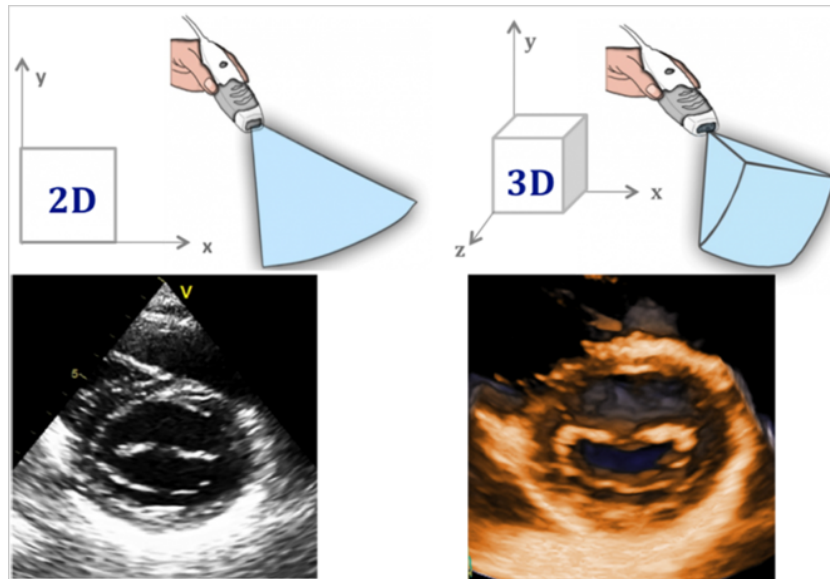


Figure 2.17: 2D and 3D echocardiography allows the visualisation of the structure of the mitral valve. While 2D Echocardiography shows the mitral valve from the ventricular perspective, 3D echocardiography shows the mitral valve from the ventricular and the atrial views.

Echocardiography has transitioned from M-mode imaging to 2D (B-mode) imaging, which has impacted cardiac disease evaluation and become the gold standard for heart valve assessment and clinical management of heart disease. The first ultrasound imaging system employed a single focused transducer to produce an M-mode (reflection mode) image. M-mode imaging is a one-dimensional imaging technique that shows the movement of tissues or other body structures over time. The ultrasonic transducer used in M-mode imaging is positioned on the skin or inside a bodily cavity and emits a focused, narrow beam of ultrasound waves that are directed at a particular area of the body. The transducer then picks up ultrasonic waves that have reflected off tissues or other objects in the beam's passage. These reflections are transformed into electrical signals, and a graph of amplitude (y-axis) vs. time is then presented (x-axis). M-mode imaging is particularly helpful for analysing how structures move, such as the heart, where it may be used to gauge the wall thickness and valve opening and

closing. It can also be used to evaluate how other organs, such as the diaphragm, move when breathing. The one-dimensional nature of M-mode imaging and the fact that it can only reveal information about the structures that are in the path of the focused ultrasound beam are some of its drawbacks. Modern ultrasound imaging includes more sophisticated methods, including Doppler imaging, which can reveal details about blood flow inside the body, and B-mode imaging, which produces three-dimensional images of the body.

With advancements in technology, ultrasound imaging now includes more sophisticated methods, including 3D B-mode imaging, which shows inside-the-body features in three dimensions. Similar to a radar scanner, 3D B-mode imaging is accomplished by sweeping the ultrasonic transducer over the desired area. The ultrasound transducer fires high-frequency ultrasound waves during this motion, and the transducer picks up the echoes that bounce back. Both the amplitude of the echoes that return and the time it takes for the ultrasound waves to travel from the transducer to the tissue are recorded. A 3D picture of the tissue is then created using this data.

The time-of-flight principle is employed in 3D B-mode imaging to pinpoint the locations of the structures in the image. The time it takes for the ultrasonic waves to travel to the tissue and back can be converted into distance by knowing the speed of sound in the tissue being scanned. As a result, the time-of-flight of the ultrasonic waves can be used to determine the location of the structures within the image. The final 3D image, which can be seen from different perspectives, gives a more thorough portrayal of the tissue being examined. Several medical specialties, including obstetrics and gynaecology, cardiology, and musculoskeletal imaging, use 3D B-mode imaging. It can help in the diagnosis and treatment of a variety of medical diseases by offering precise information about the size, shape, and placement of internal structures.

In recent years, there has been more research using 3D echocardiography as it provides better visualisation, analysis and understanding of the complex structures and motion in 3D among the mitral valve apparatus components with reliable information (Kwon and Gopal, 2017; Sengupta, 2014). Moreover, the technique has widened our

understanding of the mitral valve morphology and led to the discovery of the saddle-shaped mitral annulus and mitral leaflet scallops (Lee et al., 2013).

Not only do the echocardiograms give anatomical images, but they also simultaneously visualise blood flow velocities. Color-flow Doppler echocardiography is a type of medical imaging that makes use of ultrasound to show how the heart and blood vessels' blood flow. It is a sort of Doppler echocardiography that offers color-coded blood flow images, making it simple for medical professionals to see the direction and rate of blood flow. A transducer is put on the chest during the surgery, and ultrasound waves are sent into the body. Red blood cells act as a reflector for the waves as they travel through the heart and blood vessels, producing echoes that the transducer can detect. A computer processes the data from these echoes to produce images of blood flow that are color-coded. Red indicates blood flowing in the direction of the transducer, which is shown by the transducer's colour, whereas blue indicates blood flowing outward from the transducer. Colour-flow Doppler echocardiography is very helpful for identifying cardiac diseases, congenital heart abnormalities, and heart failure, all of which alter blood flow through the heart. It can assist medical professionals in determining the severity of an illness, locating blood flow turbulence, and assessing the efficacy of treatments. Many patients chose Doppler echocardiography as their preferred imaging procedure since it is secure, non-invasive, and free of ionising radiation. One limitation found in the early 3D echocardiograms is that it requires an offline reconstruction process to mount acquired 2D images to create 3D data sets, which is complicated and prolongs off-line data analysis. The technique was improved with transducer technology, which made 3D data acquisition possible. Then, a 4D dataset or real-time 3D echocardiography (RT3DE) was introduced and widely used, which is said to be a cardiovascular ultrasound innovation (Correale et al., 2009) since the RT3DE allows the user to visualise images of the heart in real time on a monitor and assist pre-operative surgical planning. However, as there are some limitations with echocardiography, including operator dependence and poor acoustic windows in patients with emphysema, MRI has been an alternative technique and is claimed to better visualise heart valve anatomy and function than an echocardiography (Chen et al., 2009).

It is crucial to take the ultrasound wave frequency into account while performing medical imaging because it can affect the image's spatial and contrast resolution. In the z-direction, higher frequency ultrasound waves can offer superior spatial resolution (depth). This is due to the fact that the ultrasonic wave's wavelength, which is inversely related to its frequency, determines the spatial resolution of an ultrasound image. Higher-frequency ultrasonic waves are able to resolve tiny details in the z-direction because they have shorter wavelengths. Higher-frequency ultrasonic waves, on the other hand, are more easily absorbed and scattered by tissues and have a smaller penetration depth. Their capacity to photograph deeper bodily tissues may be limited as a result, and the contrast resolution may suffer.

On the other hand, lower frequency ultrasonic waves can reach deeper into tissues and offer a superior contrast resolution. They do, however, also have longer wavelengths, which results in reduced z-direction spatial resolution. The focusing abilities of the transducer define the spatial resolution of an ultrasound picture in the x and y dimensions. In order to create an hourglass-shaped beam, the ultrasound beam is often focused using a lens or a phased array transducer. The spatial resolution in these directions may vary depending on the beam's shape and degree of concentration. In conclusion, the spatial and contrast resolutions of the generated image are both influenced by the frequency of the ultrasonic waves employed in medical imaging. Although they have a shallower penetration and a lower contrast resolution, higher frequency waves offer better spatial resolution in the z-direction. Lower frequency waves have a reduced spatial resolution in the z-direction but offer superior penetration depth and contrast resolution. The transducer's ability to concentrate affects the spatial resolution in the x and y directions.

2.6.3 Computed Tomography scan (CT scan)

A computed tomography scan is an imaging technique that uses x-rays and advanced computer algorithms to combine a series of cross-sectional images taken from different angles of the inside of the body, including soft tissue, bones, blood vessels, and internal organs. A CT scan can be used to examine internal injuries and diagnose diseases, making it suitable for medical and surgical planning. To make specific structures or abnormalities more visible during CT scans, contrast chemicals are

occasionally utilised. These medications are often iodine-based and delivered orally, rectally, or through an injection into an arm vein. The structures of interest can be seen more clearly in the ensuing images because the contrast agent absorbs X-rays differently than the surrounding tissues. Using contrast-enhanced CT scans to image blood vessels, tumours, and organs is particularly beneficial. A particular type of contrast-enhanced CT called CT angiography (CTA) is used to see the blood vessels all throughout the body. An arm vein is injected with contrast material during a CTA, and the CT scanner quickly snaps a sequence of photos as the contrast material passes through the blood vessels. Clinicians can assess the structure and blood flow in various sections of the body by combining these photos to generate intricate 3D reconstructions of the blood vessels.

CT scanning has a spatial resolution of 0.5–0.625 mm with low to moderate resolution and 83–135 ms temporal resolution (Lin & Alessio, 2009). The CT scan resolution is higher than the resolution of MRI. A CT scan uses ionising radiation, which is strong enough to pass through the human body and create images on a computer. The human body absorbs some radiation during a CT scan. For a cardiac CT scan, the amount of radiation absorbed is 3 millisieverts (mSv), which is equal to around one year of the radiation absorbed from the surrounding environment. For a CT scan of coronary angiography, the radiation absorbed is 12 mSv, or equal to four years of absorption from the environment.

For mitral valve assessment, echocardiography remains the main technique, while recently CT scanning has played an increasing role in evaluating mitral valve geometry and grading the severity of mitral regurgitation and mitral stenosis. (Weir-McCall et al., 2018). Kim, Kim, Jin and Choi (2017) studied the use of CT scanning to image the mitral valve pathology prior to and after surgery. They found that because of the advances in 3D and 4D imaging techniques of the CT scan, it enabled the visualisation of the mitral valve's anatomy, geometry, and dynamics. They also claimed that a CT scan is an alternative imaging technique to echocardiography for the mitral valve assessment pre-operative and post-operative as well as to predict the surgery outcomes.

2.7 The mitral annulus segmentation

A 3D model of the mitral valve and its structures can be created from a medical image using segmentation. Medical imaging techniques like CT, MRI, and ultrasound rely on the physical characteristics of the tissues to produce images. These images are 3D arrays of values that represent various aspects of the tissues' physical characteristics, such as their electron density, proton spin relaxation times, and acoustic impedance mismatch. Therefore, a segmentation process is needed to interpret this information and identify different anatomical structures. Depending on the structure of interest and the operator's training, one can choose between manual, semi-automatic, and automatic segmentation. Manual segmentation relies on a computer programme and operator recognition of the desired structures (open-source and commercial software are available). If the structures are complicated, this method may be time-consuming and prone to mistakes. Automatic segmentation is the method that relies solely on software, and it functions in a way that the segmented structures are automatically allocated, whereas semi-automatic segmentation is the method where automatic segmentation is performed and followed by manual editing. These automatic and semi-automatic methods are desired to deal with a large database in a less time-consuming and effortless way. Still, these methods require training on how to use the segmentation tools and software. Many segmentation methods are described in the literature. Sometimes, those techniques are used together to achieve a better result (Pham, Xu and Prince, 2000). The two most common techniques are thresholding and region growing. Thresholding is a method where the image is binary segmented based on its intensity and often requires an operator's assessment of the segmentation outcome. Ideally, the structures that have voxels with intensities higher than the threshold will be grouped into one class, and those with intensities lower than the threshold will be in another class. Therefore, this method is suitable for images that have structures with contrasting intensities. Region-growing is another technique that is based on the structures' intensity. The technique gradually extracts a connected image region that has similar intensity as the starting point or seed point selected by an operator. Again, this technique requires manual interaction to set the seed point. One major drawback of the technique is that it can be interfered with by image noise,

causing the extracted images to have holes or be disconnected (Pham, Xu and Prince, 2000).

For complex mitral valve segmentation, the method used is mostly semi-automatic with some manually placed landmarks (Ionasec et al., 2010). For the mitral annulus, researchers and clinicians have used manual segmentation of 2D slices that can be accurate but time-consuming (Schneider et al., 2009). Therefore, Schneider et al. (2010) presented a semi-automatic method, setting an algorithm designed to segment the annulus from a 3D echocardiography during the systolic stage. The algorithm started by placing one point on the mitral leaflet, then located the annulus by finding the area where the thin leaflets met the heart wall, using a thin tissue detector. The process was repeated until convergence metrics were satisfied by the operator, producing an average difference between the segmented annulus and the tracked points across six hearts of 1.19 ± 0.17 mm. Later, Schneider et al. (2010) extended their research to cover the entire cardiac cycle. Tiwari and Patwardhan (2016) also used the thin tissue detector together with manual input of landmarks and a Naive Bayes classifier to estimate the mitral annulus from 3D echocardiography. The results showed the difference between the predicted values and the manual annotations on real patient cases with errors less than 2.59 mm. Andreassen et al. (2020) introduced automatic mitral annulus segmentation with 3D transesophageal echocardiography that did not need any manual input at all. The 3D data was decomposed into a 2D plane set, utilising symmetry around the centerline of the left ventricle, and then predicted the mitral annulus coordinates. The predicted data was then compared with the test data set, producing an error of 2.0 mm with a standard deviation of 1.9 mm. This fully automatic segmentation method has the potential to eliminate manual input and operator variability.

2.8 Statistical shape analysis

Statistical shape analysis is the technique to compute images that plays an important role in biomedical imaging. It offers the tools necessary to construct representative

shapes, quantify shape variations in three dimensions, or relate shape to other measures.

2.8.1 Procrustes analysis

Procrustes analysis is the method of 3D shape analysis used to determine the differences and similarities between two sets of data by using landmarks common to all of the shapes (Niu, Li and Salvendy, 2007). The technique has been further developed by Dryden and Mardia (2016) to compare a shape to a reference shape to assess the mean shape of the data and the variability of that mean shape. In the past, this Procrustes analysis has been used to analyse the shape of the spine, torso, spinal and scoliosis research (Manfreda, Mitteroecker, Bookstein and Schaefer, 2006; Plomp et al., 2015; Dryden, Oxborrow and Dickson, 2008)

2.8.1.1 Generalized Procrustes analysis

The generalised Procrustes analysis (GPA) is a statistical method used to compare three or more shapes of objects and to normalise data to determine the mean shape of the data. The method involves translation to move the centre of mass to the common origin, reflection to reflect across an axis with preserved shapes and sizes, rotation to rotate the shapes around the centre without changing the distance of each point, and scaling to elongate or shrink all points by a constant amount in a straight line from the point to the centre of mass. This superimposition of individual data sets is performed to maximise their agreement (Xiong et al., 2008) which the optimal transformation is the smallest sum of the squared distances among corresponding points in the shapes. The steps of the generalised Procrustes analysis are as follows:

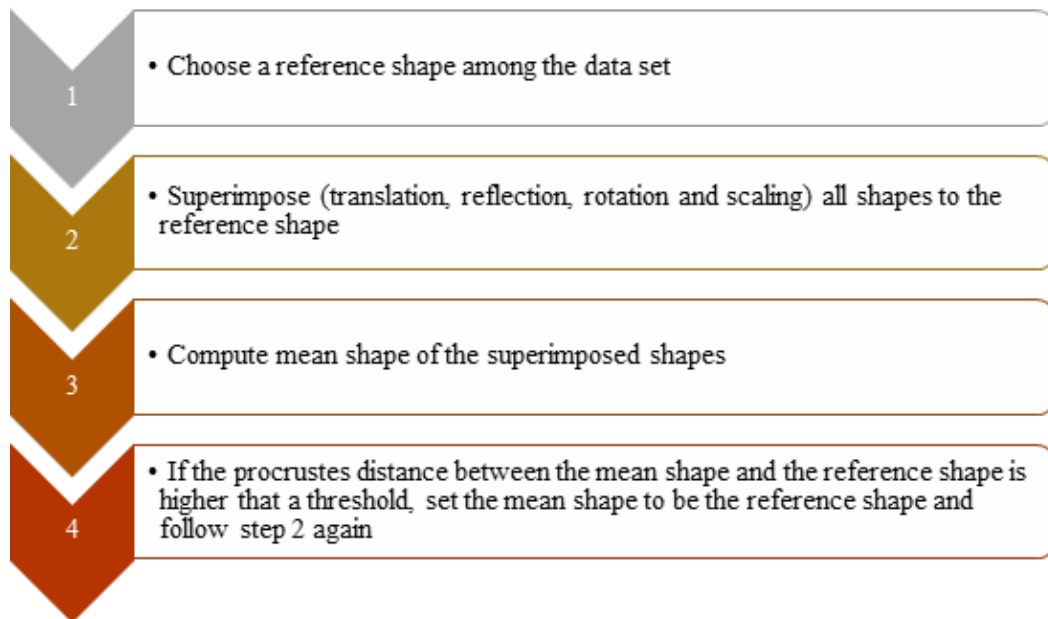


Figure 2.18: Generalised Procrustes analysis steps.

2.8.2 Principal component analysis

Principal component analysis (PCA) is a way to reduce the number of dimensions in data while making it easier to understand and keeping as much information as possible. Whilst many techniques have been developed to decrease the dimensions of the data, principal component analysis remains the most popular one (Jolliffe and Cadima, 2016). In order to be able to characterise the majority of the data variance with fewer dimensions than the actual data, the data must be transformed into a new coordinate system for the principal component analysis to work. In earlier research, the first two principal components, which comprise the top two highest variations of the data, were utilised to draw graphs in two dimensions. This procedure requires computing the principal components.

Chapter 3 Assessment of the mitral valve geometry

A 3:4 ratio of the anteroposterior and transverse diameters of the mitral annulus has been cited by many journals to represent the ratio of a healthy mitral valve. In chapter 2, it was reported that several commercial annuloplasty rings are available in various materials, shapes, and sizes, the majority of them designed based on the 3:4 ratio. However, there is limited evidence to support the ratio. Therefore, this research aimed to investigate the relationship of mitral valve dimensions using physical and digital measurements of cadaveric hearts to determine whether they conformed with the 3:4 ratio of the anteroposterior and transverse diameters of the mitral annulus, whether this ratio should be used to optimise an annuloplasty ring design, whether other mitral valve dimensions should be involved in developing an annuloplasty ring design, and whether a personalised annuloplasty ring should be developed. This chapter comprises three distinct studies. Study 1 examines the variations between different observers and methods to ensure that observers correctly identified the measurement locations before applying this method to cadaveric hearts. Study 2 investigates the dimensions of the mitral valve through cadaveric dissection, while Study 3 focuses on predicting the healthy mitral valve geometry based on the intertrigonal distance.

Methodology

The aim of using an annuloplasty ring for the mitral valve implantation is to let the ring mimic the shape of the healthy mitral annulus, supporting the coaptation of the leaflet to function normally. Therefore, to understand why the 3:4 ratio between the anteroposterior and transverse diameters was used, the dimensions of healthy mitral valves needed to be investigated. Hence, the main challenge in this study was to assess the dimensions of healthy mitral valve. Therefore, it is designed to assess the mitral valve geometry of donated cadavers whose hearts remained undamaged and did not show signs of any heart disease that might affect the shape of the mitral valve.

Before doing the mitral valve measurement from a human heart, a pig heart was tested first to find the recommended measurement methods and to ensure that the observers understood how to cut open the heart and where the measurement landmarks were.

The analysis included an investigation of the measurement methods, the errors found from using them, and the possible causes of errors.

Then the recommended measurement methods were used with cadaveric hearts. The cadavers' chests were already cut open, ready for the researcher to take the heart out. The hearts were taken out one by one, to ensure that they would be returned to the same donor. There were situations where the heart was already taken out and placed in a bag next to the body. Some of these hearts showed signs of distortion during the storage process, so they were excluded from the study. To assess the mitral valve, a transversal incision was made just superior to the valve annulus to give a clear view of its superior surface. Any blood clots and blood-stained tissue found were removed to facilitate observation of the mitral valve. The measurements of the mitral valves anteroposterior and transverse diameters were done manually using a digital callipers. For further 3D analysis of the mitral valve, Fuel 3D Scanify used a hand-held scanner to capture images of the mitral valve from different angles that covered the superior face of the mitral valve. Fuel 3D Scanify, equipped with 3.5 megapixel cameras, uses depth-sensing technologies to gain depth information from multiple images taken. The images were exported to an open-source programme called Meshlab. This software enables the process of stitching together the captured images into a single model. These models were used for the geometrical measurements. The analysis included finding the average dimensions of the anteroposterior and transverse diameters and their ratio in the cadaveric hearts.

In the next phase of this research study, the research objective was to determine the correlation between the intertrigonal distance and the 3:4 ratio of the anteroposterior and transverse diameters of the mitral valve. Since the intertrigonal distance shows no significant dilation in annular degeneration causing mitral regurgitation. Hence, understanding the relationship between the intertrigonal distance and the 3:4 ratio of the anteroposterior and transverse diameters would enable to predict the healthy mitral annular dimensions in anteroposterior and transverse diameters before it has dilated. The analysis was done to find the ratio of the intertrigonal distance between the anteroposterior and transverse diameters and to determine the possibility of using the

trigonal distance to predict the anteroposterior and transverse diameters before dilation.

Study 1 Interobserver and inter-method differences

This study aimed to confirm that the observers realised where the measurement locations were and that they measured at the same places before this method was going to be used with the cadaveric heart. For the mitral valve dimensions measurement, the study was going to measure the transverse diameter and anteroposterior diameter of the mitral valves from a pig heart before it was used to measure them from donated cadavers. The measurements included manual measurement with digital callipers and computer measurement. Therefore, it was important that the two observers, who were going to do the measurement, perform it with accuracy and produce reliable results. Therefore, this study raised awareness of interobserver differences and inter-method differences during the measurement process.

3.1.1 Method

In this experiment, a pig heart was dissected the same way that the cadavers' hearts were going to be dissected in Study 2. The heart was cut just above and below the mitral valve to show the top view of the mitral annulus. To indicate where the measurements took place, the pig heart was coloured with four landmarks along the mitral annulus (Figure 3.1). The four landmarks indicated the landmarks where the anteroposterior and transverse diameters were measured to make sure that the observers measured at the same points. Then the measurements of the anteroposterior and the transverse diameters were done.

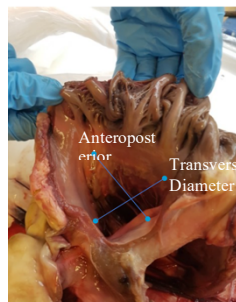


Figure 3.1: The pig heart was dissected to show the mitral annulus and the landmarks.

To study inter-method bias, one manual measurement method and two computer measurement methods were performed. The manual measurement used a digit digital callipers to place on the landmarks, and then the value was recorded. The first computer measurement was performed by using a handheld a scanner "Fuel3D". The Fuel3D Scanify, developed by Fuel3D, is a portable 3D scanner crafted for swiftly capturing high-resolution 3D scans of objects or subjects. It is a portable, handheld device that enables users to move easily around the object they wish to scan. It excels in speed, capable of capturing a 3D scan within seconds, making it ideal for swift scanning needs. It is widely employed for various purposes, including 3D printing, computer-aided design (CAD) [Fuel3D, 2014]. The Fuel3D was used to scan and produce 3D images of the mitral valve from multiple viewpoints to make sure that every angle of the annulus was captured. Then, the 3D images were transferred to Meshlab, an open-source software for processing and editing 3D meshes and preparing models for 3D printing. Meshlab was used to stitch the 3D images together to reconstruct complete 3D images of the mitral valve and to do digital measurement. The stitching process was done in pairs, meaning that two images were selected each time. The first two scan images of the hearts were selected, and around 10 spots of the areas found in both of those images were identified and merged. Therefore, the images were rotated to match each other and transformed into a new image with more details obtained from those two images, ready for the next round of merging. This step was repeated, but instead of using the other two images, the recently merged image was selected and further merged with another image from the stack until all of the images were merged together. On the other hand, the second computer measurement was done by measuring from a single scan that showed all four landmarks and did not require any merging processes between images. These two computer measurement methods were compared to investigate whether the mitral valve dimensions were affected by the scan combining process. The measurements were repeated three times, and the average values were used for the analysis.

3.1.2 Results

Figure 3.2 and Figure 3.3 show the anteroposterior and transverse diameters measured by two observers with three measurement methods: manual measurement, computer measurement with the combined scans and computer measurement with a single scan.

In Figure 3.2, the observers got similar anteroposterior diameters with the differences less than 0.2 mm except for the values measured from the combined scan image which sharply dropped and produced a higher variation around 0.9 mm. In comparison, the measurement taken from a single scan provided the dimensions closer to the manual measurement than that from a combined scan.

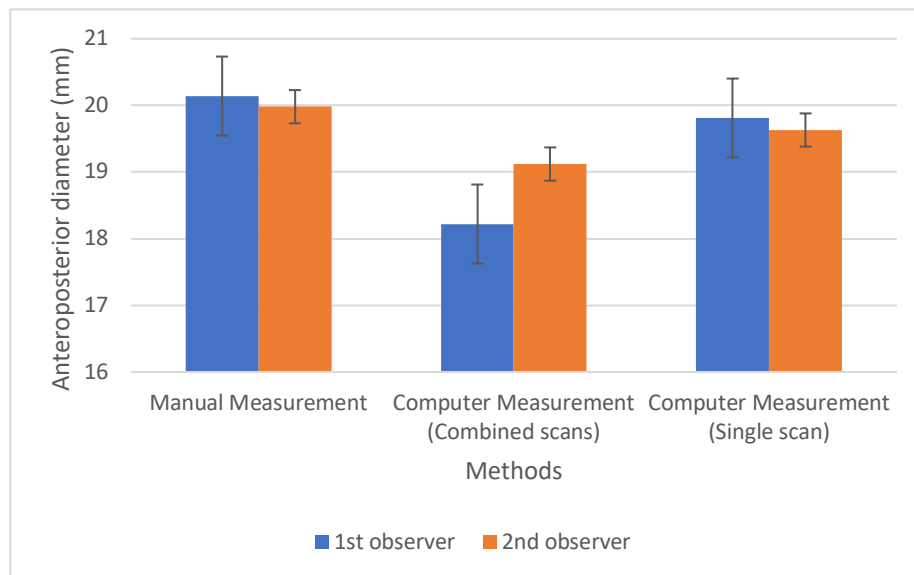


Figure 3.2: The comparison of the anteroposterior diameter performed by two observers with three measurement methods with the error bars show the standard error of the mean, measuring the variability between sample means.

Figure 3.3 shows that the computer measurement with a single scan produced the least variation among the observers which was about 0.1 mm while the other two methods had similar interobserver bias of 0.4 mm

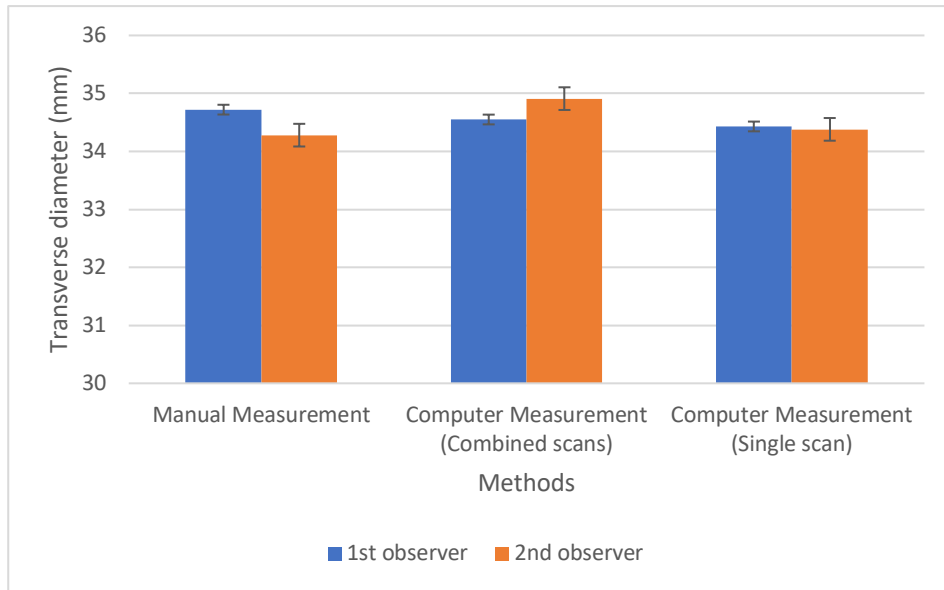


Figure 3.3: The comparison of the transverse diameter performed by two observers with three measurement methods.

3.1.3 Discussion

For the interobserver study, the mean differences in mitral valve dimension measured by the two observers were 0.3 mm by manual measurement, 0.6 mm by computer measurement with a combined scan, and 0.1 mm with a single scan. However, the paired t-tests showed no significant difference found between two observers with the P-values equal to 0.63 and 0.58 for anteroposterior and transverse diameter measurements respectively.

For the inter-method study, the experiment showed that the results measured from a single scan were better than those measured from a combined scan because the values were closer to the ones measured manually. The possible cause was that a combined scan might gradually add up errors during the combining processes and shift the landmark locations, while a single photo did not need any combining processes and showed the original landmark locations. The standard variations found from the three methods were 0.2 mm, 0.4 mm, and 0.1 mm for manual measurement, computer measurement with a combined scan, and computer measurement with a single scan. In addition, the one-way ANOVA was tested to compare between the three group means of manual measurement, computer measurement with a combined scan, and

computer measurement with a single scan. The results showed a P-value of 0.07, which was higher than the significance level of 0.05, meaning that the sample data provided strong evidence to conclude that there were no significant differences between those methods.

This section demonstrated that the two observers were capable of doing the three types of measurements and gave the results with no significant differences between them. For the measurement method, the results presented no significant differences between the three methods. Hence, all of them can be used for the mitral valve measurement. In addition, those methods had different benefits. The manual measurement was better than the other methods at identifying the annulus since it allowed the observers to touch and examine the annular area, easier for the measurement. To compare between the two computer measurement methods, the method that measured with a single scan did not require images merging steps, so it produced less error, but the drawback was that it could be used only with an image that captured all the measuring landmarks. Nevertheless, because of the complexity of the mitral valve with its saddle shape, it was hard to take a picture that showed all the landmarks, and parts of the mitral valve that could be missing from the image, making it harder for the observers to identify where the annulus was compared to a combined image. Meanwhile, the computer measurement with a combined image, which needed additional steps to merge images and form a three-dimensional model of the whole mitral valve area, was better at observing the mitral annular area since it allowed the observers to tilt the model to identify the measuring landmarks without interfering with the shape of the mitral valve, which was not rigid. For that reason, the recommended methods to use for cadaveric heart measurement were manual measurement and computer measurement with a combined scan.

The limitation was that the nail polish did not stain on the pig heart and could slide or fade away when touched with callipers.

Study 2 Relationships of mitral valve dimensions from cadaver dissection

This section was planned to study the relationship of the healthy mitral valve in terms of whether the dimensions between the anteroposterior and transverse diameters conformed to a 3:4 ratio. In order to study the geometry of the healthy mitral valve, cadaver dissection was selected instead of investigating patient scan data because the data mostly comes from patients with heart diseases, heart valve problems, and cardiac implanted devices that could possibly affect the healthy mitral valve dimensions. Also, this cadaver dissection was done together with a research student at the Queen's Medical Centre, University of Nottingham.

3.2.1 Method

Thirty-nine human hearts were collected from donated cadavers who allowed photography. The procedure started by opening the already dissected cadaver's thorax to take out the heart. The hearts were then placed on a table, ready for dissection. Then, the collected hearts were cut just above and below the mitral valve [Figure 3.4] in such a way that they remained flat and could sit properly, showing the top view of the mitral valve.

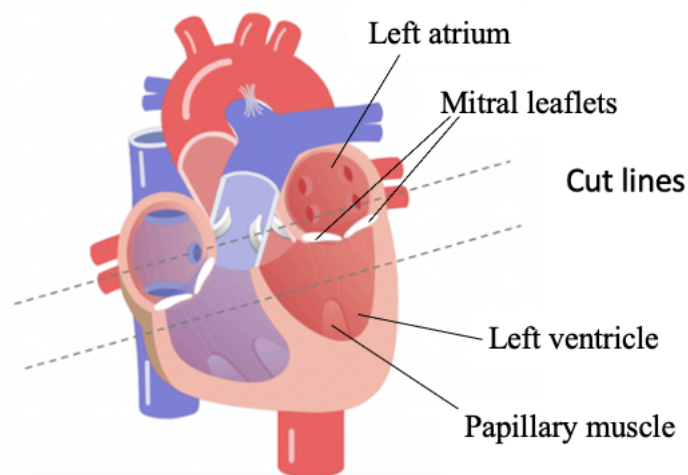


Figure 3.4: The heart with the cut directions shown as the dash lines (Phase of the cardiac cycle, 2019).

In this study, only the hearts that their mitral valve did not show significant damage or distortion were included in statistical analysis. Examples of hearts that were excluded from this study are shown in

Figure 3.5.

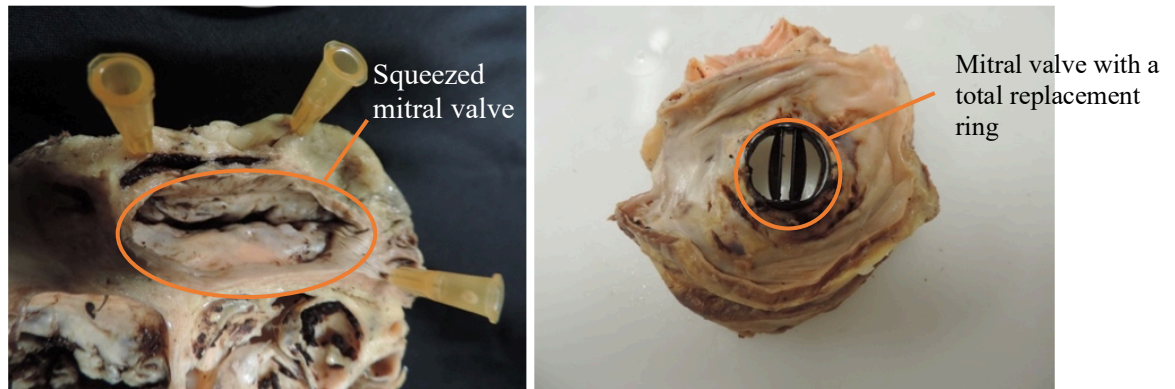


Figure 3.5: The mitral valves were excluded from the experiment because one was squeezed from storage (left) and another one had a total valve replacement ring (right) which alter the natural shape of the mitral annulus

Next, the measurement took place, where the transverse and anteroposterior dimensions of the mitral valve annulus were measured manually with digital callipers. For the computer measurement, it followed the same process used in Study 1, in which the Fuel3D software equipped with a handheld 3D scanner was used to scan and produce 3D images of the mitral valve from multiple viewpoints. Then, the Meshlab, an open-source, and versatile system designed for the manipulation and editing of unstructured 3D triangular meshes, was used to stitch the 3D images together to reconstruct the completed 3D images [Figure 3.6 and Figure 3.7] of the mitral valve and to do digital measurement.



Figure 3.6: The 3D model of a cadaveric heart clearly showed the mitral valve dimension.



Figure 3.7: The comparison between the 2D image (left) taken with a digital camera and the 3D image reconstructed using the MeshLab software.

After the 3D models of the heart were formed, showing the complete shape of the mitral annulus, the MeshLab software provided the measurement tool to quantify the anteroposterior and the transverse diameters of the mitral annulus.

For the measurement, the dimensions were measured twice for both manual and computer measurements by two observers whereas the average value were used for the analysis. The anteroposterior is the distance across the mitral valve, starting from the center of the anterior annulus to the center of the posterior annulus. While the transverse diameter or the intercommissural distance is the distance between the mitral annulus along the anterior and posterior commissures that perpendicular to the anteroposterior diameter [Figure 3.8]

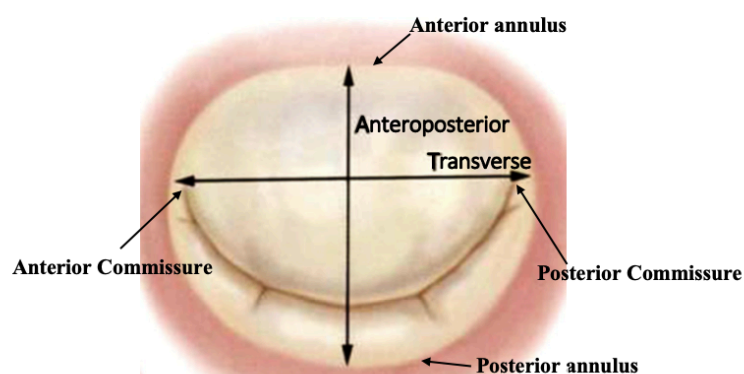


Figure 3.8: The landmarks of the mitral valve showing the anteroposterior and transverse diameters (Carpentier et al., 2010).

For the statistical analysis, this study applied the regression method to determine the connection between a dependent variable and one independent variable. This is achieved by establishing a linear equation that fits the observed data, with the objective of minimizing the sum of squared differences between the actual values and those predicted by the linear model. Moreover, the hypothesis testing with paired t-test was used to for comparing means between two measurement methods. Its primary objective was to assess whether the mean difference between paired observations exhibits a significant departure from zero.

3.2.2 Results

For the cadaver dissection, thirty-nine human hearts were collected, but only thirty-four hearts qualified as suitable for use. Three hearts were excluded as the mitral valves were damaged or squeezed from being placed at the bottom of an organ bag. Another one was excluded because it had mitral valve replacement surgery with a circular total valve replacement ring that directly distorted the actual shape of the mitral annulus. A blood-stained mitral valve was also excluded from the measurement as the 3D model was too dark to indicate where the mitral annulus was. This was because the mitral valve was stained with blood and visibly showed a dark brown colour even after light adjustment [Figure 3.9].

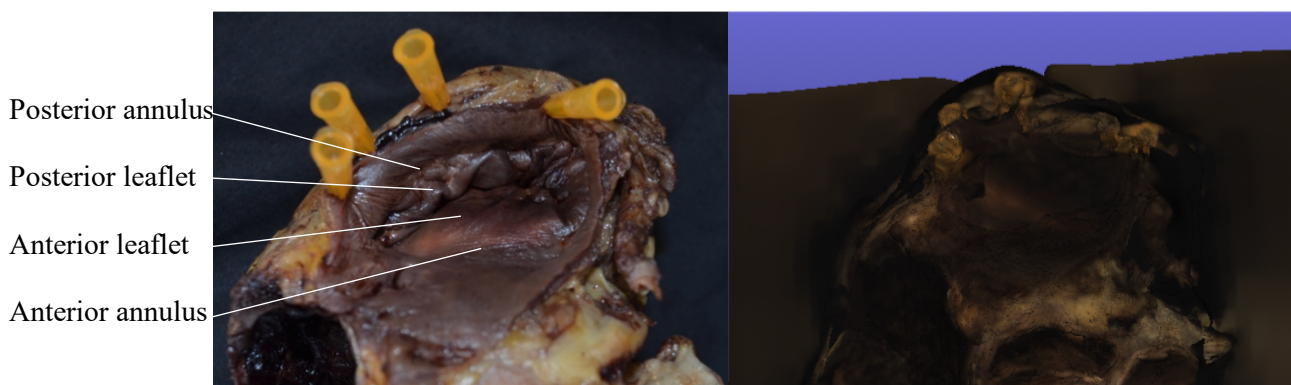


Figure 3.9: In one heart, the mitral valve was stained (left), then, the 3D model that was created in the MeshLab (right) was too dark to see the annulus.

The relationship between anteroposterior and transverse diameters, measured manually with callipers, is shown in Figure 3.10. Whilst the linear fit gives a ratio of 3:3.9, a ratio of 3:4.0 falls comfortably within the 95% confidence intervals of the gradient. The R^2 of 0.51 indicates that around 48% of the variation is not explained by the linear fit. Indeed, many individual annuli had an aspect ratio very different from 3:4 with more than half of cases falling outside the 95% confidence limits of the linear fit.

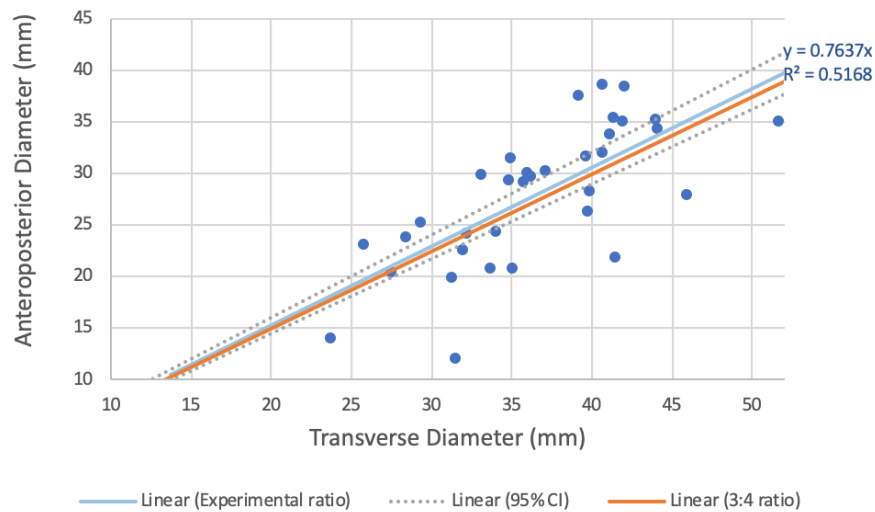


Figure 3.10: Mitral valve dimensions by manual measurement with the average ratio between the anteroposterior and transverse diameters = 3:3.9.

Figure 3.11 shows the average ratio between the anteroposterior and transverse diameters by computer measurement. The linear fit shows a ratio of 3:4.0, which was very close to and supported the 3:4 ratio between the anteroposterior and transverse dimensions of the mitral valve. However, the R^2 of 0.46 means that around 54% of the variation of the data cannot be explained by the linear fit. Moreover, as the found from manual measurement in Figure 3.10, more than half of the annuli were different from 3:4 with more than half of them falling outside the 95% confidence interval of the linear fit, showing high variation among individuals.

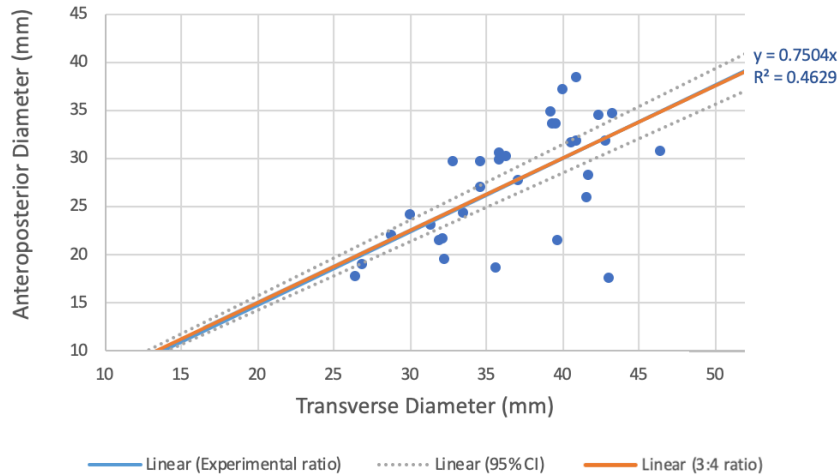


Figure 3.11: Mitral valve dimensions by computer measurement with the average ratio between the anteroposterior and transverse diameters = 3:4.0.

To compare two measurement methods, the manual measurement data were compared with the data of the computer measurement as shown in Table 1. It shows that the average anteroposterior diameter difference is 0.9 mm with a P value of 0.057, while the mean value of the differences in transverse diameter is 0.3 mm with a P-value of 0.299. These P-values are higher than 0.05, which means that the null hypothesis cannot be rejected and there is no significant difference in the data measured by manual and computer measurements.

Table 1 Statistics for relative biases for intermethod of measuring the mitral valve dimensions by manual and computer measurement. Negative bias indicates larger value by manual measurement versus computer measurement.

Dimension	Intermethod bias				
	Minimum (mm)	Maximum (mm)	Mean (mm)	SD	P-value
Anteroposterior diameter	-1.7	4.9	0.9	1.9	0.057
Transverse diameter	-1.8	2.8	0.3	1.2	0.299

3.2.3 Discussion

The results represented by the thirty-four human hearts produced equations with low R^2 values which means that the data points did not really fall on the fitted regression line and the majority of the data was outside the 95% confidence interval. Nevertheless, the average ratio between the anteroposterior and transverse diameters was 3:3.9 by manual measurement and 3:4.0 by computer measurement which was almost equal to the expected 3:4 ratio.

The residuals plot in Figure 3.12 and Figure 3.13 demonstrates the error between the predicted dimensions of the transverse diameters, predicted from the 3:4 ratio, and the measured transverse diameter from manual and computer measurements, respectively. The residuals appear to be randomly distributed around zero, which does not contradict the linear assumption. The mean absolute residual of the predicted transverse diameters is 4.7 mm for manual measurement and 4.1 mm for computer measurement. The residual plots show that with increasing diameter, the mitral annulus was getting more circular. In addition, the paired t-test has been done and proved that there was no significant difference among the predicted dimensions of the transverse diameter predicted from the ratio.

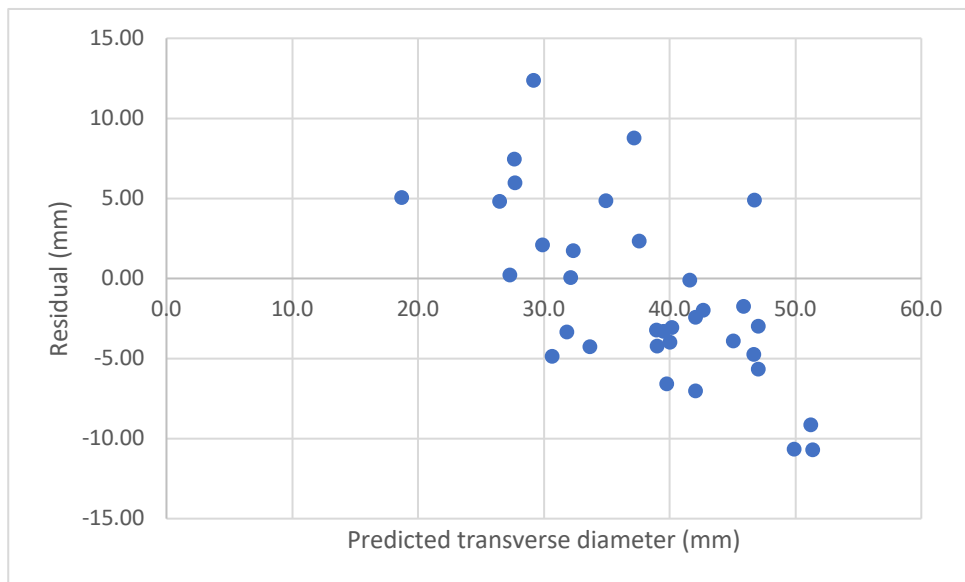


Figure 3.12: The residuals plot of the error between the predicted dimension from 3:4 ratio and the measurement dimensions of transverse diameter found from manual measurement.

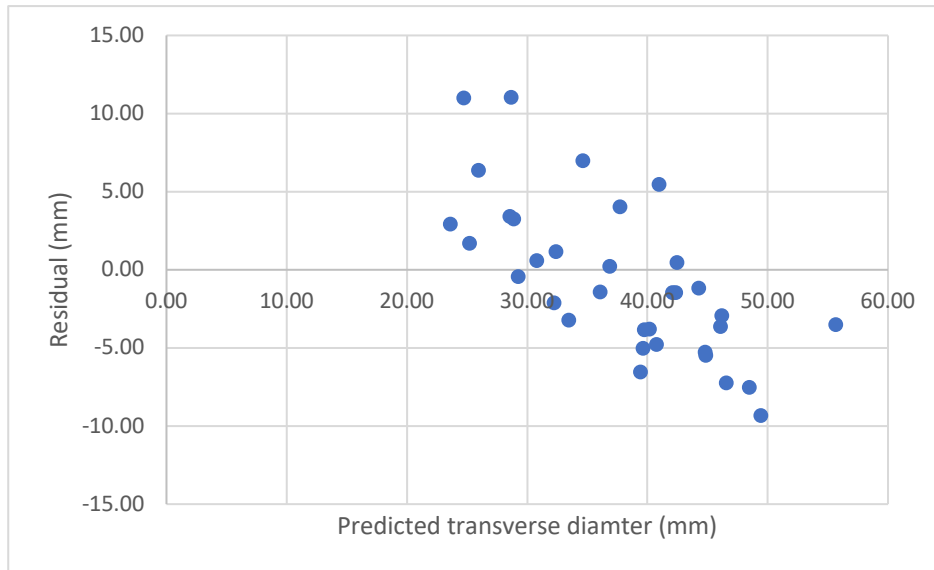


Figure 3.13: The residuals plot of the error between the predicted dimension from 3:4 ratio and the measurement dimensions of transverse diameter found from computer measurement.

This has demonstrated that the average dimension of the healthy mitral valve from the donated cadavers conformed to the 3:4 ratio between the anteroposterior and transverse diameters which is the ratio that is commonly stated and used for commercial annuloplasty rings. Nevertheless, individual dimensions were highly variable, indicating that a personalised annuloplasty ring should be considered as an alternative to standard sized commercial rings.

Two measurement methods were used to measure the mitral valve. The results have shown that both are able to measure the mitral valve with no significant difference in the measurements but with different skills and processes needed. The manual measurement with callipers allows the researcher to touch and examine the landmark area during the measurement. Sometimes, even when looking at the real heart, the annulus was not clearly recognised and required manual examination of the point where the leaflets met the annulus before the manual measurement could be taken. This supports the accuracy of the measurement. Meanwhile, the computer measurement requires some computer skills to reconstruct and measure the 3D model. The computer measurement needs MeshLab to form the 3D model of the mitral valve with fine detail. In some cases, the quality of the model is not good enough to make the mitral annulus clearly visible. For instance, there was a case when the heart was

stained with blood and visibly showed a dark brown colour. This made it harder to locate the mitral annulus, leading to some errors in computer measurement. As a result, this heart was excluded from the experiment.

Study 3 Prediction of healthy mitral valve geometry from intertrigonal distance

In Study 2, the dimensions of the healthy mitral valves were considered, which showed that the average ratio between the anteroposterior and transverse diameters of the healthy mitral valve conforms to the 3:4 ratio. The ratio is currently used in off-the-shelf implant sizing. This means that it might be possible to use a single measurement and a ratio to calculate the second. Although even within a healthy valve population there were considerable individual differences away from that ratio. Nevertheless, in degenerative diseases of the mitral valve, and particularly during dilation, these anteroposterior and transverse diameters change. Therefore, it would be better to base sizing on a parameter that does not change much. Still, there are the left and right trigones that are situated at the junction of the left fibrous borders of the mitral valve and aortic valve Figure 3.14

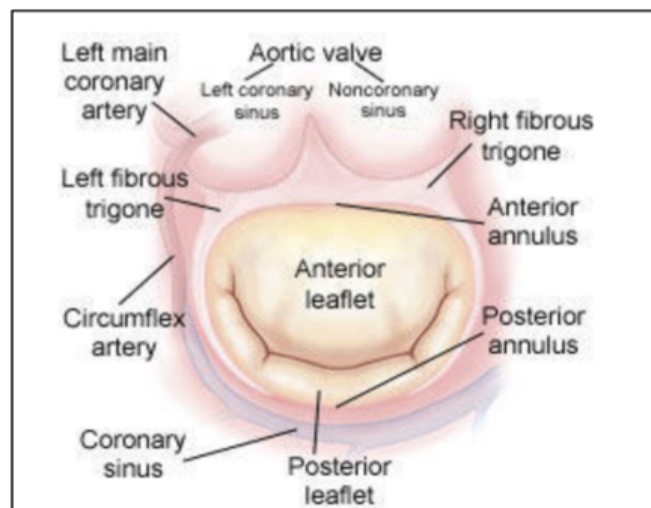


Figure 3.14: Diagram showing the mitral valve and the fibrous trigones (Pick, 2020).

It was believed trigones could not dilate for many years until recent studies proved that trigones could dilate but are less prone to dilate, resulting in an intertrigonal

distance that showed the least percentage change and does not significantly change during the cardiac cycle for both normal and regurgitant mitral valves (Jeganathan et al., 2016). Based on these findings, if the anatomical association between the intertrigonal distance, anteroposterior and transverse diameters are found, it can be hypothesised that the intertrigonal distance in patients with dilated mitral valves can be used to determine the actual dimensions of the anteroposterior and transverse diameters before dilation and is suitable to be the parameter for determining the annuloplasty ring size. Thus, based on this hypothesis, annuloplasty ring sizing can be done pre-operatively by determining the intertrigonal distance from the patient's echocardiography.

3.3.1 Method

To determine the correlation between intertrigonal distance, anteroposterior and transverse diameters of normal mitral valve, the donated cadavers' hearts were dissected to show the mitral valve and to be ready for the investigation.

Same as the method used in Study 2, the Fuel3D software equipped with a handheld 3D scanner was used to scan and capture 3D images of the mitral valves from multiple viewpoints. The 3D images were transferred to MeshLab where they were stitched together to reconstruct a completed 3D model of the mitral valve and surrounding tissues. Thirty-four heart models that showed no damage or distortion were included in the study. Then, the intertrigonal distance, anteroposterior diameter, and transverse diameter were measured and analysed [Figure 3.15]

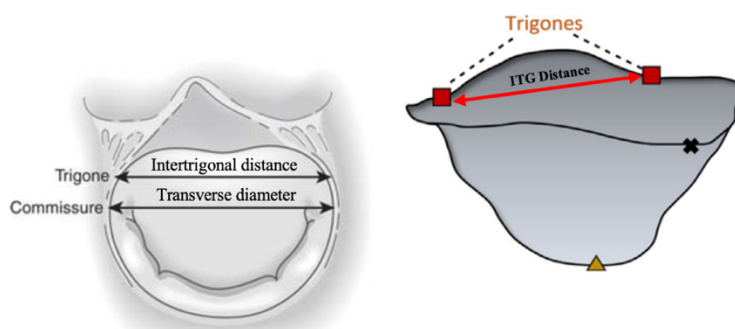


Figure 3.15: The mitral valve shows the intertrigonal distance (ITG) where the anterior leaflet attached to the fibrous skeleton between trigones (Carpentier et al., 2010, Oliveira et al., 2020).

The data obtained from the geometry measurement underwent analysis using linear regression to identify the fitted line representing the dimension relationships among the three diameters. Once the regression models were determined, the ratio between the intertrigonal distance, anteroposterior, and transverse diameters could be established. This ratio was subsequently tested using statistical analysis, specifically a paired t-test, to investigate the dimension differences between the actual measurements and the predicted dimensions derived from the ratio. In addition, the residual plot was also used to depict the differences between observed values and the predicted values from the ratio.

3.3.2 Results

The relationship between the intertrigonal distance and anteroposterior diameter is shown in Figure 3.16. The fitted line shows a ratio of 3.4: 3.0 between intertrigonal distance and anteroposterior diameter. The R^2 of 0.99 indicates that more than 99% of the data can be explained by the ratio which is greater than the R^2 found from determining the relationship between anteroposterior and transverse diameters in Figure 3.10 and Figure 3.11. Still, there is wide individual variation of measurement around this relationship with some of the data falling outside the 95% confidence interval. In addition, the ratio was tested with a paired t-test and shows there is no significant difference between the predicted value of anteroposterior diameter from the ratio and the measured value from computer measurement ($p = 0.43$).

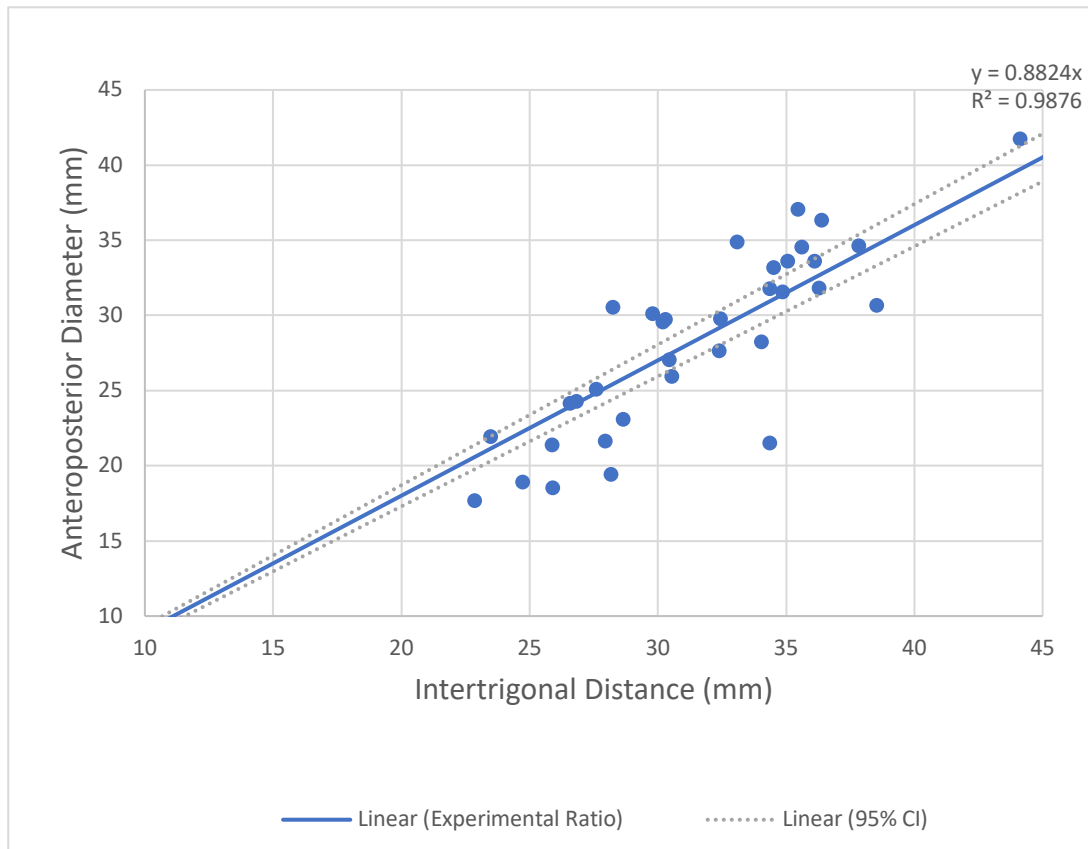


Figure 3.16: Plot of the intertrigonal distance and anteroposterior diameters of thirty-four cadavers. The solid line represents a line of fit to the data presented ($y=0.8824x$, $R^2 = 0.9876$).

The relationship between the intertrigonal distance and transverse diameter is shown in Figure 3.17. The fitted line $y = 1.174x$ results in the average ratio of 3.4: 4.0 between intertrigonal distance and transverse diameter. The data produces $R^2 = 0.99$, meaning that more than 99% of the data can be predicted by the ratio. The ratio has been tested with a paired t-test. The statistical test shows no significant difference between the predicted transverse diameter from the ratio with the measured intertrigonal distance and the computer measurement of transverse diameter ($p = 0.91$).

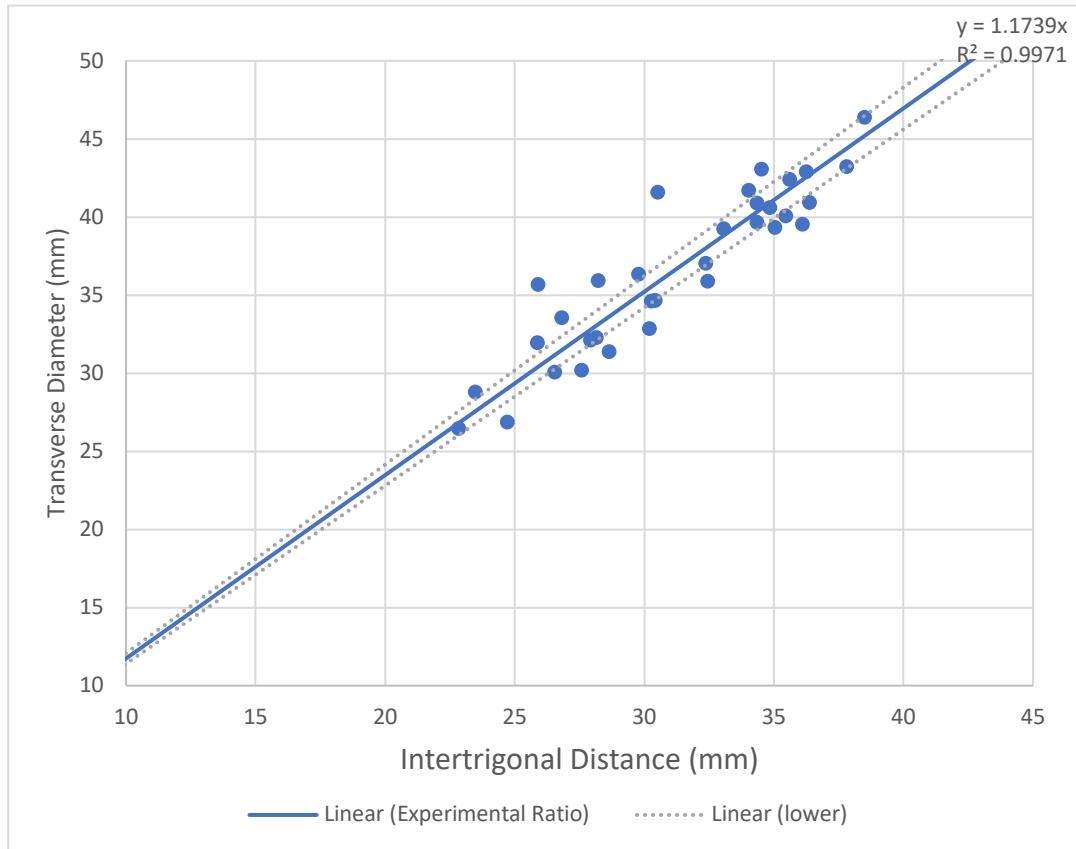


Figure 3.17: Plot of the intertrigonal distance and transverse diameters of thirty-four cadavers. The solid line represents a line of fit to the data presented ($y=1.1739x$, $R^2 = 0.9971$).

3.3.3 Discussion

The residuals plot in Figure 3.18 demonstrates the error between the predicted dimensions and the measurement dimensions of the anteroposterior and transverse diameters. The residuals appear to be randomly distributed around zero. Therefore, the random scatter residuals do not contradict the linear assumption.

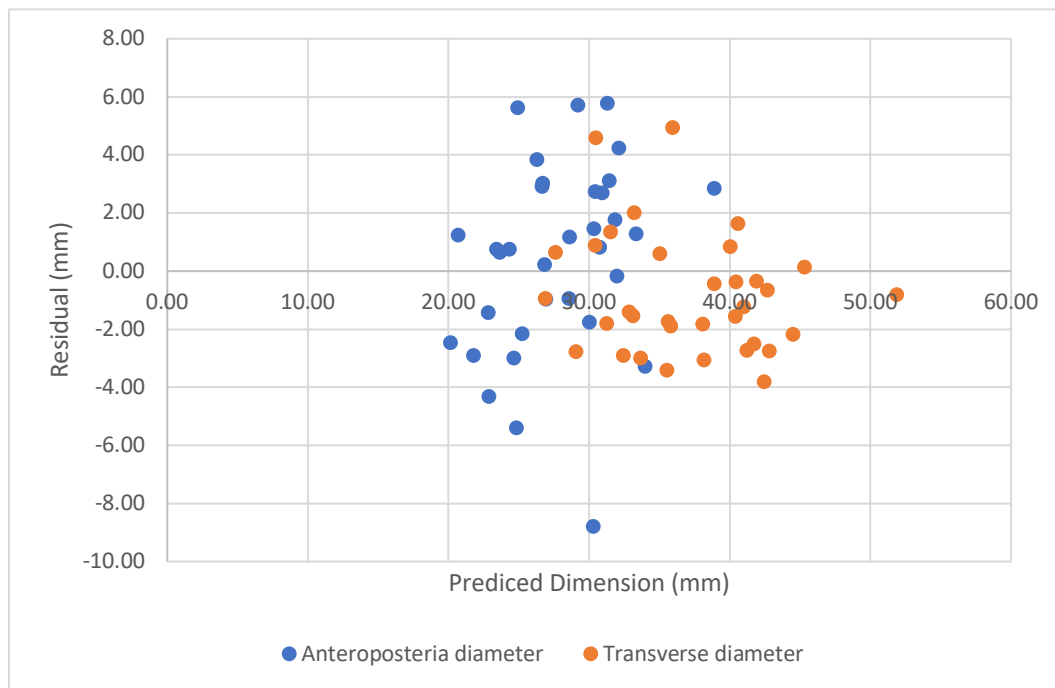


Figure 3.18: The residuals plot of the error between the predicted dimensions and the measurement dimensions of the anteroposterior and transverse diameters.

The previous section has shown that average mitral valves have a 3:4 ratio between the anteroposterior and transverse diameters, while this study shows a positive relationship when using the intertrigonal distance to predict the anteroposterior and transverse diameters. Whilst a 3.4:3:4 relationship between the intertrigonal distance, anteroposterior diameter, and transverse diameter of the healthy mitral valves has been found in this data, the spread of data that lies outside the 95% confidence interval shows that they all do not fit the relationship. The R^2 value of the regression lines shows that around 99% of the data can be explained by the 3.4:3:4 ratio, whereas the mean absolute residual of the predicted anteroposterior and transverse diameters is 2.7 mm and 1.6 mm, respectively. In addition, the paired t-test has been done and proved that there was no significant difference among the predicted dimensions of the anteroposterior and transverse diameters from the ratio. Still, in healthy valves, intertrigonal distance is fairly poor at predicting anteroposterior diameter but good at predicting transverse diameter. Then, a more sophisticated method of characterising annulus shape is needed, such as the statistical shape modelling analysis that was presented in Chapter 5 Study 2.

Conclusion

This research first demonstrated the appropriate methods for taking the mitral valve measurement. When three methods were considered: manual measurement, computer measurement with a single scan, and computer measurement with a combined scan, the appropriate ones were the manual measurement and the computer measurement with a combined scan. The manual measurement with callipers has provided more accuracy and made it easier to collect the data as the valves could be clearly visible and examined. Although the research found no significant difference in results among the three methods. Meanwhile, the computer measurement with a combined scan required more processing steps and skills and was more time-consuming. This method was beneficial in that it allowed the observers to rotate the three-dimensional models, obtained from the combined image, without interfering with the shape of the mitral valves since it did not allow the researcher to physically interact with a highly deformable object, avoiding distortion during measurement.

The research used the recommended measurement methods to show that the average dimension of the healthy mitral valves from the donated cadavers conformed to the 3:4 ratio between the anteroposterior and transverse diameters. Moreover, the relationship between the intertrigonal distance, anteroposterior, and transverse diameters is the 3.4:3:4 ratio. Since the intertrigonal distance is known to change very little throughout the cardiac cycle, it can be used to predict the anteroposterior and transverse diameters of the healthy mitral valves before dilation for the patients who have mitral regurgitation and are suitable for predicting the annuloplasty ring size that best fits each patient.

Although the ratio can be used to represent the average healthy mitral valve dimensions, individual dimensions were highly variable, suggesting that a personalised annuloplasty ring should be considered as an alternative to commercial rings, especially for those whose mitral valve dimensions differ from the average value. Personalised annuloplasty ring is the ring that specifically designed and manufactured for an individual patient based on their unique cardiac anatomy. The decision to consider a personalised annuloplasty ring in mitral valve repair surgeries arises in various scenarios that prioritize tailoring treatments to individual patients.

One key determinant is the patient's unique mitral valve anatomy, where significant variations or deviations from standard dimensions may prompt the exploration of a personalised solution. The primary goal is to optimize the outcomes of mitral valve repair, especially in cases where individualized approaches could contribute to improved valve function and enhance long-term surgical results. Personalised annuloplasty rings become a consideration when mitigating potential complications is crucial, offering a tailored approach to reduce risks associated with using standard commercial rings. This approach is particularly relevant in challenging cases where the patient's mitral valve condition poses specific difficulties not adequately addressed by commercial rings. Additionally, ongoing research and advancements in the field continually refine the criteria for considering and implementing personalised annuloplasty rings. This led to Chapter 5, which studied the process of designing a personalised annuloplasty ring from patients' medical data.

Chapter 4 Annuloplasty ring sizing from intertrigonal distance

Choosing the suitable ring size remains critical since the implantation of an improper downsized ring affects long-term outcomes and repair durability (Ohno et al., 2019). Normally, surgeons play an important role in choosing the ring size during the operation with direct vision based on their experience, preference, and background training (Ferrao de Oliveira, 2006) because there is no sufficient scientific justification for the optimal ring choice to fit patients with different anatomies and pathologies. Also, there is insufficient scientific justification to show the correlation between the strategies and to prove which one should be the standard to optimise the degrees of undersized rings. Intertrigonal distance was proved to less prone to dilate does not significantly change its size during the cardiac cycle for both normal and regurgitant mitral valves (Jeganathan et al., 2016). Therefore, this study was designed to study the relationship between the geometry of the available commercial rings and the mitral valves when the rings were selected with an intertrigonal distance strategy. This led to an investigation into whether the sizes of the commercial rings could replicate the healthy mitral valve size and whether a personalised annuloplasty ring should be implemented. Chapter 4 comprises two studies. Study 1 explores the relationship between the dimensions of a healthy mitral valve and the sizing of ring geometry using the intertrigonal distance strategy. Study 2 determines the appropriate degree of undersizing for an annuloplasty ring to fit the mitral valve.

Methodology

To implant an annuloplasty ring, selecting the appropriate ring size is very important. The ideal size of the ring is that which best replicates the original size of the mitral annulus before it dilated due to the mitral regurgitation. Since there are many sizing strategies mentioned in the literature review in Chapter 2, none of them has been standardised as an ideal method, and the choice of ring size depends on the surgeons

during the operation. This study has been designed to investigate the sizing strategy from intertrigonal distance used to select the commercial off-the-shelf annuloplasty rings, Medtronic 3D Profile (3DP), St. Jude Medical (SJM) rigid-saddle shape ring (RSA), and the Carpentier-Edwards Physio annuloplasty ring, to investigate whether these commercial rings presented the same dimensions as the healthy mitral valve dimensions when they were selected based on intertrigonal distance. In addition, down-sizing ring might be selected in order to lower the dimension differences between the commercial rings and the healthy mitral valve. The outcome was to propose the commercial ring that best fit the healthy mitral valve and to support whether the use of a personalised annuloplasty ring was needed.

Study 1 The correlation between the healthy mitral valve dimensions and ring geometry sizing from intertrigonal distance strategy

One strategy that has been suggested is sizing from the intertrigonal distance because the trigones do not significantly dilate in patients with mitral regurgitation. In order to investigate whether sizing from the intertrigonal distance can select the ring that best fits the geometry of the healthy mitral valve or not, this study assessed the commercial annuloplasty rings that were sized from the intertrigonal distance and compared the different recommended ring geometries to the healthy mitral valve geometry obtained from cadaveric dissection.

4.1.1 Method

To study the correlation between the healthy mitral valve dimensions and the ring geometry, which the rings were sized using the intertrigonal distance strategy, the mitral valve geometry was measured from the 34 donated cadaveric hearts, the hearts that were dissected in Chapter 3. The measurement took place to measure the intertrigonal distance, transverse diameter, and anteroposterior diameter of the mitral valve. After that, the commercial ring size was determined by matching the intertrigonal distance (N-N) of the commercial ring sizers to the intertrigonal distance of the mitral valve. The commercial annuloplasty rings that were used in this study

were the Medtronic 3D Profile (MDT 3DP) in size 24–40 mm, the St. Jude Medical (SJM) rigid–saddle shape ring (RSA) in size 24–34 mm, and the Carpentier-Edwards Physio annuloplasty ring in size 24–40 mm [Figure 4.1]. Furthermore, the commercial ring sizes that were selected were compared to the cadaveric mitral valve geometry. This led to showing the geometry differences between the rings and the healthy mitral valves when the rings were selected with the intertrigonal distance.

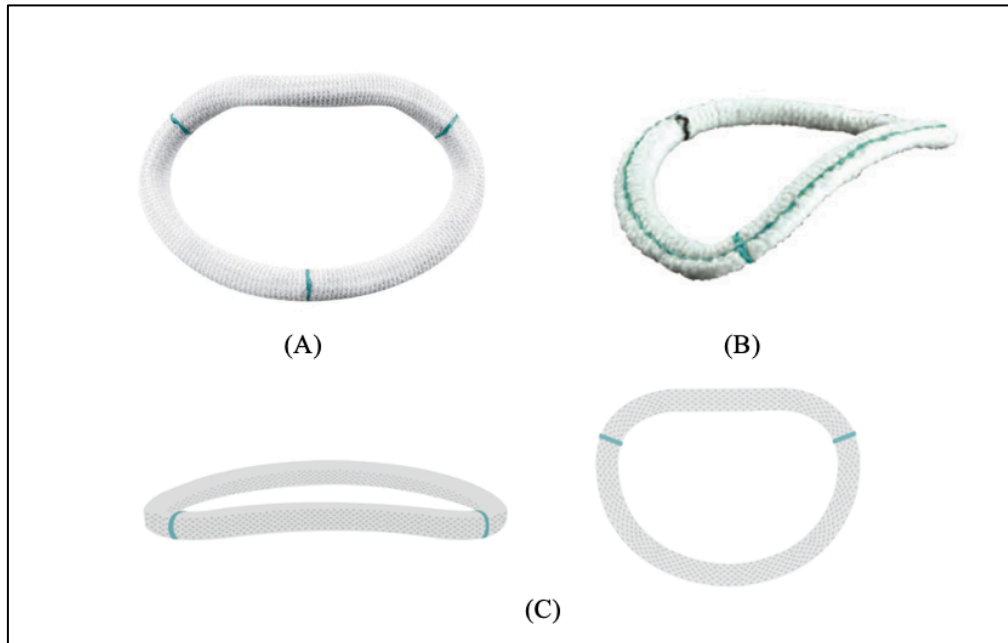


Figure 4.1: (A) Medtronic 3D Profile ring (Medtronic, 2021) (B) St. Jude Medical (SJM) rigid-saddle shape (RSA) (SJM™ Rigid Saddle Ring, 2013) (C) Carpentier-Edwards Physio annuloplasty ring (Edwards Lifesciences, 2021).

Table 2 presents the size label and the true dimensions of the three annuloplasty rings. This table was used for matching the different dimensions of the ring sizer to those of the mitral valve of each patient [Figure 4.2]. Annuloplasty ring sizer refers to a tool utilized to ascertain the appropriate size for an annuloplasty ring. The sizer assists surgeons in measuring and evaluating the dimensions of the mitral annulus, enabling them to select the most suitable annuloplasty ring size for a specific patient. The process of utilizing an annuloplasty ring sizer in mitral valve repair surgeries involves a systematic approach to determine the most suitable ring size. Subsequently, precise measurements of the mitral annulus, considering factors such as transverse diameter,

anteroposterior diameter, and intertrigonal distance, are conducted using the chosen sizer. Comparisons between obtained measurements and available sizing options guide the selection of the optimal ring size. Whilst the Carpentier-Edwards Physio ring and the Medtronic 3D Profile have a size variation of 24–40 mm, the St. Jude Medical ring has a smaller size range of 24-34 mm

Table 2: Size label and the true dimensions of the annuloplasty rings and sizers: the Carpentier-Edwards Physio annuloplasty ring, the St. Jude Medical (SJM) rigid- saddle shape ring (RSA) and the Medtronic 3D Profile (Bothe, Miller and Doenst, 2013).

Size label	Carpentier-Edwards Physio ring(24-40mm)						St.Judde Medical (SJM) rigid- saddle shape (RSA)(24-34mm)						Medtronic 3D profile (MDT 3DP)(24-40 mm)					
	Sizer diameters (mm)			Ring diameters (mm)			Sizer diameters (mm)			Ring diameters (mm)			Sizer diameters (mm)			Ring diameters (mm)		
	anteroposterior	transverse	Intertrigonal	anteroposterior	transverse	AP:T ratio	anteroposterior	transverse	Intertrigonal	anteroposterior	transverse	AP:T ratio	anteroposterior	transverse	Intertrigonal	anteroposterior	transverse	AP:T ratio
24	18.1	27.1	22	20.4	27.3	3:4	15.8	24.8	20.5	21.5	29.3	3:4	16.4	27.2	21.3	20.6	30.4	3:4.5
26	19.2	29	23.6	21.9	29.4	3:4	17.1	26.8	22.2	22.3	31.3	3:4.2	17.5	29.3	23.2	20.4	30.4	3:4.5
28	20.4	31	24.7	23.7	32.4	3:4	18.7	28.9	23.9	23.6	33.3	3:4.2	18.6	31.3	25.1	22.7	34.4	3:4.5
30	21.6	33	29.2	25	34.3	3:4	20	30.8	25.9	25.5	35.5	3:4.2	19.8	33.3	27	24.1	36.2	3:4.5
32	22.8	35	29.1	26.2	36.3	3:4.2	21.4	32.9	27.9	26.5	36.9	3:4.2	20.8	35.3	28.9	23.6	36.9	3:4.5
34	24.1	37	32.8	28.4	38.6	3:4	22.8	34.9	29.5	27.8	38.9	3:4.2	21.9	37.2	30.1	24.8	38.7	3:4.5
36	25	38.9	32.7	29.6	40.9	3:4.2							22.9	39.3	32.6	25.8	40.6	3:4.8
38	25.8	41	34.8	31.1	43	3:4.2							23.9	41.4	34.4	27.7	44.5	3:4.8
40	27.8	43	36.4	32.9	44.8	3:4							25.1	43.4	36.3	27.5	44.6	3:4.8

*AP:T ratio is the ratio between anteroposterior and transverse diameter

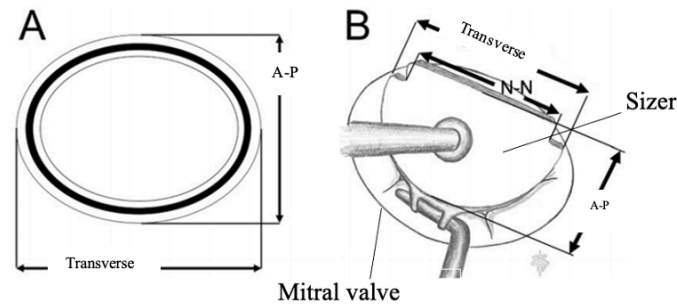


Figure 4.2: The assessment of anteroposterior (A-P), transverse diameter, and intertrigonal distance(N-N) dimensions for intertrigonal distance in (A) annuloplasty rings (B) sizers. (Bothe, Miller and Doenst, 2013)

4.1.2 Results

The results indicated the selected ring sizes of the three annuloplasty ring types: Carpentier-Edwards Physio ring (24-40mm), St. Jude Medical (SJM) rigid- saddle shape (RSA) (24-34mm), and Medtronic 3D Profile (MDT 3DP) (24-40 mm). For those mitral valves with dimensions greater or smaller than the commercial rings, the biggest and the smallest available size was selected respectively.

The comparison between the transverse diameters of the healthy mitral valves and those of the Carpentier-Edwards Physio ring, the St. Jude Medical ring and the Medtronic 3D Profile ring are shown in Figure 4.3, Figure 4.4 and Figure 4.5. They show that the healthy mitral valve has a trend line lower than the trend lines of the commercial rings at a lower intertrigonal distance. This meant that the transverse dimension of the rings was larger than that of the healthy mitral valve, resulting in the inability to reduce the size of the regurgitant mitral valve to mimic its original size if the rings are implanted. There was a point at which the mitral valves' transverse diameter began to be larger than the rings' dimension. This was because the rings had limited sizes that could not support the size variation of the mitral valves, which were larger than the sizes of the rings. This led to selecting the rings' largest size for those mitral valves whose intertrigonal distance was larger than the rings.

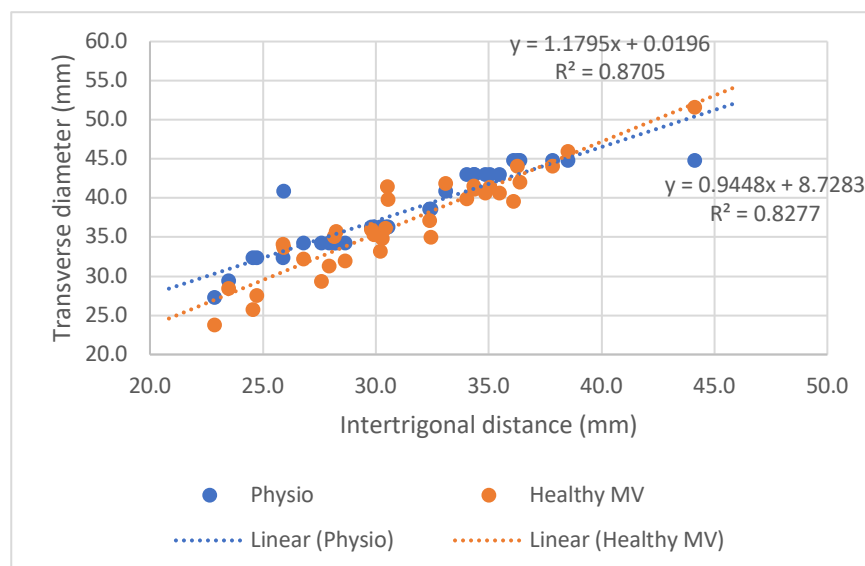


Figure 4.3: The graph of transverse diameter versus intertrigonal distance of the healthy mitral valves and the Carpentier-Edwards Physio ring.

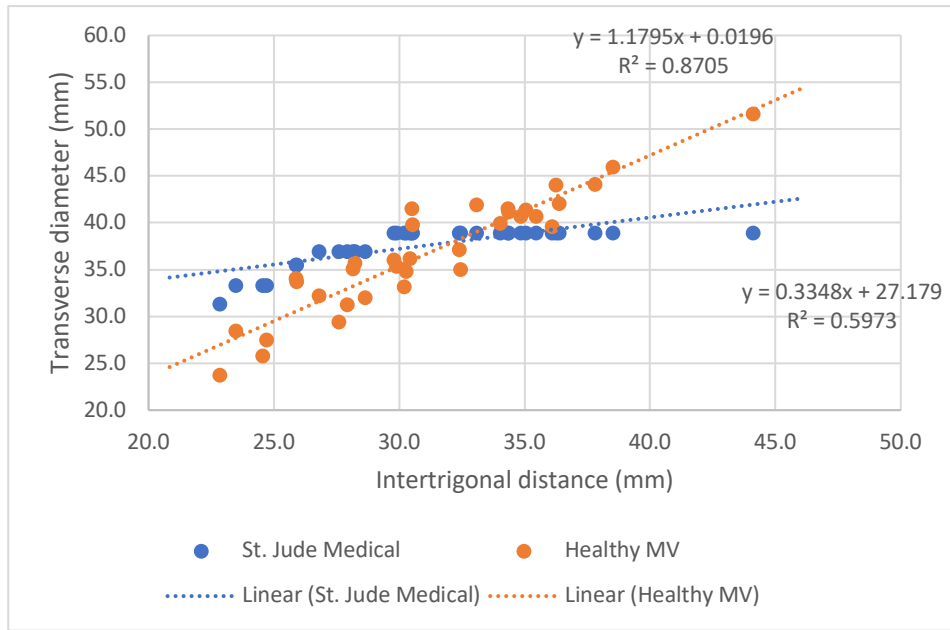


Figure 4.4: The graph of transverse diameter versus intertrigonal distance of the healthy mitral valves and the St. Jude Medical ring.

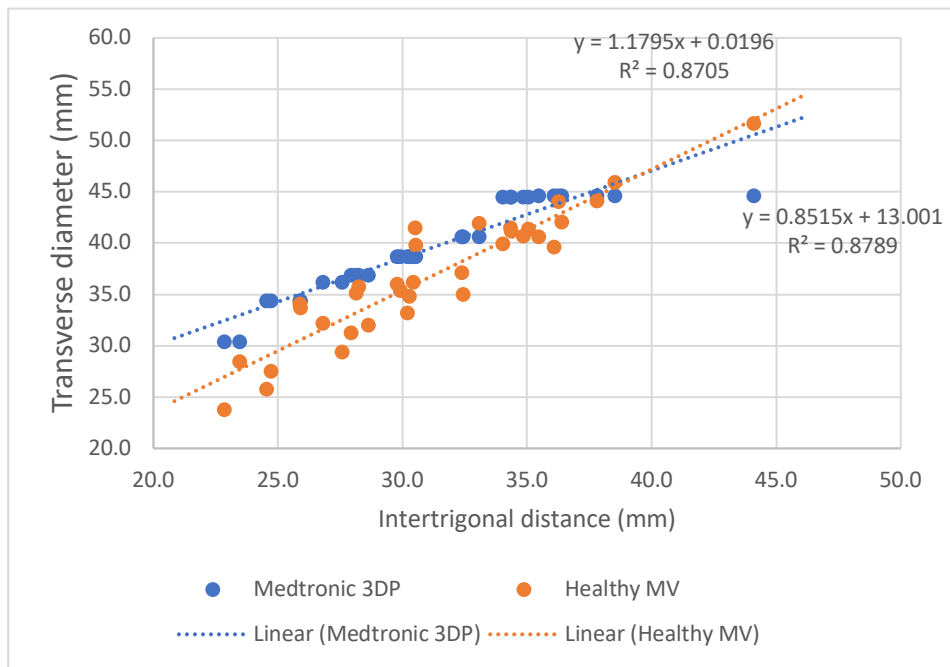


Figure 4.5: The graph of transverse diameter versus intertrigonal distance of the healthy mitral valves and the Medtronic 3D Profile ring.

Figure 4.6 determined the transverse diameter absolute error difference between the best-fit rings and the actual mitral valves, showing that the ring that had the closest transverse diameter was the Physio ring with a mean error of 2.7 mm or 7.6%. Next was the Medtronic 3D Profile ring that produced 3.5 mm of mean error, or 10.4%. Meanwhile, the St. Jude Medical ring produced the highest mean error of 3.8 mm, or 11.1%. ANOVA has been tested and found no statistically significant difference between the mean differences of the three ring types with a P-value of 0.071.

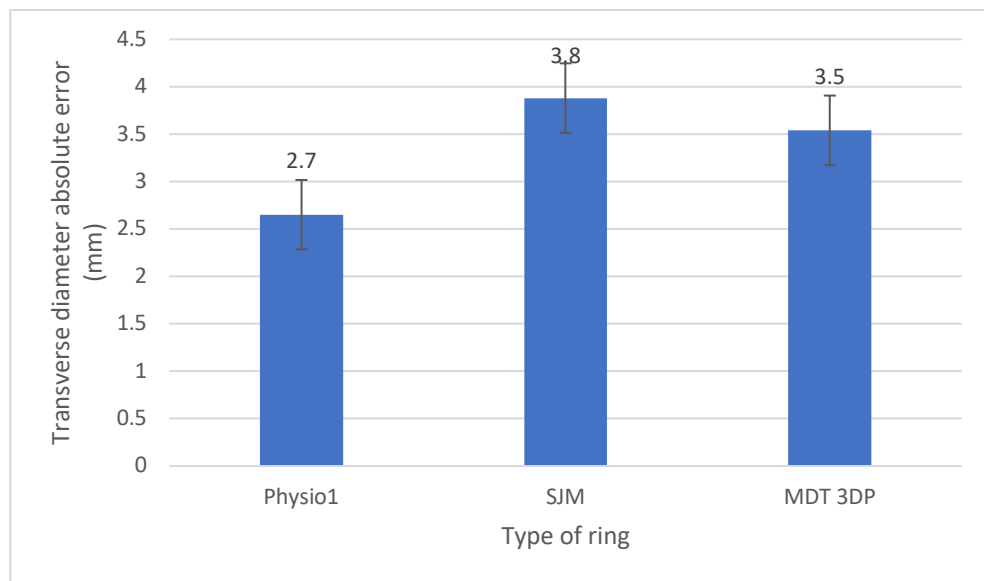


Figure 4.6: The bars present the transverse diameter difference between the commercial rings and the healthy mitral valve.

To compare the ring anteroposterior diameter to that of the healthy mitral valve, Figure 4.7, Figure 4.8 and Figure 4.9 show the trend lines of the healthy mitral valve and the Carpentier-Edwards Physio ring, the St. Jude Medical ring, and the Medtronic 3D profile accordingly. The outcomes revealed the differences in the anteroposterior dimension of the rings that deviated from the healthy mitral valve's anteroposterior dimension. The results also found that the ring dimensions were lower than the mitral valves when the intertrigonal distance increased. At higher intertrigonal distances, the anteroposterior of the rings remains stable while that of the mitral valve keeps rising. This was due to the limited ring size that could not support the mitral valves with a greater size.

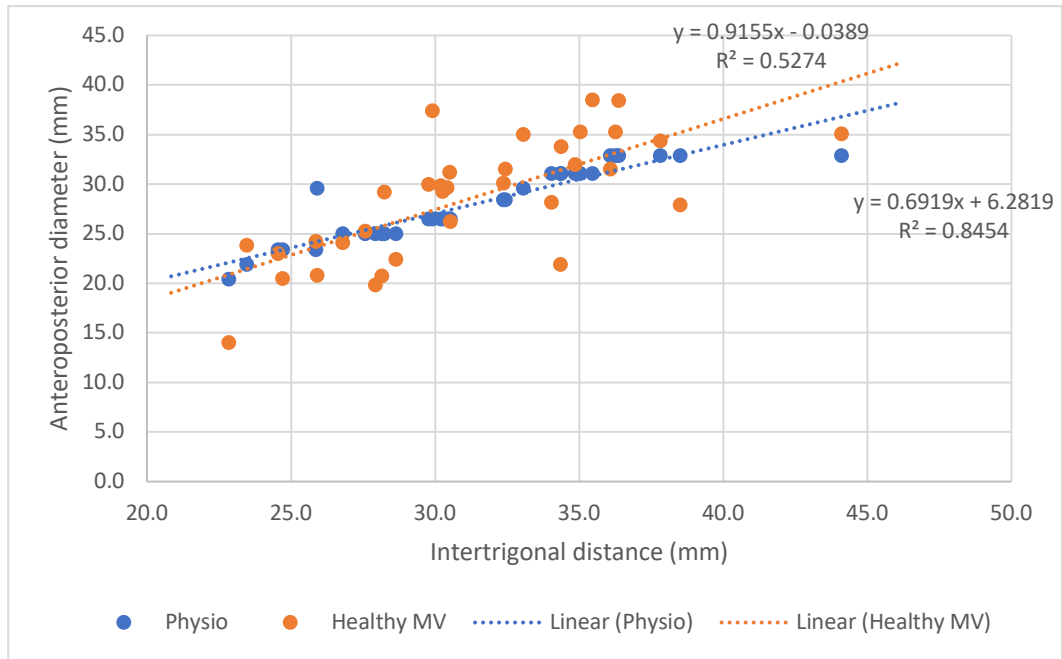


Figure 4.7: The graph of anteroposterior diameter versus intertrigonal distance of the healthy mitral valves and the Carpentier-Edward Physio ring.

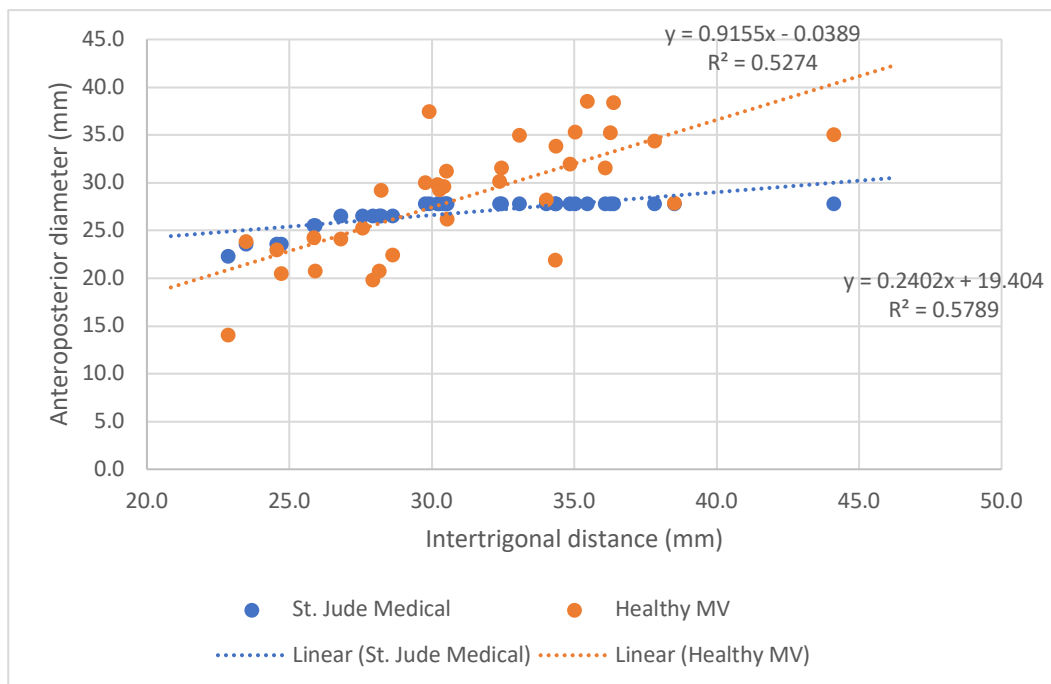


Figure 4.8: The graph of anteroposterior diameter versus intertrigonal distance of the healthy mitral valves and the St. Jude Medical ring.

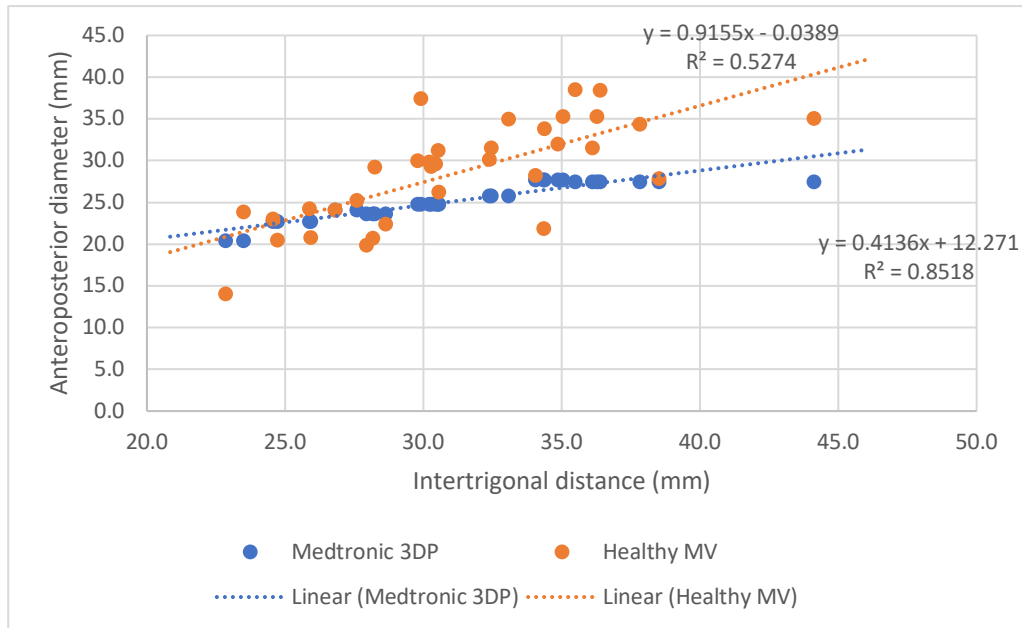


Figure 4.9: The graph of anteroposterior diameter versus intertrigonal distance of the healthy mitral valves and the Medtronic 3D Profile.

Nevertheless, Figure 4.10 was made to find the absolute error of the anteroposterior diameter between the mitral valve and the rings. The results found that the ring that had the least anteroposterior diameter difference from the mitral valve was the Carpentier-Edward Physio ring, followed by the St. Jude Medical ring and the Medtronic 3D Profile that produced the highest 4.8 mm difference or 16.2 percent error. A statistical test with ANOVA found no significant difference between the mean differences of the three groups with a P-value of 0.27.

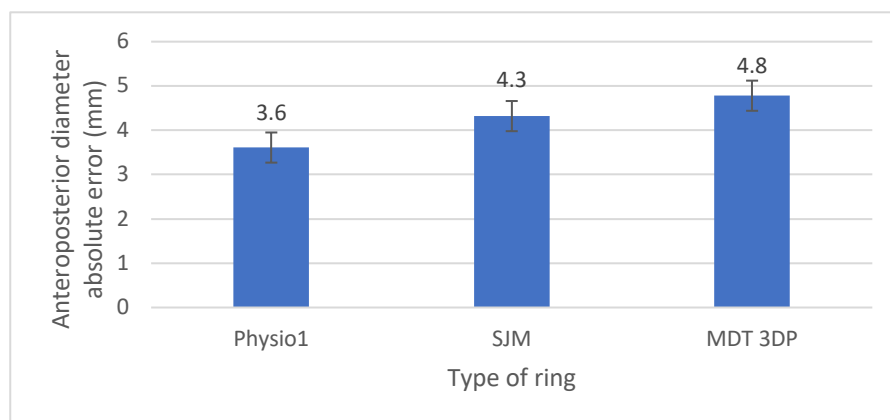


Figure 4.10: The bar presents the anteroposterior diameter absolute error difference between the commercial rings and the healthy mitral valves.

4.1.3 Discussion

When chosen based on the distance between the trigones, none of the commercial annuloplasty rings used in the study were the same size as the healthy mitral valve. Instead, the rings produced errors in both transverse and anteroposterior diameters. The Carpentier-Edward Physio ring has the closest dimensions to the donated mitral valves, followed by St. Jude Medical (SJM) rigid- saddle shape (RSA) and Medtronic 3D Profile (MDT 3DP). These dimensional differences between the three ring types found no significant difference in both transverse and anteroposterior diameters. For the rings with dimensions smaller than the mitral valve dimensions, this could potentially cause mitral stenosis and reoperation. On the other hand, the rings whose dimensions are greater than the mitral valve dimensions possibly affect the sufficiency of supporting leaflet coaptation and the reoccurrence of the mitral regurgitation. The study would propose that, among the three commercial rings with true size selection based on the intertrigonal distance, the Carpentier-Edward Physio ring is the best fit with the sample mitral valves. Still, it is important to note that by matching the intertrigonal distance of the mitral valve to the true-to-size Carpentier-Edward Physio ring, it did not meet the exact dimensions of the healthy mitral valve and produced larger dimensions in the transverse diameter and randomly larger and smaller anteroposterior diameters. Therefore, a downsized ring was considered and studied in Study 2.

Study 2 How much undersized annuloplasty ring would fit the mitral valve?

The selected commercial ring size in the previous study has shown that, in some situations, the dimensions of the rings were greater than the mitral valve dimensions, especially for the transverse diameters, where the rings had greater dimensions. This has raised the question of whether the undersized rings would have closer dimensions to the mitral valves and how much undersizing is best to fit the mitral valve. In this chapter, true-to-size, 1-size smaller, and 2-size smaller have been investigated and compared.

4.2.1 Method

Following the results found in Study 1, further study has been performed with the same method and the same commercial rings described in Study 1 which were the Medtronic 3D Profile (MDT 3DP) in size 24–40 mm, the St. Jude Medical (SJM) rigid–saddle shape ring (RSA) in size 24-34 mm, and the Carpentier-Edwards Physio annuloplasty ring in size 24–40 mm, to investigate how much undersized annuloplasty rings would fit the mitral valve. However, instead of selecting the true size ring that best fits the actual dimensions of the mitral annulus, in this study, the true size, 1 smaller size, and 2 smaller size rings of each commercial annuloplasty ring type were selected and compared to the geometry of the dissected healthy mitral valves. For those mitral valves with dimensions greater or smaller than the available commercial rings, the biggest and the smallest size were selected, respectively.

4.2.2 Results

The results found from selecting the ring size from the three annuloplasty rings: Carpentier-Edward Physio ring (24-40mm), St. Jude Medical (SJM) rigid- saddle shape (RSA) (24-34mm), and Medtronic 3D Profile (MDT 3DP) (24-40 mm), by sizing from the intertrigonal distance strategy, came up with different ring sizes. Those selected rings had various dimensions that varied between each ring type and differed from the mitral valve dimensions as well.

Figure 4.11 shows the mean error determined by subtracting the transverse diameter of the mitral annulus from the ring's transverse diameter, while Figure 4.12 presents the percentage error found between them. Since Study 1 showed that for the transverse diameter, the selected true size ring dimension presented a greater dimension compared to the mitral valve, this study found that 1 size smaller rings had the transverse diameter closer to the mitral valve with less error compared to the same type of true size rings. Meanwhile, 2 size smaller rings presented the highest errors for the Carpentier-Edward Physio ring (2.8 mm or 6.9% error) and St.Jude Medical ring (2.7 mm or 11.3% error); this 2 size smaller ring showed less error (0.9 mm or 1.0%) compared to the true size ring that was 2.7 mm or 8.7% larger than the mitral valve for the Medtronic 3D Profile rings.

Figure 4.11 and Figure 4.12 indicate that, by choosing a true-to-size ring, the transverse diameter of the ring is larger than that of the mitral valve. This can imply that if the true-to-size rings are implanted into the regurgitant mitral valve, they do not have enough efficiency to reduce the transverse diameter of the mitral valve to replicate its original size before it has dilated. Therefore, for the transverse diameter, the ring that had the closest dimension to that of the mitral valve was the Carpentier-Edwards Physio ring when the 1 size smaller ring was selected. It produced a 0.6 mm, or 1 percent error smaller than the mitral valve transverse diameter.

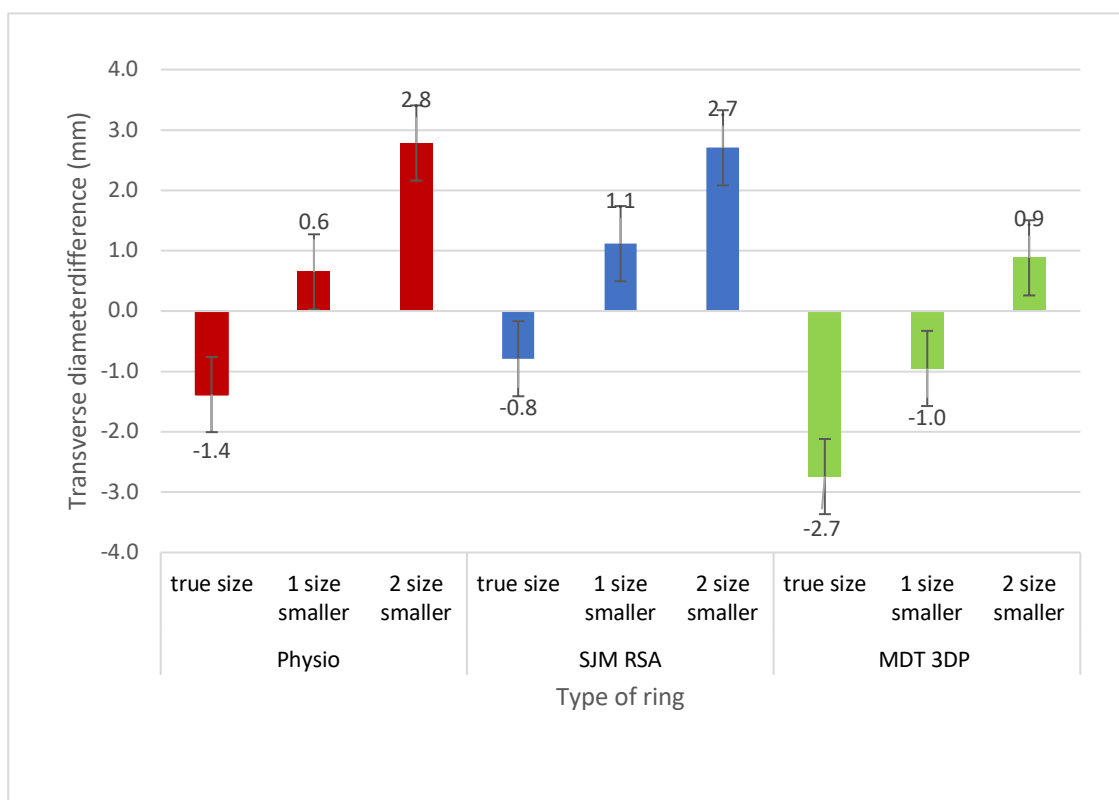


Figure 4.11: The bar presents the transverse diameter mean error (mm) between the three sizes of the commercial rings and the healthy mitral valves.

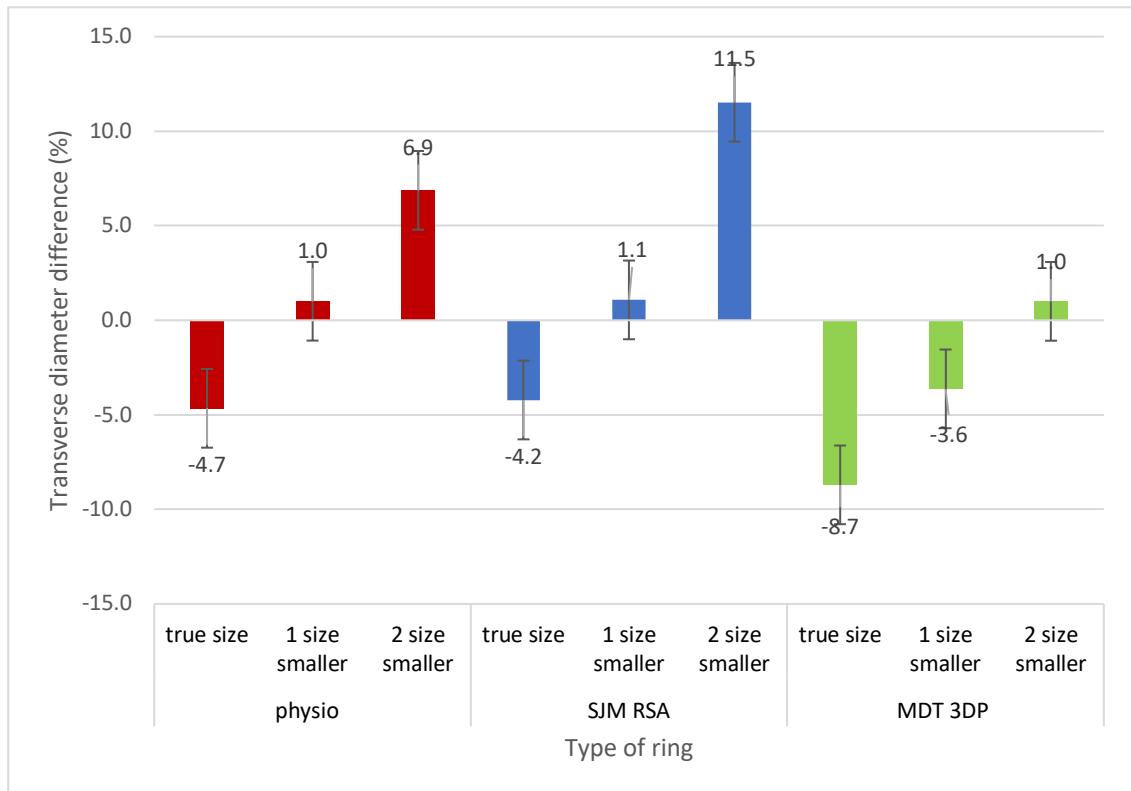


Figure 4.12: The bar presents the transverse diameter mean percent error between the three sizes of the commercial rings and the healthy mitral valves.

Previously, Figure 4.7, Figure 4.8 and Figure 4.9 revealed that the trend lines of the true-to-size rings of the three ring types and the mitral valve were quite divergent and deviated, and it could not be concluded that the anteroposterior diameters of the true-to-size rings are bigger or smaller than that of the mitral valve. However, Figure 4.13 and Figure 4.14 were used to present the mean error, found by subtracting the mitral valves' anteroposterior diameter by that of the rings, and the percent error among them, respectively. The figures clearly show that the true-to-size rings of the three ring types have the least error compared to the smaller sizes, and those rings anteroposterior are smaller than those of the mitral valves. They also indicate that the smaller the ring size, the higher the errors in anteroposterior diameter. Therefore, this study demonstrated that the ring that had the closest anteroposterior diameter to the mitral valve was the true size Carpentier-Edward Physio ring with a 0.7 mm mean error or 0.7% error, followed by the St. Jude Medical true size ring with a 1.6 mm mean error or 1.8 percent error.

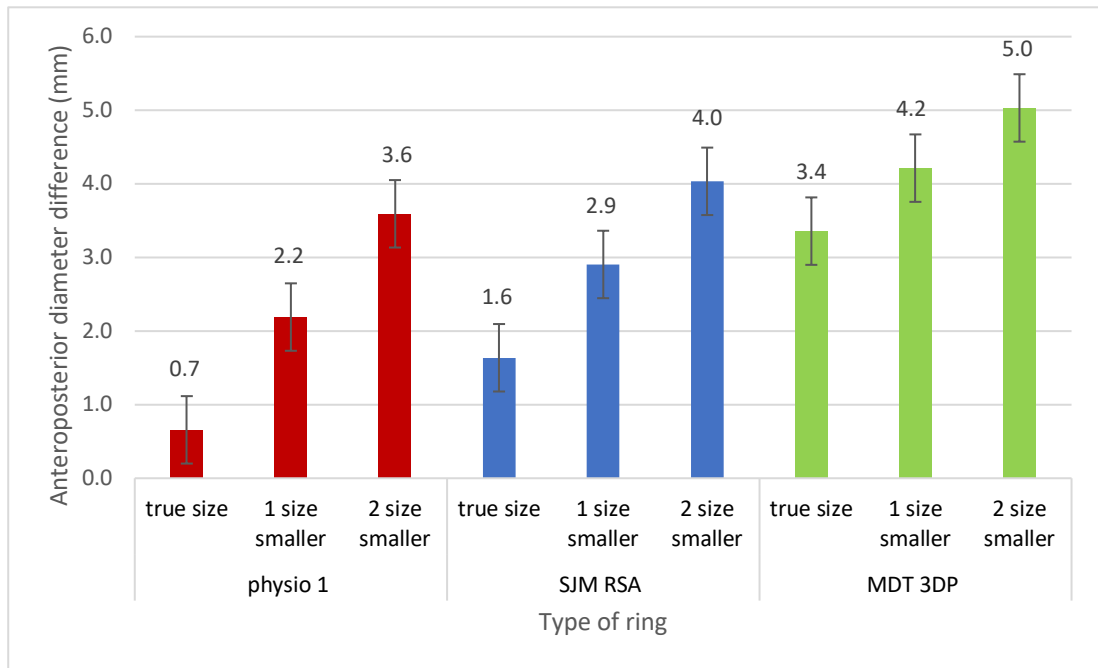


Figure 4.13: The bar presents anteroposterior diameter error (mm) between the three sizes of the commercial rings and the healthy mitral valves.

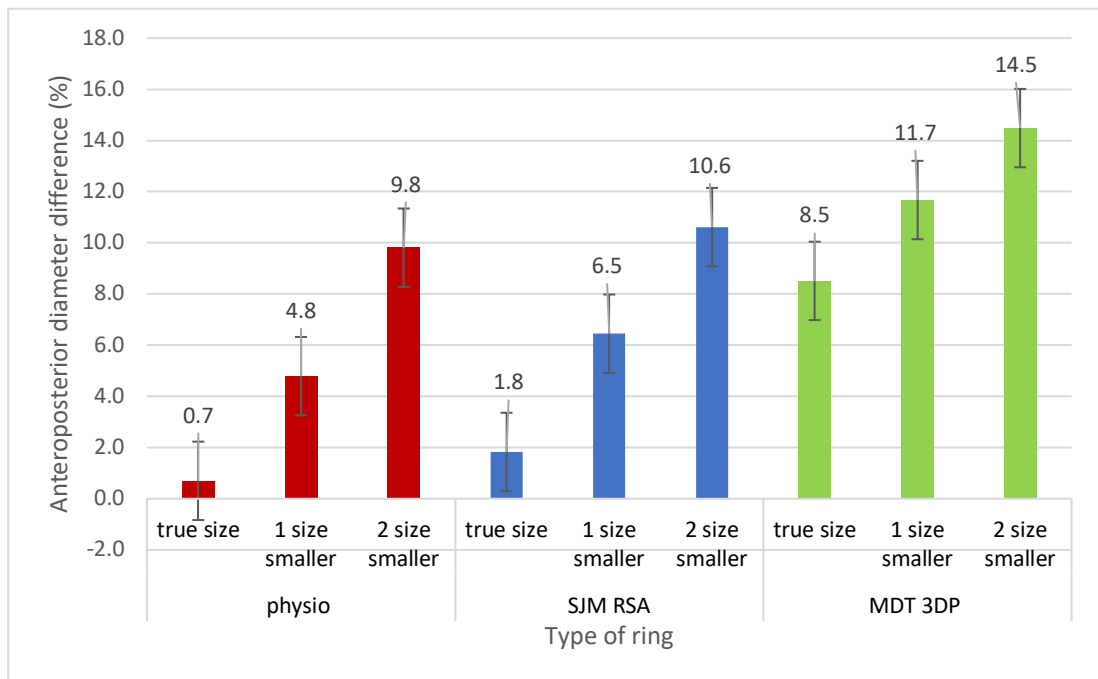


Figure 4.14: The bar presents anteroposterior diameter percent error between the three sizes of the commercial rings and the healthy mitral valves.

4.2.3 Discussion

The results have shown that none of the rings used in this study had exactly the same dimensions as the donated mitral valves when the rings were selected based on the intertrigonal distance strategy. For the transverse diameter, the study found that the true-size rings from the three commercial rings had larger distances than the mitral valve. That was why the undersized rings were investigated. The outcomes have proven that the one-size smaller ring had the closest distance to the mitral valve compared to the true-size ring. However, when the two-size smaller ring was chosen, the level of undersizing was too much that its transverse diameter was smaller than the mitral valves and caused the highest error out of the three ring sizes. In this study, the ring that was found to have the closest transverse diameter to the mitral valve was the one-size smaller ring from Carpentier-Edwards Physio, which produced a 2.23 mm mean absolute error and a 6.16% error. For the anteroposterior diameter, the graphs were so random and diverse that at lower intertrigonal distances, the rings' dimension seemed to be larger than the mitral valve. On the other hand, with a higher number of intertrigonal distances, the rings tended to be smaller than the mitral valve in the anteroposterior diameter. Therefore, the study mainly focused on determining the absolute error among them. The results have shown that the true-size ring had the closest dimension and the fewest errors, followed by the one-size smaller ring and the two size smaller rings, respectively. This can imply that the greater the level of the downsizing ring, the greater the errors it produces. This is probably because the downsized rings were smaller than the mitral valves, so when the level of downsizing was increased, the errors got higher. The ring that had the closest anteroposterior diameter was the true-size Carpentier-Edward Physio ring with a 2.23 mm mean absolute error and 6.16% error.

The study has proposed that among the commercial rings; Carpentier-Edward Physio ring (24-40mm), St. Jude Medical (SJM) rigid- saddle shape (RSA)) (24-34mm), and Medtronic 3D Profile (MDT 3DP) (24-40 mm), the ring that had the closest dimensions to the mitral valve when selected based on the intertrigonal distance was the Carpentier-Edward Physio ring. However, the level of downsizing cannot be concluded due to the fact that the one size smaller ring had the closest transverse diameter while the true size ring had the closest anteroposterior diameter to the mitral

valve geometry. In addition, this study found that due to the limited size of the rings, they do not have the dimension to support the mitral valve with a higher intertrigonal distance, supporting the use of a personalised ring.

In conclusion, the findings of this study provide valuable insights into the selection of commercially available annuloplasty rings and suggest potential improvements in their design. The use of data, particularly the intercommissural distance, has been assessed for choosing the most suitable commercial annuloplasty ring. Among the tested options, the Carpentier-Edwards Physio annuloplasty ring demonstrated the closest match to mitral valve dimensions, making it a favorable choice for mitigating mitral regurgitation.

However, the study highlights discrepancies between the dimensions of commercial annuloplasty ring and healthy mitral valves, indicating room for enhancement in commercial designs. Further research and collaboration between clinicians and manufacturers are recommended to refine existing annuloplasty ring, potentially incorporating personalised features to better match individual anatomical variations.

Regarding the need for bespoke annuloplasty ring, the study underscores the significance of personalised solutions, especially in cases where individual mitral valve anatomy deviates significantly from standard dimensions. The process of designing and manufacturing personalised annuloplasty ring involves various steps, from obtaining high-quality medical imaging data to 3D reconstruction, dimensional analysis, and CAD-based design.

In practical terms, the decision to opt for a bespoke annuloplasty ring should be guided by a thorough assessment of the patient's mitral valve geometry. Collaboration between medical professionals and engineers is crucial in determining when a personalised solution is warranted. The study's findings contribute to the broader understanding of annuloplasty ring selection and design, paving the way for future advancements in mitral valve repair procedures. As medical technology evolves, ongoing research and innovation will play a pivotal role in refining the use of data, improving commercial designs, and expanding the application of personalised annuloplasty ring in clinical practice.

Conclusion

This chapter is about the comparison between the dimensions of popular commercial rings that are available and the mitral valve dimensions by using the intertrigonal distance strategy. The commercial rings come in different sizes and shapes that directly affect the mitral valve reduction when the rings are implanted.

The results found that none of the commercial rings used in this study produced the exact dimensions of the mitral valve and produced some residuals, although the undersized ring was also considered. Moreover, some ring types have dimensions larger than that of the mitral valve, making them unable to reduce the mitral valve dimension and thus solve the mitral regurgitation.

The Carpentier-Edward Physio ring had the most potential to reduce the height and width of the mitral valve, which helped the mitral valve coaptation, among the commercial rings that were shown in this study.

The results also showed that the size ranges available from those three ring types were not suitable since they did not have size ranges that matched the population of the mitral valves that showed a large intertrigonal distance. The findings have raised the possibility of using a personalised annuloplasty ring to better fit the mitral valve dimensions. A personalised annuloplasty ring refers to a uniquely crafted and custom-manufactured device utilized in mitral valve repair interventions. It is designed to suit the distinctive anatomy of an individual patient, setting it apart from standardized, commercially available annuloplasty rings that come in predetermined sizes. This personalised approach seeks to optimize the compatibility and performance of the annuloplasty ring, ultimately improving the overall success and outcomes of mitral valve repair procedures.

The key contribution of this chapter lies in uncovering the correlations between the dimensions of a healthy mitral valve and the commercial annuloplasty rings employed in this study. Specifically, the emphasis is on instances where ring selection is based on the distance between the trigones, a parameter recognized for its minimal dilation in diseased mitral valves. Additionally, the thesis explores the feasibility of adopting an undersized annuloplasty ring, as opposed to a true-size ring, to achieve a more

accurate reproduction of the dimensions of a healthy mitral annulus. The limitations of this experiment are the limited number of commercial rings and the ring information used in the study.

Chapter 5 Personalised annuloplasty ring design to fit individuals

Chapter 4 demonstrated that human mitral valves are highly variable, and their shape might not be best fitted with the shape of available commercial annuloplasty rings, leading to the idea of developing personalised annuloplasty rings to serve individual differences. However, previous studies (Díaz Lantada et al., 2009; Sundermann et al., 2013) have revealed that the application of personalised annuloplasty rings has been limited due to the time-consuming procedure, the cost, and the difficulties in imaging the mitral annulus, designing, and manufacturing the ring. Therefore, this chapter presents processes for developing personalised annuloplasty rings from patients' medical data that aim to address the limitations of previous studies. Chapter 5 comprises three individual studies. Study 1 concentrated on refining techniques for isolating and 3D reconstructing the mitral annulus. In study 2, efforts were made to fill in the gaps in the posterior annulus of the mitral annulus model, which was initially obtained in Study 1. Study 3 showcased the feasibility of selecting personalised annuloplasty ring sizes based on medical scan images taken before a patient's operation.

Methodology

The literature review in Chapter 2 supports the use of a personalised annuloplasty ring. Nevertheless, the cost and difficulty of designing and manufacturing personalised annuloplasty rings were the limitations that it could not overcome over the commercial annuloplasty ring. Hence, this study was to develop a method for designing a personalised annuloplasty ring for each patient. The first step was to visualise and identify the mitral annulus from patients' medical images. This method was developed using two MRI scans of patients who have mitral regurgitation and one echocardiography. The purpose of using both MRI and echocardiography was to determine whether the mitral annulus could be visualised and segmented with those

data types and whether they required different steps in producing a three-dimensional model of the mitral annulus. The process to visualise patients scan images can be done with various software applications that allow visualisation of files using the standard medical image format Digital Imaging and Communications in Medicine (Dicom) file and the analysis of the heart, especially the mitral valve, for example Materialise, QLAB software from Philips, and Tomtec software, meaning that any of them can be utilised. Dicom is a protocol for medical image management and communication. The purpose of Dicom is to enable the interoperability of systems used to store, display, transmit, process, and print medical images through the integration of imaging devices in Dicom format.

The research was further studied with available open-source software called ITK-SNAP and Blender. The benefit of using open-source software is that others can repeat this work. ITK-SNAP allowed the visualisation of the patients scan images and came with embedded tools that allowed the mitral annulus extraction. The extraction methods of the mitral annulus included the thresholding method, and a point-based method, the method that gradually placed red landmarks on the multiple layers of the scan where there was the intersection between the leaflets and the annulus, in order to allocate the annulus shape. After the mitral annulus was segmented, the next step was to create a 3D model of the annuloplasty ring out of the mitral annulus shape. Furthermore, it requires choosing a suitable size and shape to provide correction to the regurgitant mitral valve. In this research, the outcome found from the mitral annulus extraction was the shape ideal for the personalised annuloplasty ring design. This was because the mitral annulus shape was so varied among individuals that a personalised annuloplasty ring would be a better fit for an individual compared to available commercial rings.

Another challenge found from this study was that often the echocardiography did not show the whole area of the leaflet insertion to the mitral annulus, meaning that only part of the mitral annulus could be extracted, showing part of it. This situation could possibly happen in a clinical data set if part of the area of interest was not visible. Thus, this study has proposed a method to overcome the problem by predicting the missing posterior annulus from the set of data obtained during the cadaveric dissection. The study involved using R Studio, a programming software for statistical

computing and analysis, to perform functions included in the packages. The data processing included Generalised Procrustes Analysis (GPA) and a linear regression model that predicted the missing posterior annulus.

The next phase of this study section was to pilot the possibility of annuloplasty ring sizing with pre-operative medical data from different strategies and to understand the correlation of these sizing strategies in terms of whether they selected the same ring size. Because of the difficulty in obtaining the commercial rings and the data on the ring dimensions, these have been the limitations found in this study. Therefore, the comparison of the ring sizing was limited to four strategies: the height of the anterior mitral leaflet (AML) and the intercommissural distance with true size, one size smaller, and two size smaller rings. The workflow in this chapter was shown in Figure 5.1

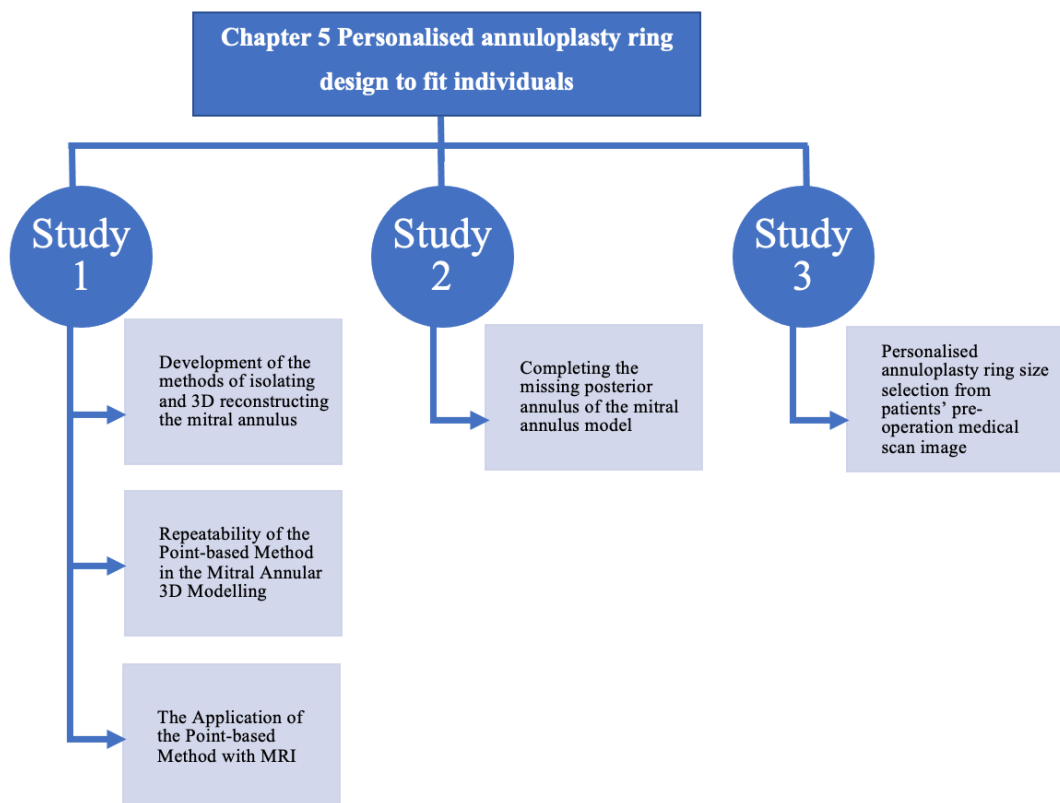


Figure 5.1 The workflow of the studies in Chapter 5

Study 1 Development of the methods of isolating and 3D reconstructing the mitral annulus

The first step in making an annuloplasty ring that fits each patient was to study how to get the shape of the patient's mitral annulus and turn it into a virtual 3D model. This process is one of the main limitations in designing a personalised annuloplasty ring due to the fact that the soft tissue is not easily recognised in medical images as the density of the mitral annulus is very similar to the leaflets and surrounding muscular tissue. In this chapter, patients scan images from 3D echocardiography were studied with CAD - CAM software. Materialise software includes Mimics and 3-Matic. Mimics is a 3D design and modelling software that creates 3D models in STL format from stacks of 2D images or medical data through segmentation, while 3-Matic is a software that uses CAD designs to modify the STL output data from Mimics. In this work, the licenced software has been tested with two different methods, the thresholding method and the point-based method, to determine which is the most suitable and reliable one for this application.

5.1.1 Method

The development of the method to reconstruct the mitral annulus in three dimensions from echocardiography data was conducted using two different methods: a thresholding method and a point-based method. These methods were performed by following the steps.

5.1.1.1 The point-based method for isolating and 3D reconstructing the mitral annulus

The first step was to upload the sample echocardiography to the Materialise Mimics in Dicom file. This file shows views of the mitral valve and surrounding tissue in three windows: axial, coronal, and sagittal views. Another window was provided to view the 3D image during the 3D modelling process [Figure 5.3]. Next, the mitral annulus was allocated by looking at the leaflet insertion area to the mitral annulus. Once the area was identified, the paint tool was used to gradually place red landmarks on the area on the multiple layers of the scan images. This step resulted in a set of points on the annulus that were identified in three dimensions to extract the shape of the mitral annulus [Figure 5.2]. Later, once the shape of the mitral annulus was extracted. The

3D image was exported to Materialise 3-Matics. In Materialise 3-Matics, a line was drawn to connect the red landmarks to form a curve. Then, a circle was swept along the line to create a 3-dimensional shape for the mitral annulus ring. The process was repeated to determine the repeatability of the method. The results was analysed by investigating the usability, repeatability, and accuracy of the method to extract the mitral annulus shape.

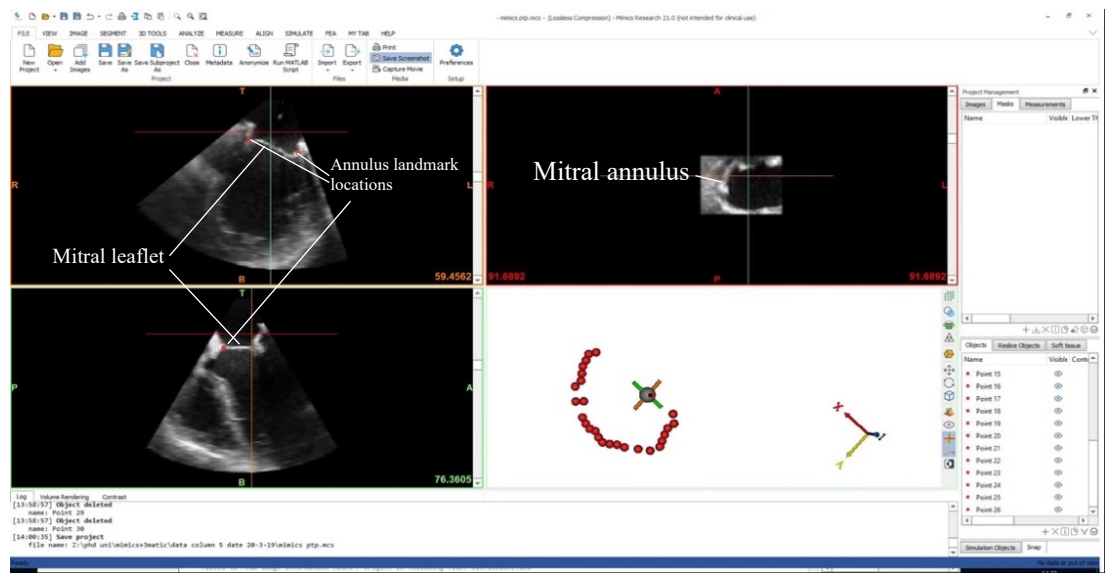


Figure 5.2: The echocardiographs of the mitral valve were displayed in Materialise Mimics in the three views and one 3D image during point-based method.

5.1.1.2 Method for developing of imaging, isolating and 3D reconstructing the mitral annulus using a thresholding method

In comparison with the point-based method, the thresholding method was performed with the same echocardiographic data used with the point-based method. The Dicom file from the sample echocardiography was uploaded to Materialise Mimics.

Then, the segmentation process to isolate the mitral annulus started with the new mask tool and the thresholding tool. The thresholding tool was used to highlight the area of interest. In this case, the mitral valve area was highlighted to distinguish it from the other structure. To make sure that most parts of the mitral valve were included, soft tissue surrounding the mitral valve was included as well because the mitral valve and these parts had similar density and low contrast. Therefore, the thresholding method could not separate them [Figure 5.3].

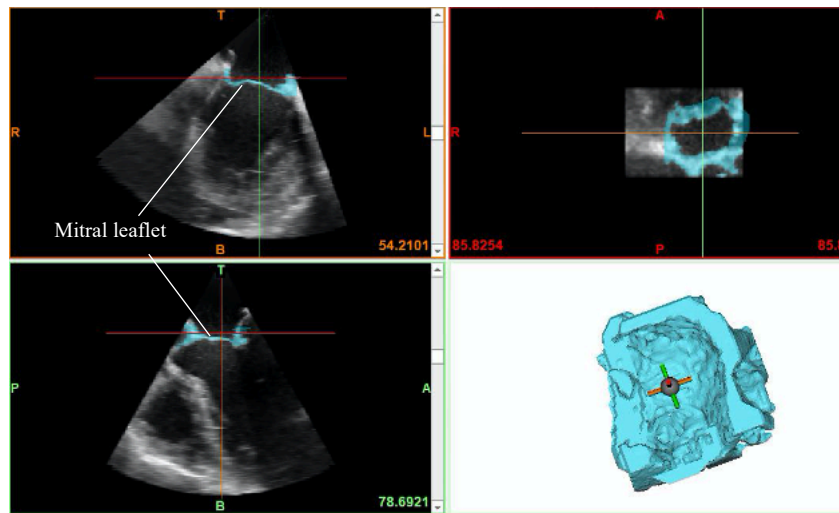


Figure 5.3: The echocardiographs of the mitral valve were displayed in Materialised Mimics in the three views and one 3D image, showing the mitral valve and surrounding tissue.

To solve the problem, the crop tool and erasing masks were applied to remove the irrelevant parts layer-by-layer. On the other hand, some areas of the mitral valve were not covered and needed to be added layer-by-layer as well by using the edit masks. These methods were mainly based on the knowledge of the person in deciding which area was part of the mitral valve and should be included or not. After the segmentation, the 3D object was calculated and exported to the Materialise 3-Matic software. In 3-Matic, the curve was drawn attached to the inside of the object to show the mitral annulus shape [Figure 5.4]. Then, a circle was created on a sketch plane and followed by a sweep tool to create a 3D shape of the annulus.

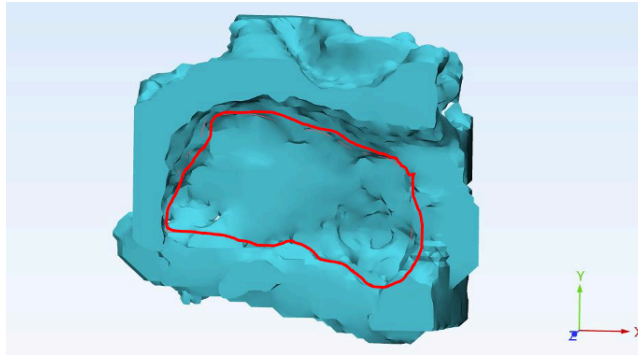


Figure 5.4: The mitral annulus was shown as the red line drawn attached inside of the extracted 3D object(blue) which included both the mitral valve and surrounding tissue.

The same echocardiographic data was tested twice with the same method to see whether this method was repeatable. The results were analysed by investigating the usability, repeatability, and accuracy of the method to extract the mitral annulus shape.

5.1.2 Results

5.1.2.1 Point-based method

The point-based method was able to extract the mitral annulus shape. The shape found from using the point-based method is shown in Figure 5.5. The red landmarks displayed the 3D shape of the mitral annulus. However, the quality of the sample data was not good enough so some intersection points could not be seen, with the results that the annulus shape that was created was not a complete ring [Figure 5.6]. As this method focused only on placing landmarks on the annulus area, the knowledge needed to perform this step was to accurately read the scan and indicate where the leaflet insertion area to the annulus was.

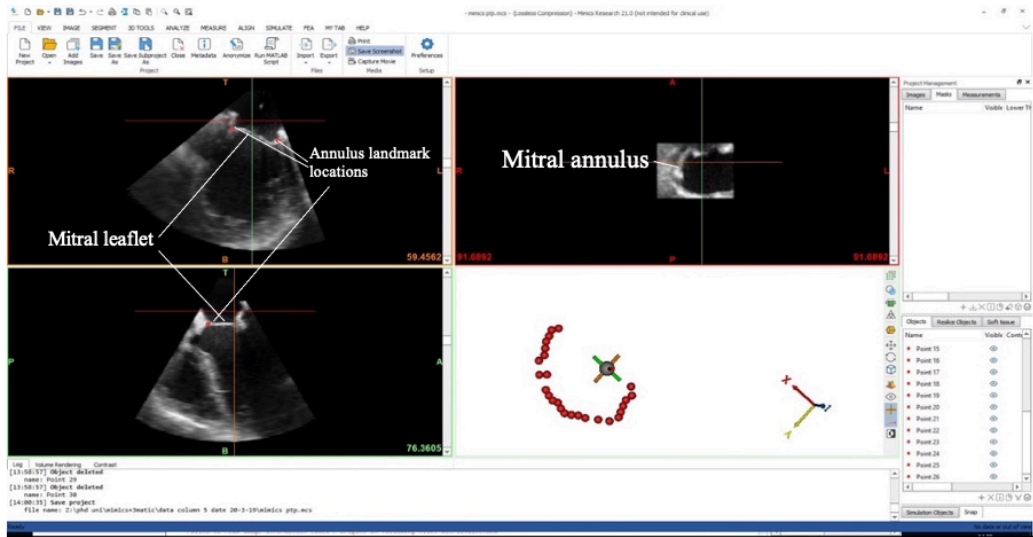


Figure 5.5: Point-based method with the red landmarks showing the mitral annulus shape.

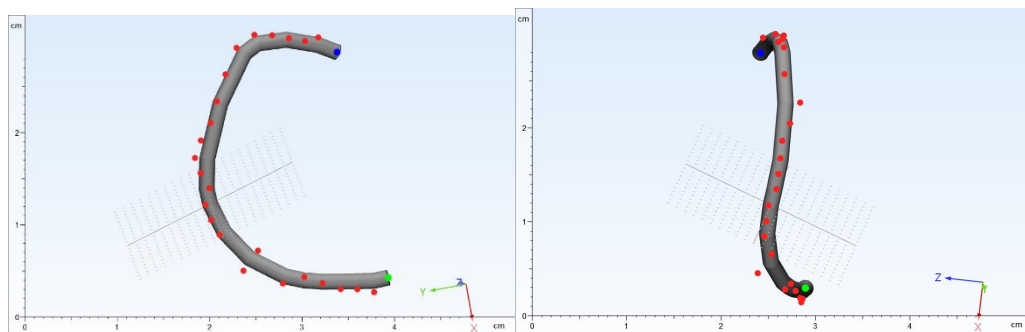


Figure 5.6: Top view (left) and side view (right) of the 3D shape of the mitral annulus created with the point-based method.

The same data was tested twice with the same point-based method resulting in the shapes shown in Figure 5.7. The half-rings produced were slightly different in shape compared to each other.

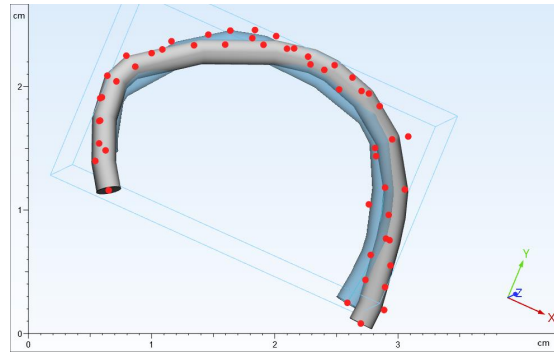


Figure 5.7: Two half-rings produced with the same data and point-based method showing the shape similarities and differences: first produced (blue), second produced (grey).

5.1.2.2 Thresholding method

The thresholding method was able to isolate the mitral annulus shape from the segmented structure. The shape found from the sample echocardiography was shown in Figure 5.8.

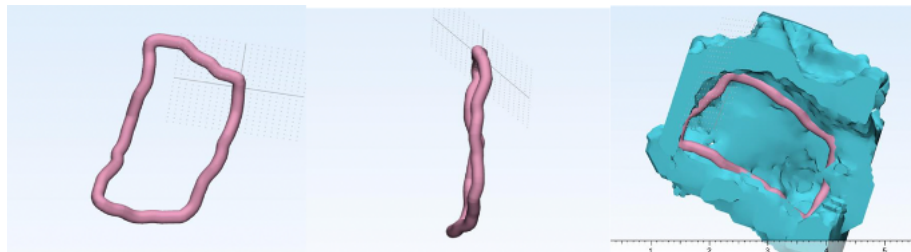


Figure 5.8: Top view (left) and side view (middle) of the complete 3D shape of the mitral annulus. The 3D annulus shape in the thresholded mitral valve from Mimics (right).

The results showed that creating the 3D model twice did not produce exactly the same shape [Figure 5.9] even though the shapes were quite similar as well as the dimensions. The first 3D ring had a transverse diameter of 26.25 mm and an anteroposterior diameter of 14.61 mm, while the second ring had a transverse diameter of 25.92 mm and an anteroposterior diameter of 13.26 mm. The differences were due to the method

of manually drawing the attached curve inside the object on the annulus area because the annulus was not clearly shown in the 3D objects using the thresholding method.

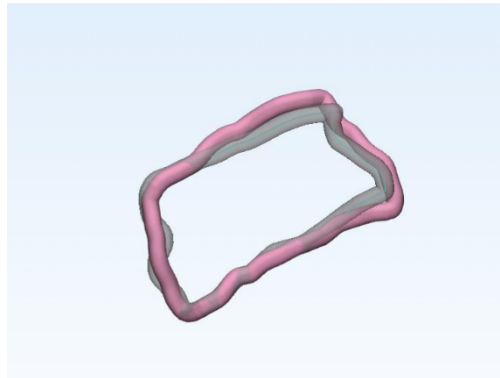


Figure 5.9: The comparison of the 3D reconstruction of the mitral annulus using the thresholding method twice. The pink ring shows the first result while the grey ring shows the second result obtained.

5.1.3 Discussion

For the methods to determine the shape of the mitral valve, the research showed that Materialise Mimics with 3-Matics was able to form the 3D shape of the mitral annulus from the echocardiographic data. The study started with the point-based method that was able to indicate the mitral annulus by looking at the leaflet insertion area to the mitral annulus. Then the thresholding method was introduced because it was a refinement method that defined the surface area of the mitral valve before locating the mitral annulus. As mentioned earlier, the thresholding method relied a lot on the knowledge and decision making of the person who performed the segmentation to remove or add any area to the part, which could cause some human errors; it also required more processes and time. On the other hand, the point-based method appeared to be more accurate with fewer steps and was less time-consuming as the person performing the method mainly focused on placing landmarks on the annulus on the scans to make sure that only the annulus was included. In addition, as the surrounding tissue was not involved, as it was in the thresholding method, no removing steps were required.

Based on the experiment, the raw data made it easier to find landmarks of the mitral annulus than the segmented image. Hence, the most accurate and suitable method that has been performed appears to be the point-based method. Nevertheless, due to the fact that the Materialise program with both thresholding and point-based methods produced some errors in determining the mitral annulus shape, the 3D shapes produced from the same data were slightly different. This raised awareness of the validity of the method, which then led to the study in Section 5.1.4. Hence, the next step of this research was to continue with more trials to determine the statistical error parameters produced with the same programme and with the point-based method.

5.1.4 Repeatability of the Point-based Method in the Mitral Annular 3D Modelling

Repeatability of the 3D modelling process is crucial to ensure that the extracted 3D shapes do not vary when the process is repeated, showing the validity of the process. As a result, in this study, Materialise with Mimics and 3-Matics has been studied to visualise patient scan data, allocate the mitral annulus, and generate the annular 3D model. The 3D model is very important in showing the actual mitral annulus shape of each patient, as it is used in developing patient specific annuloplasty rings for annuloplasty surgery. Section 5.1.2 has shown the possibility of using a point-based method and proposed that this method was better than the thresholding method. Thus, it is very important and necessary to examine the validity of this point-based method using the same echocardiography data used in the previous study, presenting the non-completed mitral annular shape as the data did not show all the insertion points from the leaflet to the annulus that are necessary for creating the 3D model.

5.1.4.1 Method

Since the point-based method has an element of operator judgement, it is important to understand its reproducibility. The study used echocardiography data with voxel sizes of 1 mm. The data was the same one used in Section 5.1.1. A ring design was generated five times from the data using the same point-based method described in Section 5.1.1.

The models' dimensions were compared by looking at the mean and the 95% confidence interval to investigate the variability of the annular length, anterior annular, transverse diameter, and the distance from the starting to the ending points, assessing their variability, and verifying whether the point-based method consistently yielded identical results through multiple iterations of the process.

5.1.4.2 Results

The 3D modelling processes were performed and repeated five times. To compare those five annular models with each other, different dimensions of the shape were measured. Annular length showed the total length of the half-ring annulus; anterior annular length was measured from the starting point of the anterior annulus to the intersection point where the posterior annulus began; transverse diameter was the straight line showing the distance between the commissural points where the anterior annulus met the posterior annulus, and the distance from the starting point to the ending point of the annular curve.

The annular lengths of the five models were measured and are shown in Figure 5.10. The average length was 54.1 mm, the standard deviation was 1.0 mm, and the coefficient of variation was 1.77%. Also, all of the data was within the 95% confidence interval.

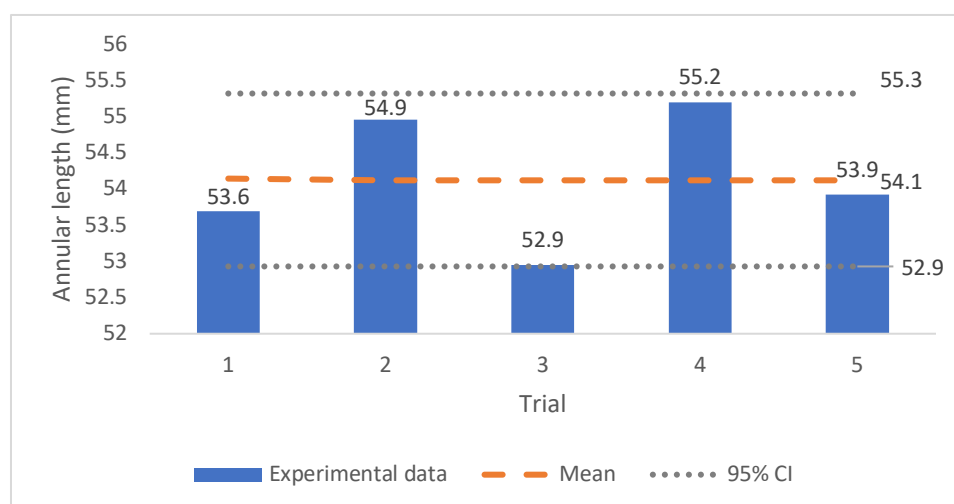


Figure 5.10: Comparison between the annular lengths of the five 3D models of the mitral annulus produced from the same data with mean equal to 54.1 mm.

The anterior annular lengths of the five models [Figure 5.11] produced an average of 38.9 mm and the standard deviation was 1.0 mm with around 2% potential variability. Moreover, all of the data fell within the 95% confidence interval.

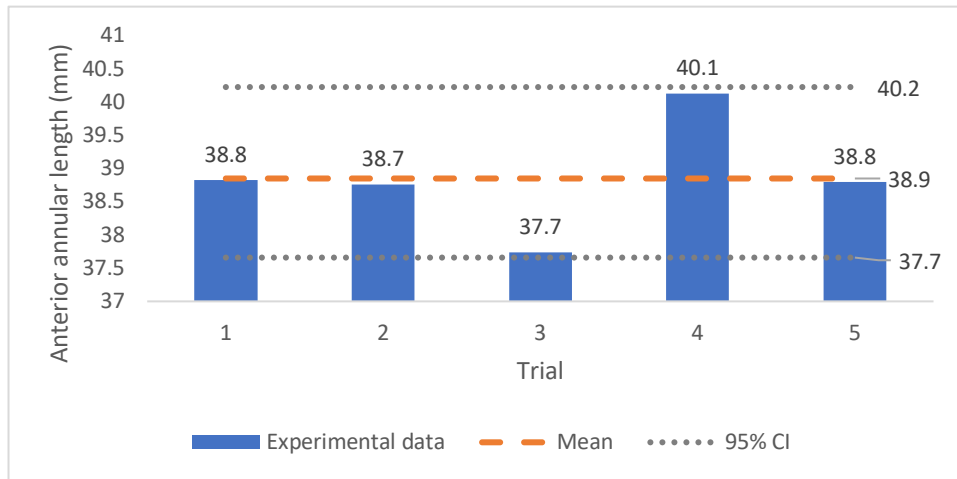


Figure 5.11: Comparison between the anterior annular lengths of the five 3D models of the mitral annulus produced from the same data with mean equal to 38.9 mm.

The commissural diameters of the models [Figure 5.12] produced an average equal to 26.8 mm, the standard deviation was 1.0 mm, and the coefficient of variation was 3.62%. Moreover, one of the data points lies just outside the lower bound of the 95% confidence interval, with a difference of 1.3 mm from the mean data.

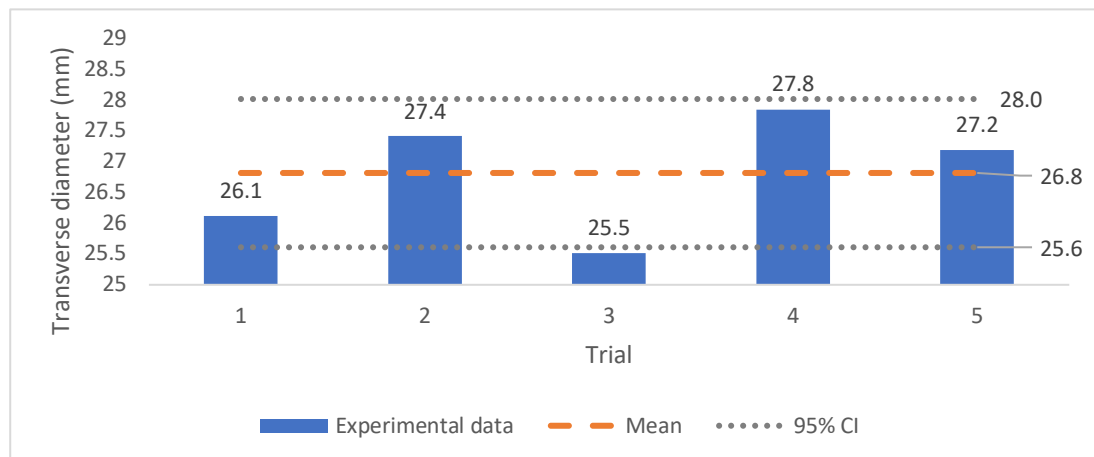


Figure 5.12: Comparison between the commissural diameter of the five 3D models of the mitral annulus produced from the same data with mean equal to 26.8 mm.

The distance between the starting and ending points of the mitral valve curve [Figure 5.13] had an average equal to 27.7 mm, the standard deviation was 0.9 mm, and the coefficient of variation was 3.47%. Moreover, all of the data fell within the 95% confidence interval.

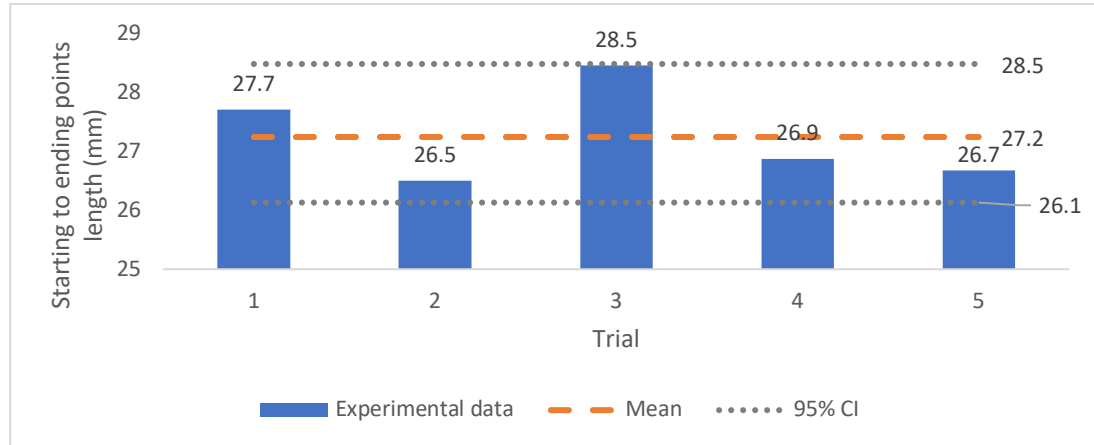


Figure 5.13: Comparison between the distance from the starting to ending points of the five 3D models of the mitral annulus produced from the same data with mean equal to 27.7 mm.

5.1.4.3 Discussion

The five mitral annular models produced from the same stack of the patient's echocardiography with the point-based method were quite similar and stable in terms of the shape observed from different views. They had relatively similar dimensions, with standard deviations of around 1 mm. With the voxel size being equal to 1 mm, it means that the measurement cannot be more precise than 1 mm and that the standard deviation of 1 mm is acceptable. Most of the data from the four-dimensional parameters lie within the 95% confidence interval, except for one point from the commissural diameter parameter that lies slightly outside the lower boundary. Moreover, coefficients of variation varied between 1% and 4%, which indicated relatively low variations in data distribution from each other. This means that the mitral annular models did not have significant dimensional differences when the 3D modelling process was repeated five times, indicating that this point-based method is a reliable and repeatable method.

The limitation of this research is that the data used in the experiment did not show a complete cardiac cycle, otherwise, more dimensional parameters could have been examined and a better comparison made between the models.

5.1.5 The Application of the Point-based Method with MRI

This study determined the application of the design processes used in echocardiography to the medical images of MRI and investigated whether any other additional steps were needed. Two samples of MRI patient data and one echocardiographic sample were included in this study. So far, it has been established that the point-based method was able to extract the mitral annulus shape, which was the prototype for the annuloplasty ring design, and that this method was more suitable and reliable than the thresholding method. Nonetheless, the software used in the study was Materialise Mimics and 3-Matic, which required licences. Hence, this section aimed to reduce the cost of producing a personalised annuloplasty ring by using the same point-based method with available open-source software that can be downloaded online and does not require any licence fee. In the study of ITK-SNAP, an application to segment structures in 3D medical scans was used to visualise and segment the mitral annulus from patients' MRI images. Meanwhile, Blender, an open-source computer graphic software, was applied to edit the extracted mitral annular shape and to create a 3D model.

5.1.5.1 Method

To determine the point-based method with MRI data, the same point-based method was performed with the ITK-SNAP, an open-source software application that comes with embedded tools that enable to visualise patient scan images, and the software is available to be downloaded online. Following the same point-based steps used in Section 5.1.1.1, the method started by importing the Dicom file obtained from MRI. In ITK-SNAP, the uploaded file was presented in three views, allowing visualisation of the volumetric image in four windows. Similar to Materialise Mimics, the three

windows displayed the image in the horizontal axial, coronal, and sagittal planes. The remaining window was to display the 3D model during the segmentation process [Figure 5.14]

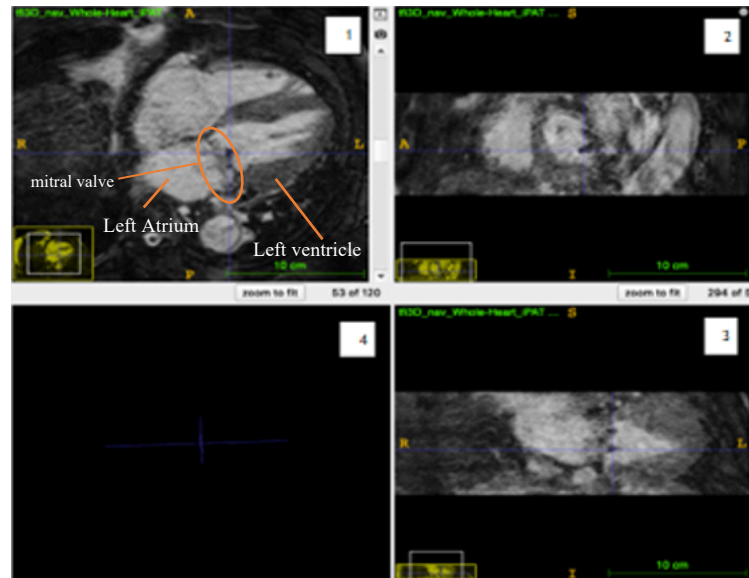


Figure 5.14: The MRI of the heart that shows the mitral annulus was shown in four windows display the image views in horizontal axial (1), sagittal plane (2), coronal plane (3), and 3D model view (4).

Then, the area of interest, which was the leaflet insertion area for the mitral annulus, was observed and identified. After that, the embedded paintbrush tool with a brush type circle was selected to place red landmarks along the mitral annulus area on the stack of images [Figure 5.15].

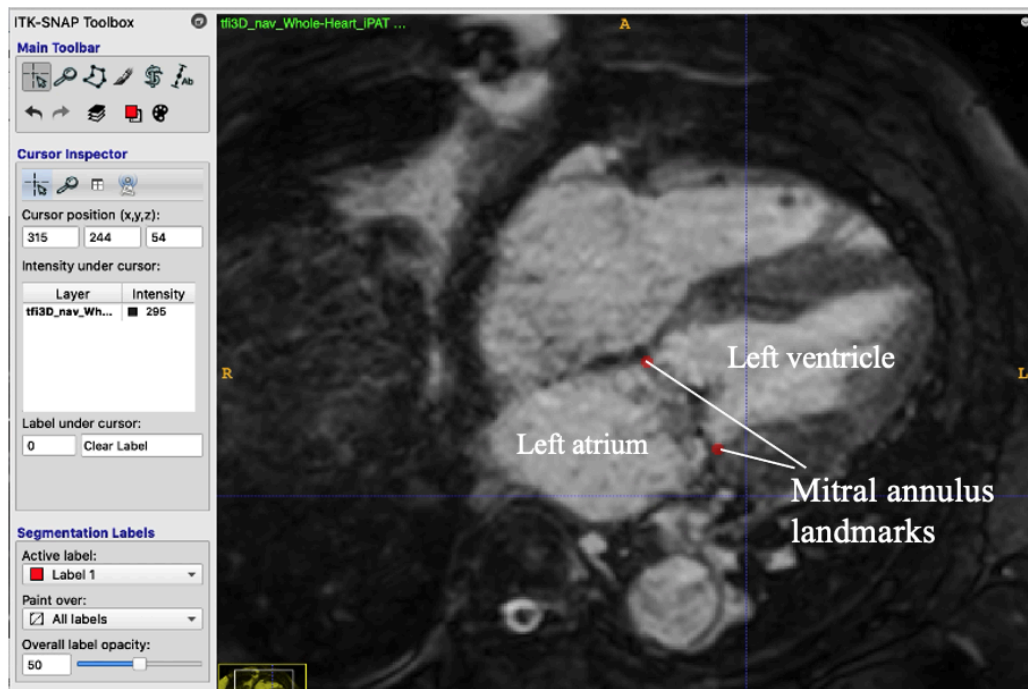


Figure 5.15: ITK-SNAP image for locating the annulus area (marked with red landmarks) using the point-based method process.

When the mitral annulus was not clearly visible in medical data, therefore, additional steps such as contrast adjustment were applied to all layers of the image. For echocardiography, it presents the contrast based on the boundaries between different acoustic impedances. However, the MRI presents contrast based on volume values of the environment of the hydrogen nuclei. To change the image contrast to be more like echocardiography data, edge attraction is a way of converting volume contrast to boundary contrast. In this software, the edge attraction tools were used to better visualise the annulus area, which was a step added on to the point-based steps. This mode was used to adjust the edge blurring, intensity, and contrast of the image. The selection of the edge blurring scales was a necessary and careful step because with a higher number of blurring scales, only the intense edges became visible while the fine details with lower qualities of edge could be lost. Once the red landmarks were allocated and the segmentation was completed [Figure 5.16], the 3D images were exported into an STL file. The next step is to use Blender, an open-source programme to edit 3D models. In Blender, the stl file was imported, the vertex was selected one

by one along the curve, and then the vertex path was connected to form a curve line. In edit mode, the thickness of the curve was added to form the 3D model of the mitral annulus.

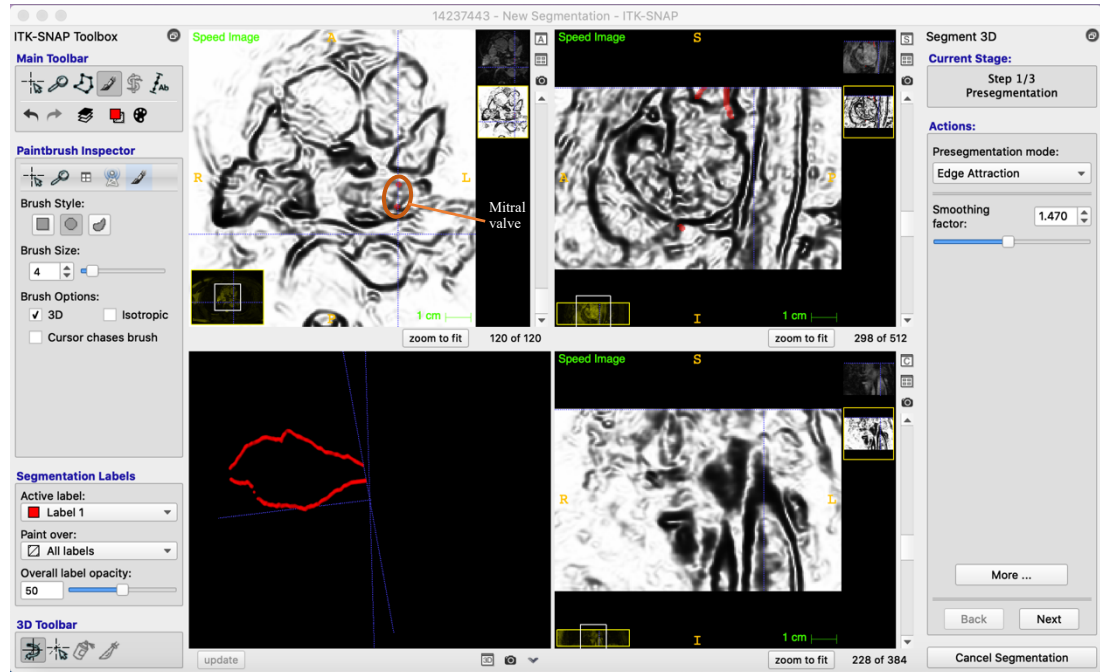


Figure 5.16: The four windows present the medical image after the Edge attraction adjustment and a red model represents the segmented mitral annulus.

5.1.5.2 Results

The results of the study showed 3D models of the mitral valves. It indicated that the two samples of MRI data showed the complete mitral annulus shapes, and those shapes could be extracted using the same point-based method as the method used with echocardiography data. However, with the MRI data, the edge attraction technique was added to the annulus segmentation step. It was used to adjust the contrast of the data to better show the contrast of the data and make it easier to visualise the mitral annulus insertion area.

Figure 5.17 shows the three-dimensional mitral annulus shape extracted from one of the MRI data sets using the point-based method. The extracted annulus shape was the ideal shape for designing a personalised annuloplasty ring.

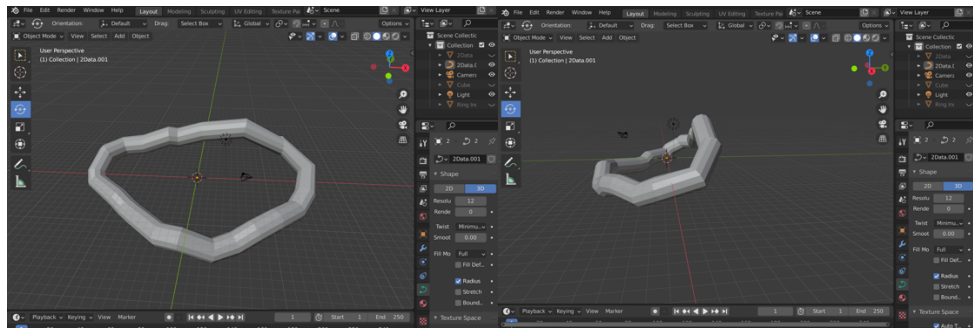


Figure 5.17: The model of the extracted mitral annulus.

Designing a personalised annuloplasty ring based on the extracted annulus shape involves a comprehensive process tailored to a specific medical condition related to mitral valve issues. The initial step entails obtaining high-quality medical imaging data, typically from MRI or echocardiography scans, of patients with the targeted condition. Following this, specialized software is employed for image processing to enhance image quality and accurate segmentation, isolating the mitral annulus from surrounding cardiac structures. The subsequent phase involves 3D reconstruction techniques to convert 2D medical images into a precise 3D model of the mitral annulus. Detailed dimensional analysis is then conducted, investigating the relationships between anteroposterior diameter, transverse diameter, and intertrigonal distance. With these correlations established, the process proceeds to personalised annuloplasty ring sizing and design, determining the optimal size and shape based on the extracted annulus dimensions. Once the design is finalized and validated, the manufacturing phase commences, producing the personalised annuloplasty ring using suitable materials.

5.1.5.3 Discussion

The process of extracting the mitral annulus by using the point-based method and placing landmarks along the intersections between the leaflet's insertion and the mitral annulus was able to be achieved with the MRI data. With the MRI data, the same steps that were applied to the echocardiography could be applied. However, in order to improve the visualisation of the mitral annulus in MRI data, the edge attraction tool

was an additional step needed to change the contrast of the MRI data to be more like the data from echocardiography.

Similar to the processes used to segment the mitral annulus from echocardiography, the tools that were used to extract the annulus shape of MRI data were not complicated and did not require specific skills, supporting the ease of the processing.

For designing and creating the personalised annuloplasty ring shape, the ITK-SNAP and Blender software were sufficient to perform the process and prepare the 3D model ready for 3D-printing, although the steps of creating the personalised annuloplasty ring were more complicated and needed more design steps compared to the 3-Matics software.

Although Mimics and 3-Matics support the ease of the annuloplasty ring design for 3D printing, the software requires a licence, which results in the higher cost of the manufacturing of personalised annuloplasty rings. Meanwhile, ITK-SNAP and Blender are open-source computer software that are also efficient enough to design and create the 3D models of the personalised annuloplasty rings. The study has shown that it is possible to perform the same point-based ring generation using ITK-Snap and Blender in place of Mimics and 3-Matic, respectively. Since the softwares are open source, they can be downloaded and used by any user who has 3D modelling skills, lowering the cost of designing the rings.

In conclusion, this study showed that both MRI and echocardiography data can be used to extract and create the three-dimensional shape of the mitral annulus with the point-based method, although the edge attraction step might be needed to improve the quality of the MRI data in order to support the visualisation of the mitral annulus.

Study 2 Completing the missing posterior annulus of the mitral annulus model

Study 1 has already proven that the patient scan data, the echocardiography, and the 3D magnetic resonance (MRI), together with CAD – CAM software, are able to form

a 3D model of the mitral annulus, which is the model for the personalised annuloplasty ring. However, in some cases when the patient scan data does not show the whole shape of the mitral annulus, it is not possible to visualise and form the whole 3D shape of the mitral annulus. Therefore, the echocardiographic scan, which was used in Chapter 5 Study 1 and Study 2, showed half of the mitral annulus, was used together with R language and Rstudio, a programming language for statistical analysis, to fill in the missing part and fulfil the shape.

5.2.1 Method

The study has found that one of the sample datasets did not allow the visualisation of the leaflet insertion area on the mitral annulus, resulting in the ability to extract only half of the mitral annulus, leaving the other half missing, and therefore, the ability to design a personalised annuloplasty ring out of the data. Therefore, this study determined the process of filling in the missing posterior annulus from the echocardiography using R studio software with the packages that enable statistical analysis.

This study first used Rstudio, and the 34 patient data sets obtained from the cadaveric heart with the healthy mitral valve to establish a shape model of the healthy mitral annulus. The R coding can be found in the Appendix. This process required Generalized Procrustes Analysis (GPA) to translate and rotate the thirty-four shapes of the mitral annulus without scaling, no scaling to preserve the original size of the mitral annulus and to align all the mitral annulus to have the least sum of squared distance before determining the mean shape of the healthy mitral valve. The reason to include only the complete mitral annulus models that were included in the GPA was because if the incomplete one was included, it could interfere with the mean shape.

Thirty coordinates of each of those 34 mitral annuli were identified after the GPA processes. The coordinates were used to determine the mean shape of all points of the mitral annulus, resulting in the mean shape of the mitral annulus from the cadaveric hearts.

The latter step was to estimate the missing half of the mitral annulus using linear regression and Procrustes analysis. The linear regression model was used to find the correlation between the mean shape of the healthy mitral valve and the incomplete shape of the sample mitral annulus that only provided half of the annulus. Therefore, the 12 coefficients were determined for the x, y, and z coordinates, and the regression models were formed, resulting in a model ready for the prediction.

To test the quality of the fit of the linear regression model, the predicted coordinate values obtained from the model and the real coordinates provided from the half-ring data were compared by determining the residuals. The ideal residual is zero, or the sum of the residuals is as close to zero as possible, meaning that the predicted and the real value are approximately the same. For a model that best fits the data, the R-squared must be 1 or as close as possible. On the other hand, if the model is poorly fit with the data, the R-squared will be close to 0. In this study, adjusted R-squared was used because of its ability to make a more accurate view of the correlation between variables than R-squared because R-squared does not consider different independent variables against the model while adjusted R-squared does. R-squared cannot decrease if more independent variables are added to the model, but it will increase once the model is more complex, even if the added independent variables do not add anything to the prediction. Moreover, the adjusted R-squared will increase only if it can reduce the error of the predictions. Therefore, for the model with more than one variable, it is probably better to look at the adjusted R-squared.

Once the linear regression model was found and tested, it was applied to predict the missing half of the mitral annulus. Then, the predicted part filled in with the existing shape, presenting a complete mitral annulus.

After that, the Procrustes analysis was carried out on all thirty-five annuli, thirty-four mitral annulus and a new filled complete annulus to align the new complete shape to the remaining thirty-four shapes in x, y, and z coordinates. Finally, the coordinates of the new filled shape were found.

5.2.2 Results

To determine the mean shape of all points of the mitral annulus from cadaveric hearts, Generalized Procrustes analysis (GPA) was applied to translate and rotate the thirty-four shapes of the mitral annulus without scaling. The optimal mean shape of the complete sample mitral annulus with the dimension of the anteroposterior was measured as 26.73 mm and the dimension of the transverse diameter was 36.56 mm, resulting in a ratio of 3.0:4.1 between the anteroposterior and transverse diameters as shown in Figure 5.18.

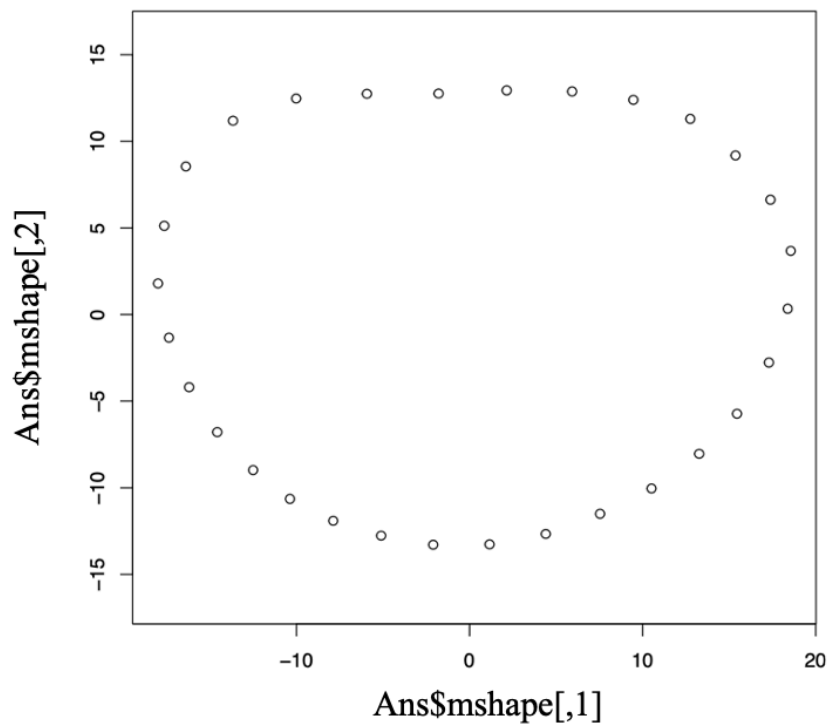


Figure 5.18: The mean shape of the mitral annulus determined from the thirty-four sample cadaveric hearts.

After that, to predict the missing posterior annulus, three linear regression models with 12 parameters were calculated for the affine fit of the half annulus to the mean shape of the rest. The affine fit found from this data was:

$$Y_1 = -9.29 + 1.181x + 0.08y - 1.06z$$

$$Y_2 = -5.14 - 0.08x + 0.87y - 0.51z$$

$$Y_3 = 3.48 - 0.17x - 0.87y + 4.25z$$

where x , y , and z were the input values from the mean shape, while Y_1 is the predicted x coordinate, Y_2 is the predicted y coordinate, and Y_3 is the predicted z coordinate. These models were tested to find the residuals between the predicted values and the observed values of the 15 coordinates provided by the incomplete annulus. The residuals found were less than 2.87 mm for Y_1 and less than 1.99 mm for Y_2 and Y_3 , with the adjusted R-squared equal to 0.9935 for Y_1 , 0.9462 for Y_2 , and 0.7453 for Y_3 , meaning that around 99%, 95% and 75% could be predicted from the linear regression model for x , y , and z coordinates, respectively. Then the regression model was used to predict and fill in the incomplete shape and form the model in Figure 5.19. The black landmarks show the observed data from an MRI scan, while the red landmarks are the predicted data for the other half of the model from the linear regression model. The red landmarks were connected to the black landmarks at the end points to form the complete annulus shape shown in Figure 5.20.

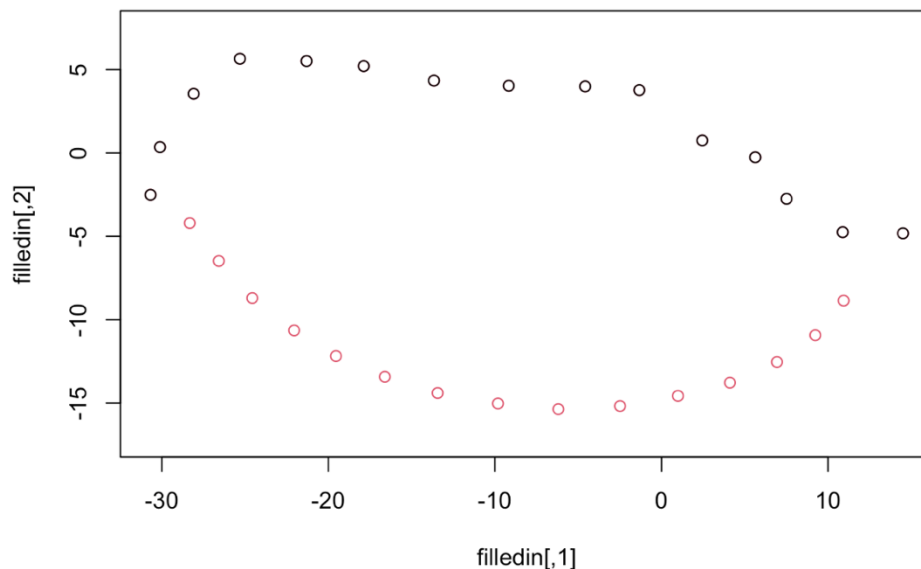


Figure 5.19 The incomplete model shows as black landmarks while the red landmarks are the predicted data from the regression model.

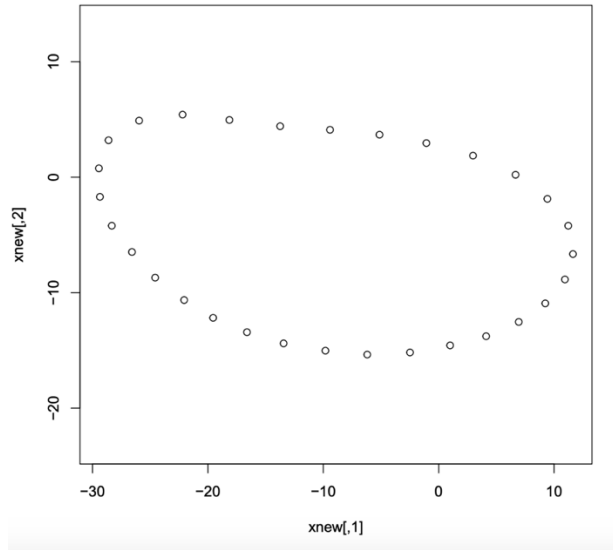


Figure 5.20: The new filled mitral annulus model from the predicted data.

The Procrustes analysis was carried out to rotate the 34 mitral annulus models, which are the blue shapes in Figure 5.21 and the new filled annulus model in red, which was the half annulus model that had already been filled in to complete the annulus shape. This Procrustes analysis was to determine the optimal alignment between the new filled model and the rest. After the Procrustes analysis, the coordinates of the new filled model were found, showing 30 coordinates in 3 dimensions.

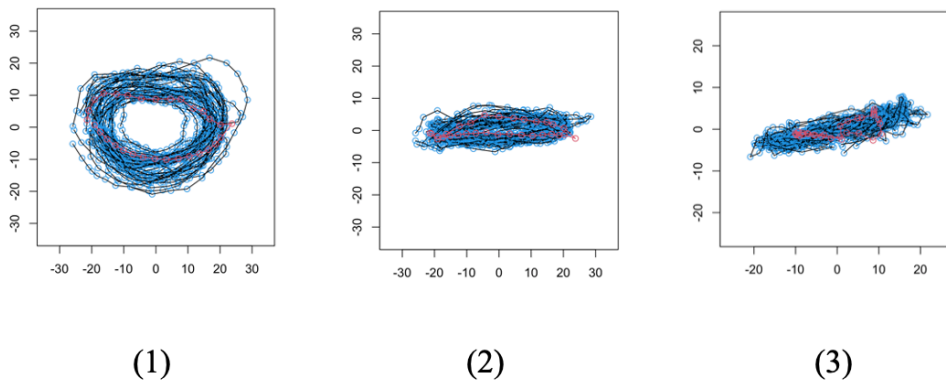


Figure 5.21: Figure 5.20 The filled mitral annulus model (red) and the observed annulus model (blue) were analysed with the Procrustes analysis to analyse the distribution of the models and to provide the minimum sum of squared distance of the models at each landmarkk (1) the Procrustes rotated shapes of x-y coordinates only,

(2) the Procrustes rotated shapes of x-z coordinates only, (3) the Procrustes rotated shapes of y-z coordinates only.

5.2.3 Discussion

The mean shape of the healthy mitral annulus was determined using Generalized Procrustes analysis (GPA). The results presented were that the mean shape had a ratio of 3.0:4.1 between the anteroposterior and transverse diameters, which was slightly different from the ratio cited by the literature in Chapter 2 that the ratio between the anteroposterior and transverse diameters is 3:4. In this study, the linear regression model was used to predict the missing posterior annulus, and it was tested to find the quality of the fit of the model by looking at residuals between the predicted and real values. The ideal residual is zero, or the sum of the residuals is as close to zero as possible, meaning that the predicted and the real value are approximately the same. In this study, the residuals found between the predicted values of the half annulus and the real values from x, y, and z coordinates were relatively small, with the highest value being less than 2.87 mm for x and less than 1.99 mm for y and z coordinates. The adjusted R-squared values found were 0.99, 0.95, and 0.75 for x, y, and z coordinates, respectively. This means that the model can explain 99%, 95%, and 75% of the variability of the data in x, y, and z coordinates, respectively. The F value in the regression is the result of a test in which the null hypothesis is that all of the twelve coefficients found in the regression model are equal to zero, meaning that the model has no predictive capability. In other words, the F statistic test is used to consider whether the twelve coefficients improve the model. The results found that the p-values for the x, y, and z coordinates were $6.794e^{-13}$, $7.721e^{-08}$ and 0.000369, respectively, which were smaller than the significance level (0.05), leading to rejecting the null hypothesis. This has provided sufficient evidence to conclude that the regression model improved the fit and fits the data better than the model with no independent variables.

In conclusion, the R studio, together with the Procrustes analysis and the regression model, were able to fill in the missing posterior annulus found from patient scan data prior to operation, for which this study used MRI scans. Once the process has found

the relationship between the mean shape of the healthy mitral valve and the incomplete mitral valve, predicting the missing part becomes possible.

The potential limitation found in this study was the lack of demonstration regarding the effectiveness of the proposed method in reconstructing a complete annulus when dealing with a reduced dataset. It recognises the need for further validation or testing in scenarios with limited data to ensure the reliability and effectiveness of the proposed reconstruction approach.

Study 3 Personalised annuloplasty ring size selection from patients' pre-operation medical scan image

Following the extraction and 3D modelling of the mitral annulus shape in Study 1 for the design of a personalized annuloplasty ring, the subsequent crucial step involves selecting an appropriate ring size. This decision holds significant importance in minimizing the risk of failure and the need for reoperation. In this section, the 3D models of the two designed personalised rings were sized based on different sizing strategies: the height of the anterior mitral leaflet and the intercommissural distance. The 3D models, which were adjusted to fit each strategy, were then compared to determine the possibility of selecting a ring size pre-operatively for further personalised ring design development.

5.3.1 Method

The method for selecting ring sizes commenced with measuring the intercommissural distance (CC) and the height of the anterior mitral leaflet (AML) from the patients' scan images. There were two sets of MRI that were used in this study. Subsequently, appropriately sized rings were chosen, mirroring the approach used in the cadaveric section (Ohno et al., 2019). This involved aligning the dimensions of the sizers of commercial rings with the actual dimensions of the patients' mitral valve using various sizing strategies.

The sizing strategies employed in this study included the height of the anterior mitral leaflet (AML), intercommissural distance (CC) — true size, intercommissural distance (CC) — one size smaller, and intercommissural distance (CC) — two sizes smaller. The preference for sizing the anterior mitral leaflet (AML) was due to its primary role in mitral valve closure during systole. Thus, a strategy was implemented to ensure that the annulus was approximately the same size as the AML post ring implantation, allowing the remaining AML tissue to fully coapt (Al-Maisary et al., 2017).

These sizing strategies were applied to select ring sizes for four commercial rings: Carpentier-Edward Physio ring (sizes 24–40), Carpentier-Edward Physio ring II (sizes 26–38), St. Jude Medical (SJM) rigid-saddle shape (RSA) (sizes 24-34), and Medtronic 3D Profile (MDT 3DP). The geometries of the selected rings were then compared to the dimensions of the previously generated 3D models of the annulus to assess any deviations between the rings and mitral valve dimensions. This process was repeated not only for true-sized rings but also for one and two sizes smaller rings. The workflow of this study is shown in Figure 5.22

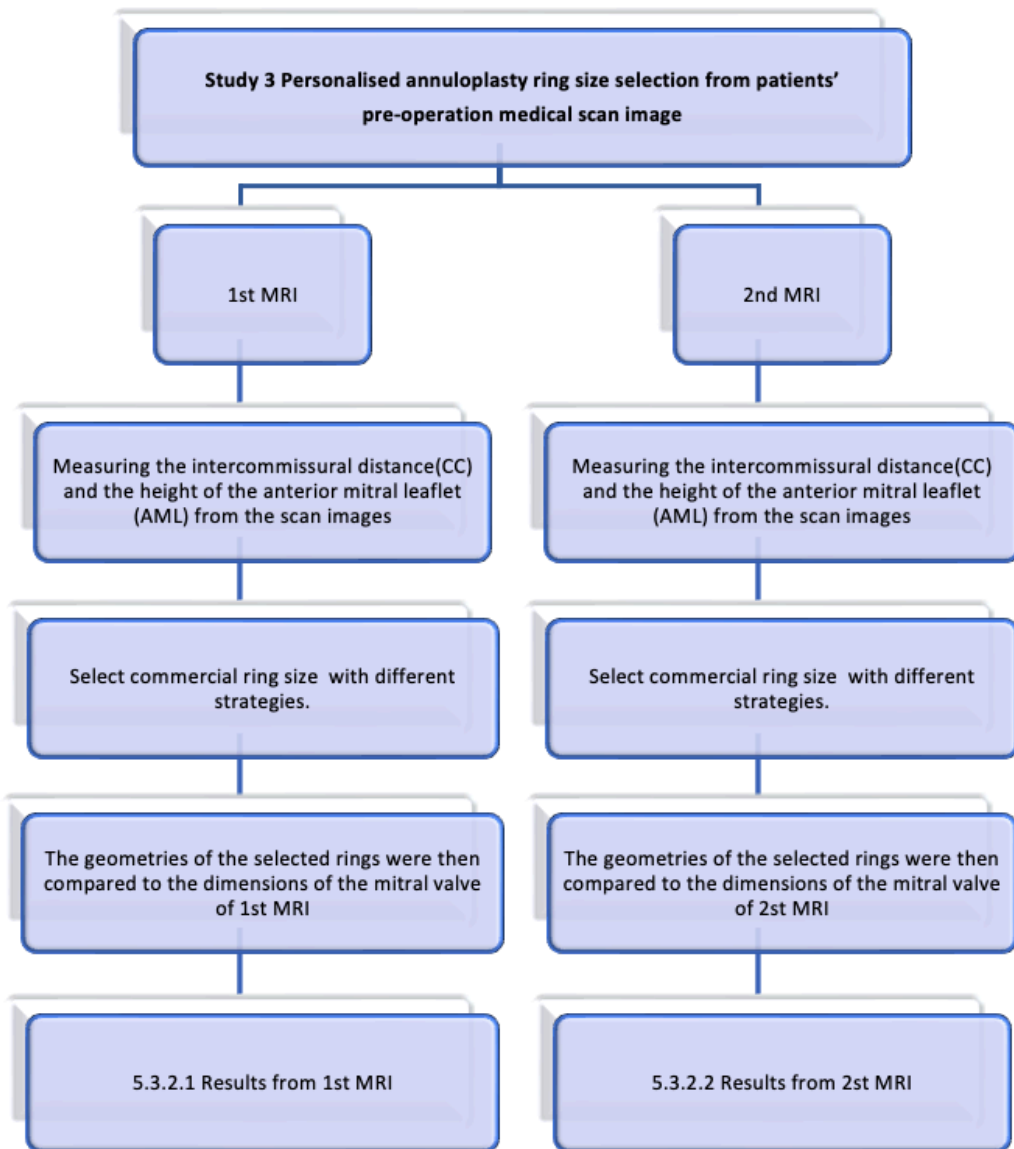


Figure 5.22: Workflow of the Personalised annuloplasty ring size selection from patients' pre-operation medical scan image.

Table 3 Size label and the true dimensions of the annuloplasty rings and sizers: the Carpentier-Edwards Physio annuloplasty ring, the Carpentier-Edwards Physio II annuloplasty ring the St. Jude Medical (SJM) rigid- saddle shape ring (RSA) and the Medtronic 3D Profile.

Size label	Carpentier-Edwards Physio ring (24-40mm)				Carpentier-Edwards Physio II ring (26-38mm)				St.Jude Medical (SJM) rigid- saddle shape (RSA) (24-34mm)				Medtronic 3D profile (MDT 3DP) (24-40 mm)			
	sizer		Ring		sizer		Ring		sizer		Ring		sizer		Ring	
	Anteroposterior	Transverse	Anteroposterior	Transverse	Anteroposterior	Transverse	Anteroposterior	Transverse	Anteroposterior	Transverse	Anteroposterior	Transverse	Anteroposterior	Transverse	Anteroposterior	Transverse
24	18.1	27.1	20.4	27.3					15.8	24.8	21.5	29.3	16.4	27.2	20.6	30.4
26	19.2	29	21.9	29.4	21.12	26.26	19.37	26.2	17.1	26.8	22.3	31.3	17.5	29.3	20.4	30.4
28	20.4	31	23.7	32.4	22.91	27.97	21.1	28.13	18.7	28.9	23.6	33.3	18.6	31.3	22.7	34.4
30	21.6	33	25	34.3	24.42	27.11	22.26	29.99	20	30.8	25.5	35.5	19.8	33.3	24.1	36.2
32	22.8	35	26.2	36.3	24.95	27.55	23.73	32.13	21.4	32.9	26.5	36.9	20.8	35.3	23.6	36.9
34	24.1	37	28.4	38.6	26.25	30.01	26.1	34.48	22.8	34.9	27.8	38.9	21.9	37.2	24.8	38.7
36	25	38.9	29.6	40.9	28.3	32.18	27.47	37.07					22.9	39.3	25.8	40.6
38	25.8	41	31.1	43	30.15	33.57	29.53	37.74					23.9	41.4	27.7	44.5
40	27.8	43	32.9	44.8									25.1	43.4	27.5	44.6

5.3.2 Results

5.3.2.1 Results from the 1st MRI

The results obtained from the first patient's data is shown in Table 5. For the Carpentier-Edward Physio ring, three sizing strategies resulted in selecting the same ring size, which was size 24, while one size bigger (size 26) was selected when the ring was sized by the intercommissural distance. Actually, when the rings were selected by the intercommissural distance, either with their true size or one or two sizes smaller, it should not result in the same ring size. However, due to the limited size, sometimes, smaller size ring was not available, resulting in selecting the same size ring. The situation of having the same size ring for a one-size smaller ring and two-size smaller rings also happened with the Medtronic 3D Profile ring.

Interestingly, for the Carpentier-Edward Physio ring II, the ring selected from the height of the AML was four sizes smaller than sizing from the intercommissural distance, and it was two sizes smaller than sizing from the intercommissural distance with two-size smaller. For the St. Jude Medical ring, the ring selected based on the height of AML was the same size as the ring selected based on the intercommissural distance, which was size 28 and was the biggest size among the methods. Meanwhile, the Medtronic 3D Profile selected from the height of AML was the largest size (size 28), followed by the rings measured based on the intercommissural distance with true size, one size small, and two sizes smaller, respectively.

Table 5 presents the ring size selection for the first set of data. The Carpentier-Edward Physio ring (sizes 24–40), the Carpentier-Edward Physio II ring (sizes 26–38), the St. Jude Medical (SJM) rigid-saddle shape (RSA) (sizes 24-34), and the Medtronic 3D Profile (MDT 3DP) (sizes 24–40) were selected based on the height of the AML and the intercommissural distance with different levels of downsizing.

Table 4: Ring size selection for the first data. Note, AML is the anterior mitral leaflet, CC is the intercommissural distance or the transverse diameter.

Sizing Method	Carpentier-Edward Physio			Carpentier-Edward Physio II			St. Jude Medical			Medtronic 3D Profile		
	size	Ring		size	Ring		size	Ring		size	Ring	
		Anteroposterior (mm)	Transverse or CC (mm)		Anteroposterior (mm)	Transverse or CC (mm)		Anteroposterior (mm)	Transverse or CC (mm)		Anteroposterior (mm)	Transverse or CC (mm)
Height of AML	24	20.4	27.3	26	19.37	26.2	28	23.6	33.3	28	22.7	34.4
CC (true size)	26	21.9	29.4	34	26.1	34.48	28	23.6	33.3	26	20.4	30.4
CC (one size smaller)	24	20.4	27.3	32	23.73	32.13	26	22.3	31.3	24	20.6	30.4
CC (two size smaller)	24	20.4	27.3	30	22.26	29.99	24	21.5	29.3	24	20.6	30.4

The anteroposterior rings were compared and are shown in Figure 5.23. The graph indicates that the anteroposterior diameter of each type of ring is totally different in every ring selection method. For Carpentier-Edward Physio and Physio II, the highest ring heights were used when the rings were selected by using the intercommissural distance- true size. On the other hand, for the St. Jude Medical and Medtronic 3D Profile, the biggest ring heights were selected when the height of AML was applied compared to the other ring sizing strategies.

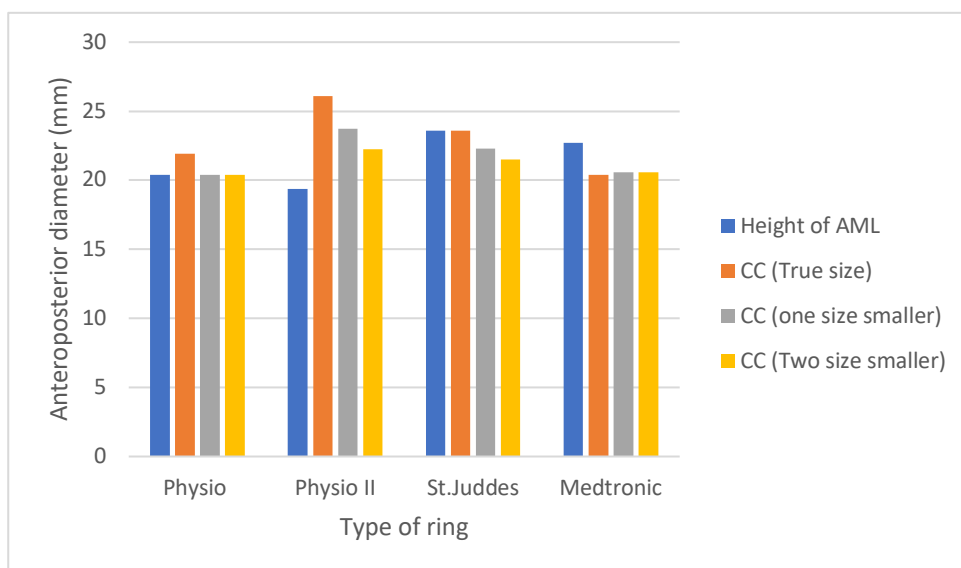


Figure 5.23: The graph presents the height of the rings selected based on the height of the anterior mitral leaflet (AML) and the intercommissural distance (CC). The intercommissural distance (CC) is the measurement between the two commissures, which are the points where the valve leaflets meet and coapt within the mitral valve.

Figure 5.24 presents the residual chart, showing the difference in the dimensions between the ring's height and the mitral valve anteroposterior diameter. The ring that had the least residual in anteroposterior diameter was the Carpentier-Edward Physio ring II when using the intercommissural distance strategy with a one size smaller ring. The Carpentier-Edward Physio II ring was selected by the intercommissural distance, which produced a negative value for residual, meaning that the ring height was larger than the mitral valve anteroposterior diameter and was not able to reduce that dimension when implanted. In contrast, the highest difference between the dimensions was found in the Carpentier-Edward Physio II when using the height of the AML strategy. This led to the highest mitral valve reduction in the anteroposterior dimension.

Figure 5.25 shows the difference between the ring height and the anterior mitral leaflet (AML) diameter. The height of the rings was larger than the AML, presenting positive values. In contrast to the results found in Figure 5.22, the Carpentier-Edward Physio II had the closest height to AML when selected using the height of AML strategy.

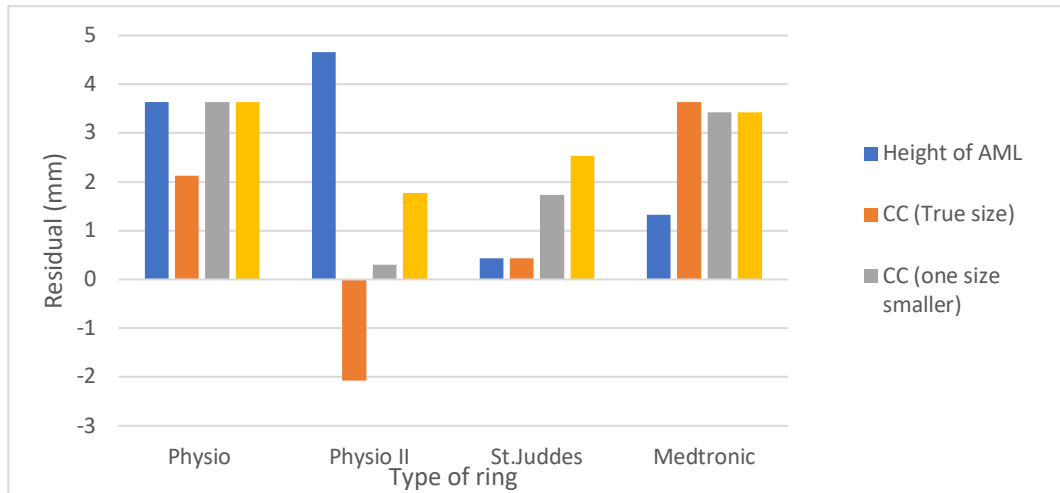


Figure 5.24: The residual charts show the anteroposterior diameter of the mitral valve minus the ring height when the rings were selected based on the height of the anterior mitral leaflet (AML) and the intercommissural distance (CC).

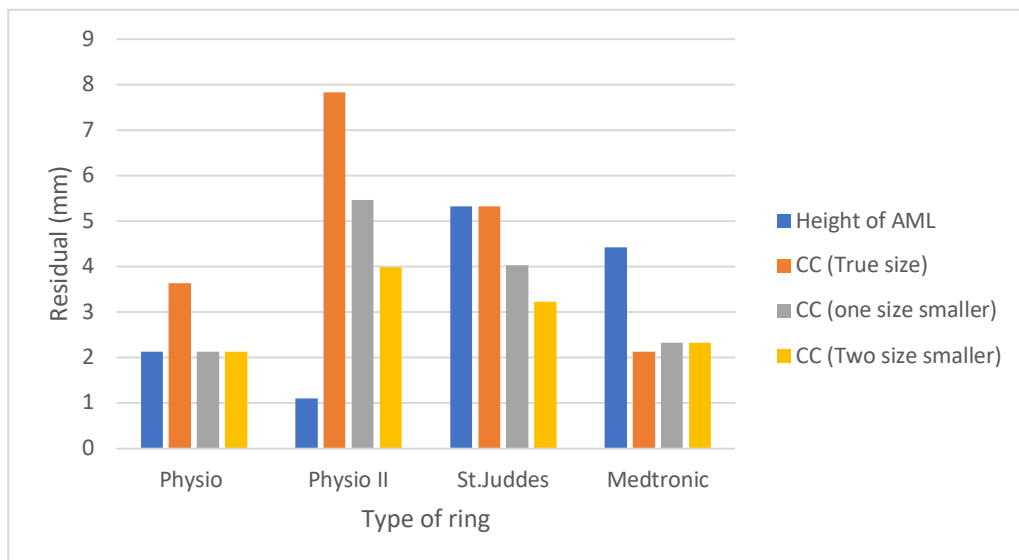


Figure 5.25 The residual charts show the ring anteroposterior minus the height of anterior mitral leaflet of the mitral valve when the rings were selected based on the height of the anterior mitral leaflet (AML) and the intercommissural distance (CC).

The intercommissural distance of the rings are presented in Figure 5.26. Again, the ring dimensions were totally different between each ring type, ranging from around 26 to 34.5 mm, with the smallest ring width (26.2 mm) coming from the Carpentier-Edward Physio II when chosen from the height of the AML.

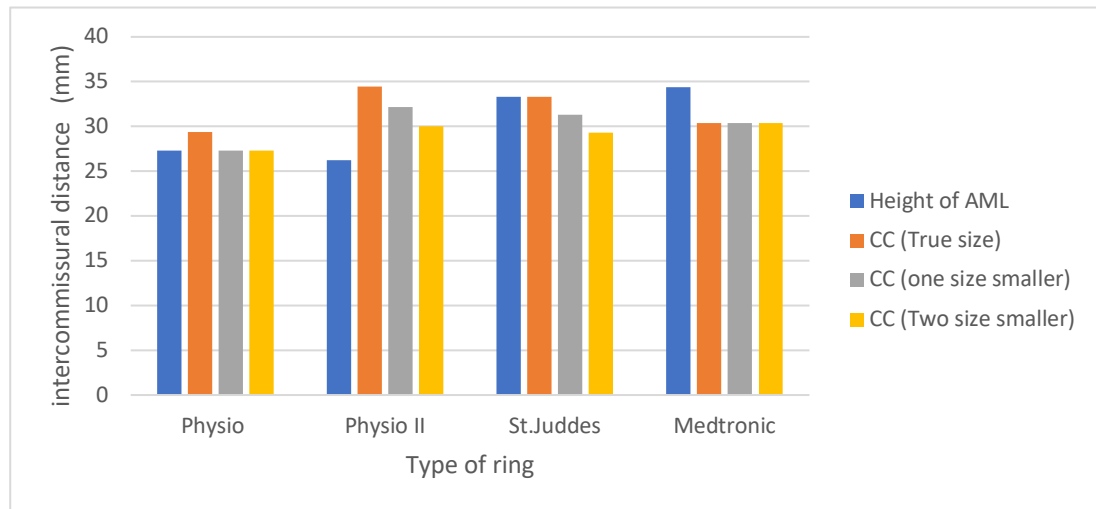


Figure 5.26: The graph presents the intercommissural distance of the rings selected based on the height of the anterior mitral leaflet (AML) and the intercommissural distance (CC).

The intercommissural distance of the rings and the mitral valve were compared in Figure 5.27. The positive values indicate that the mitral valve’s intercommissural distance diameter is wider than the rings, while the negative values indicate that the rings have a larger width than the mitral valve’s. The ring that had the smallest transverse diameter was the Carpentier-Edward Physio II by using the height of the AML strategy, demonstrated the highest reduction in the mitral valve intercommissural distance when implanted. Also, the Carpentier-Edward Physio II ring selected using the intercommissural distance strategy had the biggest intercommissural distance among the rings and produced a -4.2 mm residual value, showing that the ring is 4.2 mm wider than the transverse diameter of the mitral valve when implanted. Interestingly, all of the Medtronic 3D Profile had a width larger than the mitral valve, showing the negative values in every sizing strategy.

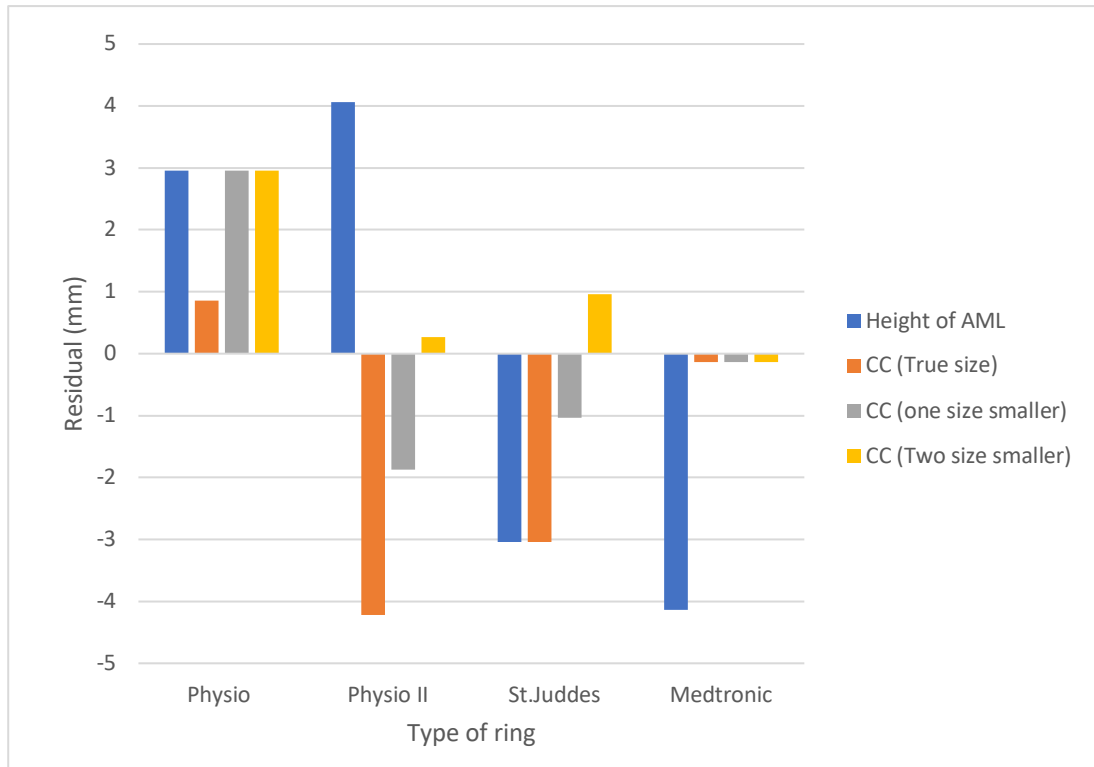


Figure 5.27: The residual chart shows the intercommissural of the mitral valve minus the ring width when the rings were selected based on the height of the anterior mitral leaflet (AML) and the intercommissural distance (CC).

5.3.2.2 Results from the 2nd MRI

The ring size selection for the second patient's data is shown in Table 6. Similar to the first data results, for Carpentier-Edward Physio, the ring selected from the height of AML was the same size as the ring selected from the intercommissural distance with one size smaller ring, while the true size ring selected from the same method was the largest one among the four methods. For Carpentier-Edward Physio II, the ring selected from the height of AML and the intercommissural distance were even further apart than the results obtained from the first data. The ring selected based on the height of the AML was size 26, which was six sizes smaller than the ring selected based on the intercommissural distance (size 38). Similar to the Carpentier-Edward Physio ring, the St. Jude medical ring selected based on the height of AML was the same size as

the ring selected from the intercommissural distance-one size smaller. Meanwhile, the Medtronic 3D Profile selected based on the height of AML and the intercommissural distance were the same size and were larger than the other sizing method

Table 5: shows the ring size selection for the second data. The Carpentier-Edward Physio ring (size 24-40), the Carpentier-Edward Physio II ring (size 26-38), St. Jude Medical (SJM) rigid- saddle shape (RSA) (size 24-34), and Medtronic 3D Profile.

Sizing Method	Carpentier-Edward Physio			Carpentier-Edward Physio			St. Jude Medical			Medtronic 3D Profile		
	size	Ring		size	Ring		size	Ring		size	Ring	
		Anteroposterior (mm)	Transverses or CC (mm)		Anteroposterior (mm)	Transverses or CC (mm)		Anteroposterior (mm)	Transverses or CC (mm)		Anteroposterior ((mm)	Transverses or CC (mm)
Height of AML	30	25	34.3	26	19.37	26.2	32	26.5	36.9	32	23.6	36.9
CC (true size)	32	26.2	36.3	38	29.53	37.74	34	27.8	38.9	32	23.6	36.9
CC (one size smaller)	30	25	34.3	36	27.47	37.07	32	26.5	36.9	30	24.1	36.2
CC (Two size smaller)	28	23.7	32.4	34	26.1	34.48	30	25.5	35.5	28	22.7	34.4

*AML is the anterior mitral leaflet, CC is the intercommissural distance or transverse diameter

The ring anteroposterior diameters were compared and are shown in Figure 5.28. The graph indicates that the anteroposterior diameter of each type of ring was different, depending on the ring selection method. Among the rings, the Carpentier-Edward Physio II had the shortest anteroposterior diameter when it was selected using the height of AML strategy, making it the ring that was most likely to reduce the mitral valve anteroposterior diameter when implanted.

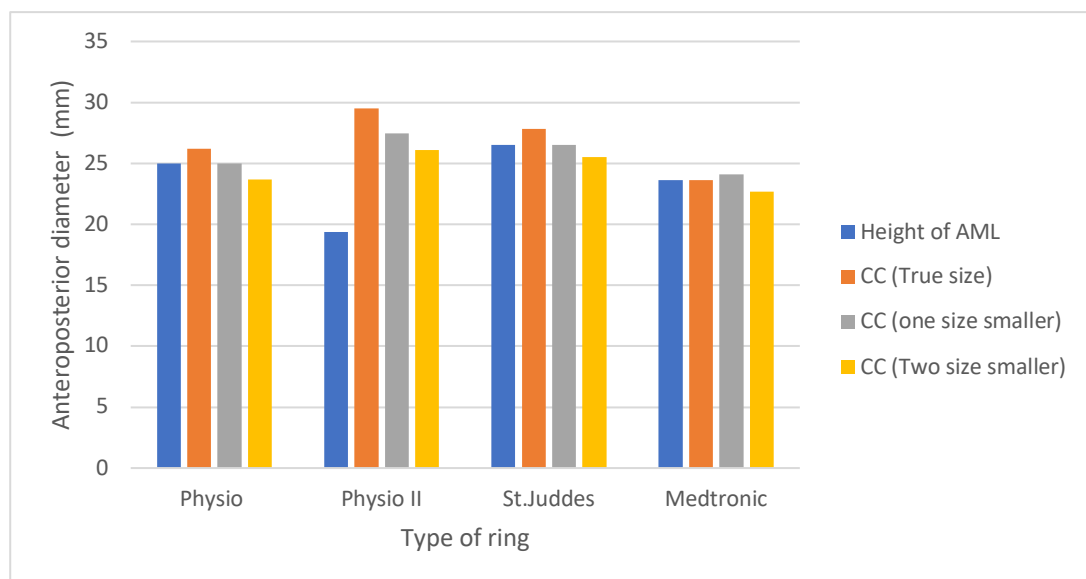


Figure 5.28: The graph presents the anteroposterior diameter of the rings selected based on the height of the anterior mitral leaflet (AML) and the intercommissural distance (CC).

Figure 5.29 is the residual chart, which shows the difference in size between the rings and the anteroposterior diameter of the mitral valve. The ring that had the least residual was the St. Jude medical ring when it was selected using the height of AML and the intercommissural distance strategy with a one-size smaller ring. Negative values were found in some of the Carpentier-Edward Physio II and St. Jude medical rings, meaning that the ring height was larger than the mitral valve anteroposterior diameter and would not be able to reduce that dimension when implanted. In other words, the highest difference between the dimensions was found in the Carpentier-Edward Physio ring II when using the height of the AML strategy. This highest residual leads to the highest mitral valve reduction in the anteroposterior dimension.

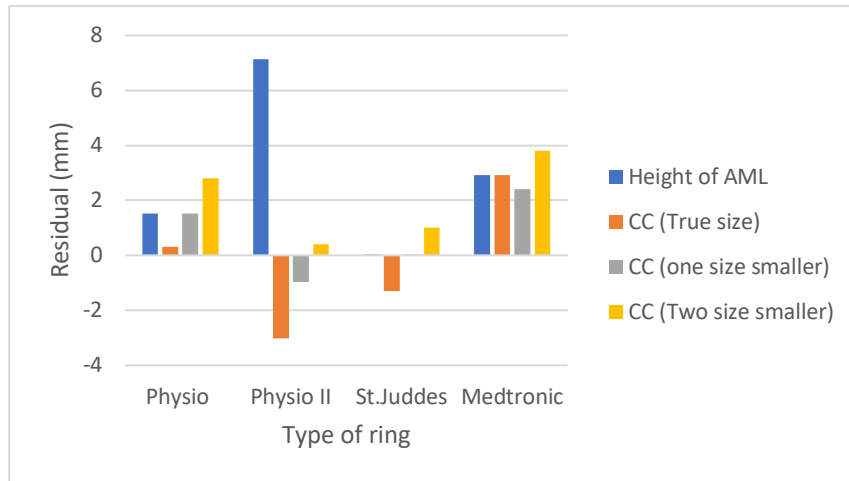


Figure 5.29: The residual charts show the anteroposterior diameter of the mitral valve minus the ring height when the rings were selected based on the height of the anterior mitral leaflet (AML) and the intercommissural distance (CC).

Figure 5.30 shows the difference between the ring height and the anterior mitral leaflet (AML) diameter. When the height of the rings was greater than the AML, positive values were presented, while those less than the AML were presented as negative values. The only ring height that was smaller than the height of the AML was the Carpentier-Edward Physio II, while the ring that had the closest height to the AML was from the Medtronic 3D Profile when selected with the intercommissural with two sizes smaller strategy.

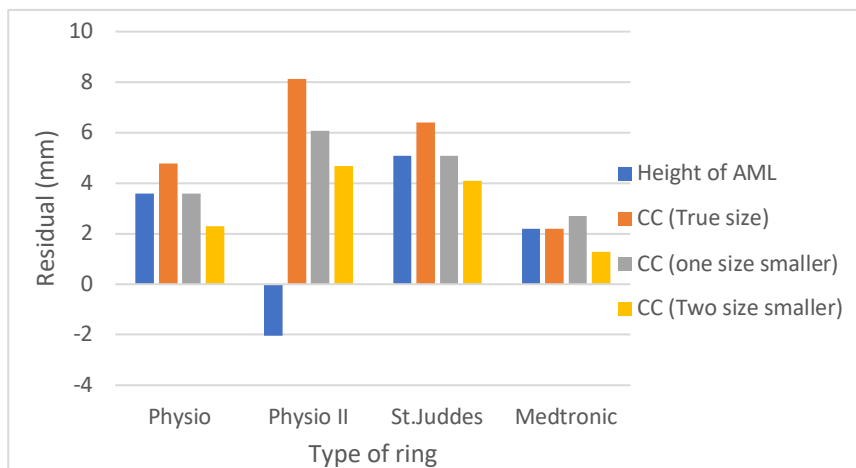


Figure 5.30 The residual charts show the ring height minus the height of anterior mitral leaflet of the mitral valve when the rings were selected based on the height of the anterior mitral leaflet (AML) and the intercommissural distance (CC).

The intercommissural distance of the rings are presented in Figure 5.31. The rings width was still different between each ring type, ranging from around 26.0 to 39.0 mm. The smallest ring width was from the Carpentier-Edward Physio II when chosen from the height of AML (26.2 mm), and the largest one was found from the St. Jude when chosen from the intercommissural distance (38.9 mm).

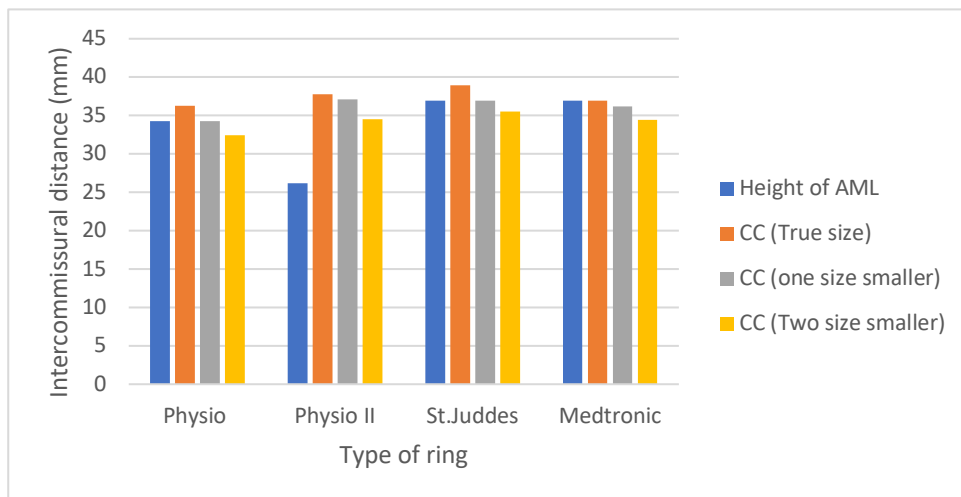


Figure 5.31: The graph presents the intercommissural distance (mm) of the rings selected based on the height of the anterior mitral leaflet (AML) and the intercommissural distance (CC).

The comparison between the intercommissural distance of the rings and the mitral valve is presented in Figure 5.32. The positive values indicate that the mitral valve's intercommissural distance was wider than the ring's, while the negative values indicate that the rings had a larger intercommissural distance than the mitral valve's and were not able to reduce the width of the mitral valve after implantation. The ring that had the smallest width was the Carpentier-Edward Physio II when selected using the height of the AML strategy, which produced an 8.8 mm smaller width than that of the mitral valve, demonstrating the highest reduction in the mitral valve intercommissural distance when implanted. In contrast, the St. Jude medical ring selected by the intercommissural distance strategy had the biggest width among the rings, and produced -3.9 mm of the residual value, showing that the ring is 3.9 mm wider than the intercommissural distance of the mitral valve. Importantly, all of the St. Jude medical rings had a width larger than the mitral valve, showing the negative values in every sizing strategy.

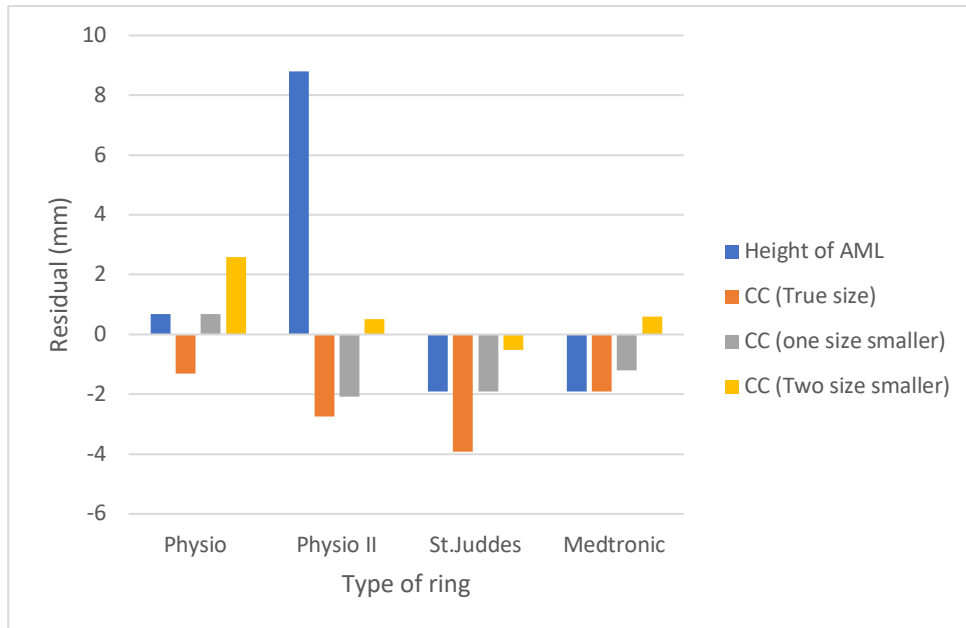


Figure 5.32: The residual chart shows the comparison between the transverse diameter of the rings and the mitral valve selected based on the height of the anterior mitral leaflet (AML) and the intercommissural distance (CC).

5.3.3 Discussion

This section was an illustration of the method to select ring size pre-operatively from patients scan data. For the first and second sets of data, the number of commercial rings was selected based on the height of the AML and the intercommissural distance of the mitral valve with a true-size ring, a one-size-smaller ring, and a two-size-smaller ring. It was found that the size of the Carpentier-Edward Physio ring was the same when sized from the height of the AML and the intercommissural distance with one size smaller rings. However, for the first set of data, the two-size smaller ring was the same as the one-size smaller ring when sized from the intercommissural distance. Actually, they should not have the same size, but because of the limited ring sizes, the two-size smaller ring cannot be smaller than the smallest available ring. This situation also occurred with the Medtronic 3D Profile in the first set of data, leading to the rings selected from the intercommissural distance with one smaller ring and two smaller rings being the same size. This situation can occur when the mitral valve is small, and the available commercial ring is not small enough to support the levels of an undersized ring.

For the Carpentier-Edward Physio II ring, the ring size selected from the height of AML was the smallest one among the other sizings, making it the method most likely to reduce the highest levels of the dimensions of the mitral valve among the four methods in these two cases. For the St. Jude Medical ring, the larger ring size was selected by sizing from the intercommissural distance, which was the same as the results found from the Carpentier-Edward Physio ring and Physio II. However, the first data found that the rings selected from the height of AML and the intercommissural distance were the same size. This situation was also found in the second set of data with the Medtronic 3D Profile. In contrast, the bigger Medtronic 3D Profile was selected when using the height of AML compared to the other methods. The results have shown that for these two pilot cases, the ring size selection of the different sizing strategies was varied for every ring type that has been used in this study. Therefore, this study has found that the different sizing strategies directly affect the ring size selection, affecting the implantation outcome and the ability to reduce the mitral annulus dimensions.

In order to determine the difference in the dimensions and to determine how much the rings can reduce the mitral valve dimensions after implantation, the selected rings were compared to the mitral valve dimensions: the height and width of the mitral valve, and the height of the anterior mitral leaflet. By emphasising reducing the overall dimensions of the mitral valve, the height and width of the mitral valve were considered. The outcome was evaluated by determining the residual differences in the height and width of the mitral valves and the rings. The higher residuals show a higher ability to narrow down the mitral valve dimensions. Meanwhile, the negative value of the residuals shows that the ring dimension is larger than that of the mitral valve, lacking the efficiency to reduce the mitral valve in that dimension. The outcome from the first and second data has presented the resemblance. It has been shown that the ring that has the greatest residuals and the ability to narrow down the mitral valve in both the height and width dimensions is the Carpentier-Edward Physio II when it is sized by the height of the AML strategy. This section has demonstrated the possibility of selecting a ring size that would fit the dimensions of the patients' mitral valve from their scan images, which can be done before the operation and is beneficial for designing a personalised annuloplasty ring size to fit individuals.

Conclusion

One of the major aims of this study was to determine whether personalised annuloplasty rings could be designed prior to surgery from patient scan images. The results of this study have shown that the patients scan images, both echocardiography and MRI data, allow the visualisation of the mitral annulus, which could be extracted and transformed into a 3D model. This study has used various software to visualise the data and form and edit 3D models. It has been demonstrated that software, either with a paid licence such as Materialise with Mimics and 3-Matics or open-source software such as ITK-SNAPs and Blender, are able to design a 3D model of the mitral annulus prior to the design of personalised annuloplasty rings. However, the methods required for each software were different as they did not have the same functions and tools.

For the method to determine the shape of the mitral valve, the research shows that Materialise Mimics with 3-Matics is able to form the 3D shape of the mitral annulus and replicate its shape at different stages from echocardiographic data. The most accurate method that has been performed is the point-based method, where the mitral annulus is marked with red landmarks to present the annulus area on each of the scans. Nevertheless, this method produces errors showing differences in mitral valve shape from the same image of echocardiographic data. Therefore, a later study was tested to determine error statistical parameters. To show the potential variation of the 3D modelling process on the mitral valve dimension when the process is repeated, the use of Materialise Mimics with 3-Matics, a point-based method, has been studied to find the possibility of error occurrence that can affect the process of generating a 3D structure of the mitral annulus from patient scan data. The results showed no significant differences among the five repeated trials. It has presented the work to ensure that the Materialise software and the point-based method, in combination with information from medical imaging, are a reliable and repeatable method that provides good results. Therefore, the use of this technique together with medical imaging is suitable for assessing the geometry of the mitral valve.

Future studies are therefore to use this technique in developing a personalised annuloplasty ring design and developing sizing strategies in order to optimise the outcome of the mitral valve repair.

Even if it were possible to create the 3D model of the mitral annulus from the patient's scan images, there were situations when the mitral annulus found in the scan images could not be seen, showing half of the annulus. This has led to the study to fill in the missing part which was the posterior annulus using R Studio. R Studio uses the R language to perform statistical analysis functions that are embedded in the software. In this study, Generalise Procrustes analysis and a linear regression model were used to determine the relationship between the thirty-four observed mitral annulus that show the complete shape and the data that showed only half of the annulus. Once the linear regression was determined, the missing posterior annulus locations were predicted. The predicted data was joined to the remaining parts, forming the complete shape of the mitral annulus. This study has demonstrated methods to fill the missing posterior annulus from the prediction using R Studio.

By determining the size of the commercial annuloplasty rings to fit each of the two sets of data pre-operatively with the commercial rings used in the study, it has been shown that the ring that has the greatest ability to narrow down the mitral valve in both the height and width dimensions is the Carpentier-Edward Physio II when it is sized by the height of the AML strategy. This study presented the possibility of selecting the annuloplasty ring size from medical images taken prior to the operation, which is important step for designing a personalised annuloplasty ring to fit an individual.

Limitations of this experiment are the limited number of commercial rings, the ring information used in the study, and the limited number of patient scan data

Chapter 6 Discussion

This discussion chapter covers the major findings from the studies. It explains how the obtained results contribute to the literature on annuloplasty rings, specifically personalised annuloplasty rings. Moreover, this chapter shows how the outcomes achieved the research aims and objectives.

6.1 General discussion and major findings

This research significantly contributes to enhancing the selection process of current commercial rings, guiding the consideration of personalised rings, evaluating the potential for improved commercial ring design, and outlining the methodology for personalised annuloplasty ring designs. The key outcomes are as followed.

To better select of current commercial rings, The study assessed the dimensions of healthy mitral valves and compared them with commercially available rings, the study provides insights into the suitability of existing rings. It identifies which commercial rings closely match the dimensions of a healthy mitral valve, aiding surgeons in making more informed choices during mitral valve repair surgeries. The research highlights the specific sizing strategies that align commercial rings with the anatomical variations observed in mitral valves.

The study underscores the high variability in individual mitral valve dimensions, emphasizing the need to consider personalised annuloplasty rings. It provides a rationale for opting for personalised rings in cases where standard-sized commercial rings may not precisely replicate the unique geometry of a patient's mitral valve. Insights into the limitations of commercial rings in accommodating diverse anatomies guide the decision-making process on when to shift towards personalised solutions.

In addition, the research assesses the accuracy of current commercial rings in mimicking healthy mitral valve dimensions, offering a basis for evaluating their design efficacy. It identifies potential areas for improvement in the design of

commercial rings, providing valuable feedback to manufacturers. Findings may contribute to the optimization of existing commercial ring designs to better align with the varied anatomical characteristics of mitral valves.

The study outlines a comprehensive methodology for designing and manufacturing bespoke annuloplasty rings tailored to individual patients. It details the use of patient-specific scan data, emphasizing the importance of considering both shape and size in the design process. The research suggests employing advanced tools and software, such as ITK-SNAP and Blender, for accurate 3D modelling and customization.

The proposed workflow involves a step-by-step process, including gap filling using statistical analysis in R Studio, offering a clear guide for researchers.

In summary, this work serves as a foundational resource that not only refines the selection of current commercial rings but also advocates for the consideration of personalised solutions. Additionally, it contributes insights that could potentially inform the future design enhancements of commercial annuloplasty rings.

6.1.1 Assessment of the mitral valve geometry

The objective of this study was to gain a profound understanding of the geometry of commercial annuloplasty rings, specifically designed with a 3:4 ratio between the anteroposterior and transverse diameters to emulate the ideal geometry of a healthy mitral valve. To achieve this, an assessment of mitral valves from heart disease-free cadavers was conducted, aiming to ascertain the authentic geometry of the mitral valve before the onset of any conditions that could impact its shape.

The assessment involved three distinct measurement methods: manual measurement using callipers, computer measurement with a single image, and computer measurement following 3D reconstruction. The findings revealed that manual measurement, allowing direct tactile examination, was comparatively simpler than computer-based methods, especially when using a single image. The computer measurement with a combined image necessitated the reconstruction of 3D models from images taken at varying angles, introducing potential errors during the merging process, and requiring additional steps for accurate measurement. Conversely,

measuring from a single image, without the need for merging, exhibited fewer errors, as it presented the original landmark locations.

While each method had its limitations, the study found no significant differences in the results obtained. Crucially, the average geometry of healthy mitral valves adhered to the 3:4 ratio, commonly employed in commercial annuloplasty rings to mimic the pre-dilation mitral valve shape. This reaffirms the applicability of the 3:4 ratio as an ideal design parameter for annuloplasty rings. However, the substantial variability in individual mitral valve dimensions among the donated cadavers underscores the need to consider personalised annuloplasty rings as an alternative to standard-sized commercial rings.

Another crucial finding was the identification of the 3.4:3:4 ratio between the intertrigonal distance, anteroposterior diameter, and transverse diameters in healthy cadaveric hearts. This ratio, studied to predict mitral valve dimensions before dilation using the intertrigonal distance, presents an avenue for determining appropriate ring sizes to match the original size of the mitral valve. This innovative approach offers a promising method for personalised annuloplasty ring selection based on individual patient characteristics, potentially revolutionizing mitral valve repair procedures.

6.1.2 Annuloplasty ring sizing with intertrigonal distance

Choosing an appropriate ring size is a critical aspect of mitral valve repair surgery, as the implantation of an improperly sized ring can significantly impact long-term outcomes and the durability of the repair (Ohno et al., 2019). Striking the right balance is crucial, as insufficient downsizing may fail to restore mitral valve function, while excessive downsizing can lead to complications such as dehiscence, restricted valve movement, and mitral stenosis, ultimately resulting in the need for reoperation. Despite the importance of this decision, there is a lack of scientific justification for optimal ring choice and size selection, often relying on surgeons' subjective judgment based on their experience, preferences, and training.

In the context of creating personalised annuloplasty rings, considerations extend beyond shape to include size. Understanding the relationship between ring sizing strategies and commercially available rings raises questions about the degree of downsizing required and which ring type closely matches the dimensions of a healthy mitral valve in terms of anteroposterior and transverse diameters. Consequently, this study aimed to determine whether the commercial rings investigated—the Medtronic 3D Profile, St. Jude Medical (SJM) rigid-saddle shape ring (RSA), and the Carpentier-Edwards Physio annuloplasty ring—presented dimensions identical to those of a healthy mitral valve, effectively mimicking its original dimensions.

The findings revealed that none of the commercial rings matched the dimensions of the mitral valve when selected based on the intertrigonal distance, resulting in errors in both anteroposterior and transverse diameters. However, the study indicated that the Carpentier-Edwards Physio ring closely approximated the dimensions of healthy mitral valves, producing the fewest errors. This was followed by the St. Jude Medical (SJM) rigid-saddle shape (RSA) and the Medtronic 3D Profile (MDT 3DP). It is noteworthy that even when selected based on intertrigonal distance, the Carpentier-Edwards Physio rings did not precisely match the dimensions of healthy mitral valves, exhibiting variations in the transverse distance and random fluctuations in the anteroposterior diameter.

Subsequent research further refined these findings, suggesting that the one-size smaller ring of the Carpentier-Edwards Physio ring closely aligned with the transverse diameter, while the true-size ring closely matched the anteroposterior diameter of the mitral valve geometry. This understanding supports the use of personalised annuloplasty rings, highlighting the intricacies involved in achieving optimal sizing for mitral valve repair procedures.

6.1.3 Personalised annuloplasty ring design to fit individuals

This research marks a significant advancement in the pursuit of personalised annuloplasty rings for mitral valve repair. The comprehensive exploration of methodologies, encompassing both echocardiography and MRI, for designing a

bespoke annuloplasty ring demonstrates a meticulous approach to patient-specific solutions. The comparison between the thresholding and point-based methods, facilitated by cutting-edge software like Materialise and open-source alternatives such as ITK-SNAP and Blender, highlights the adaptability of techniques to reduce design costs without compromising accuracy. Another software of extracting and 3D modelling the mitral annulus shape was applied to fill in the missing part of the 3D model.

The integration of R Studio into the workflow, enabling the prediction of missing posterior annulus, addresses a critical challenge in the design process. This not only enhances the feasibility of creating personalised rings but also underscores the interdisciplinary nature of this research, merging medical imaging, software development, and statistical analysis. Besides obtaining the shape of the mitral annulus for designing the annuloplasty ring, it is also crucial to explore the possibility of predicting the size of the annuloplasty ring from medical scans.

The exploration of ring sizing strategies, especially the correlation between commercial ring selection and mitral valve dimensions, provides valuable insights. The pilot study, although with a limited number of cases, lays the groundwork for the potential selection of ring size from preoperative data, a crucial step towards individualized interventions.

Despite the commendable achievements, certain limitations are inherent in this study. The reliance on cadaveric hearts for determining mitral valve dimensions introduces a potential gap in replicating real-world patient scenarios. The small sample size, though consistent with pilot studies, calls for future investigations with a more extensive and diverse patient pool to enhance the generalizability of findings.

Moreover, the use of open-source software, while cost-effective, introduces certain limitations in terms of advanced 3D editing capabilities. Future work could explore collaborations or advancements in open-source tools to bridge this gap.

To fully realize the potential of personalised annuloplasty rings, future research should aim at establishing a standardized approach that seamlessly integrates into clinical

workflows. Collaboration with medical professionals, including surgeons and cardiologists, is imperative to refine and validate the developed methodologies in real-world surgical scenarios.

The study sets the stage for further exploration into predictive modelling for annuloplasty ring sizing, potentially incorporating machine learning algorithms. This could lead to the development of a robust decision support system for clinicians, aiding in the selection of the most appropriate ring size for individual patients.

6.2 Revising aim and objectives

This research has been studied to assess the mitral valve geometry in order to develop a method to design a personalised annuloplasty ring for patients who suffer from mitral regurgitation. This research has

- Determined the methods for the mitral valve measurements.
- Investigated the geometry of the mitral valves in healthy cadaveric hearts
- Determined the ratio between the mitral valves' anteroposterior and transverse diameters.
- Determined the relationship between the intertrigonal distance, anteroposterior, and transverse diameter of the mitral valve.
- Investigated the possibility of using intertrigonal distance to predict healthy mitral valve dimensions.
- Investigated the application of selecting ring size from an intertrigonal distance strategy.
- Developed the method to design a personalised annuloplasty ring with echocardiography and MRI.
- Determined the method to fill in the gap of the mitral annulus model.
- Determine the possibility of personalised annuloplasty ring sizing pre-operatively.
- Investigated ring size selection from different sizing strategies.

6.3 Limitations

This research study has several limitations that need to be considered. Firstly, the sample size of patient scan data used in the study is relatively small, and this may limit the generalizability of the findings to a broader population. Additionally, the study faced constraints in accessing certain patient data, which restricted the overall comprehensiveness of the research. Financial limitations also impacted the study, particularly in terms of software availability and the inability to acquire commercial rings due to their high costs. Consequently, information about the rings was derived from existing literature, influencing the overall scope of the research.

This thesis encompasses various aspects aimed at enhancing mitral valve repair procedures, particularly through the development and assessment of annuloplasty rings. The initial focus involves evaluating the 3:4 ratio between anteroposterior and transverse diameters of the mitral annulus, commonly used in commercial annuloplasty ring designs. Through cadaveric dissection and physical measurements, the study investigates the validity of this ratio and explores other mitral valve dimensions for potential optimization of ring designs. Furthermore, the development of 3D modelling software for isolating and reconstructing the mitral annulus from patient scans contributes to personalised annuloplasty ring design. The study suggests that commercial rings may not adequately replicate individual mitral valve shapes, emphasizing the necessity of personalised annuloplasty rings for optimal mitral valve function.

Chapter 7 Conclusion and Future Directions

7.1 Conclusion

This study outlines the exploration of creating personalised annuloplasty rings using patients' scan images for potential applications in mitral valve repair. The research demonstrates the feasibility of designing annuloplasty rings tailored to individual needs.

For assessing mitral valve geometry, three measurement methods were employed: manual measurement with a caliper, computer measurement with a single image, and computer measurement with a combined image. Recommended methods include manual measurement for tactile examination and computer measurement with a combined image for multi-angle visualization, aiding mitral valve model rotation. Mitral valves measured from a single image with all measuring points displayed had fewer errors than those measured from a combined image, possibly due to gradual error accumulation and shifting of landmarks in the combining processes. However, in some cases, capturing all landmarks within an image was challenging due to mitral valve complexity.

The study revealed that average dimensions of healthy mitral valves from donated cadavers aligned with the commonly cited 3:4 ratio between anteroposterior and transverse diameters, a standard for commercial annuloplasty rings. Variability in individual dimensions suggests considering personalised annuloplasty rings as an alternative to standard-sized commercial rings. The study further demonstrated a positive relationship between anteroposterior and transverse diameters of a healthy mitral valve and the intertrigonal distance. This implies using the intertrigonal distance to predict mitral valve size before dilation, indicating a 3.4:3:4 relationship in this dataset.

The study on annuloplasty ring sizing with intertrigonal distance found discrepancies in dimensions between the selected commercial rings (Medtronic 3D Profile, St. Jude Medical (SJM) rigid-saddle shape ring (RSA), and Carpentier-Edwards Physio annuloplasty ring) and healthy mitral valves, resulting in errors in both intercommissural and anteroposterior directions. Among the commercial rings, the Carpentier-Edwards Physio ring closely matched mitral valve dimensions, with the fewest errors, followed by SJM RSA and Medtronic 3D Profile.

For personalised annuloplasty ring design to fit individuals as to extracting the shape of the mitral annulus, both thresholding and the point-based method were able to do it. However, the thresholding method relied a lot on the knowledge and decision making of the person who performed the segmentation, which required more processes and time. On the other hand, the point-based method appeared to be more accurate with fewer steps and less time consumption. Therefore, the most accurate and suitable method that has been performed appears to be the point-based method, which involves placing landmarks along the intersections between the leaflet's insertion and the mitral annulus. The mitral annulus segmentation was able to be performed with echocardiography and an MRI scan, but the MRI required the edge attraction steps to better visualise the mitral annulus.

For the patient data that did not show the whole shape of the mitral annulus and could not be used to create a complete 3D model of the annulus shape, the process of filling in the missing posterior annulus of the mitral annulus from the echocardiography could be done with R Studio coding in R language together with embedded functions, including Generalized Procrustes analysis (GPA), a linear regression model, and the data set of the observed mitral annulus that allowed the visibility of the completed shapes.

In summary, this research has detailed the exploration of developing personalised annuloplasty rings using patients' scan images, with potential applications in mitral valve repair. The study affirms the feasibility of customizing annuloplasty rings to accommodate individual variations, resulting in the generation of valuable new insights.

7.2 Future work

In addition to this research, there are a lot of potentials to explore the areas of research that can build upon the knowledge of designing a personalised annuloplasty ring. Future work in personalised annuloplasty ring design may involve refining the methods employed for isolating and reconstructing the mitral annulus. The adoption of more sophisticated techniques, including advanced imaging or computational methods, holds the potential to enhance accuracy and efficiency in the process. Additionally, further investigations into the relationship between mitral valve dimensions and other anatomical factors from live and beating hearts could provide a more comprehensive understanding for personalised ring sizing. A continuous collaborative effort with medical professionals, engineers, and software developers might result in the development of innovative tools and technologies for designing personalised annuloplasty rings. Additionally, future studies could investigate the shape of the diseased mitral annulus and design strategies for transforming it into a healthy mitral annulus using shape modelling. Moreover, assessing the feasibility of integrating 3D printing technologies into the manufacturing process may offer new possibilities for customization and precision in the production of these specialized medical devices. Finally, a functional evaluation of commercial annuloplasty rings versus personalised annuloplasty rings in vivo and in vitro could offer insights into how these rings impact operational outcomes.

References

- 3D imaging and Computer Vision Solutions: England (2014) Fuel3D. Available at: <https://www.fuel3d.com/> (Accessed: 29 September 2023).
- Accola, K., Scott, M., Thompson, P., Palmer, G., Sand, M. and Ebra, G. (2005). Midterm Outcomes Using the Physio Ring in Mitral Valve Reconstruction: Experience in 492 Patients. *The Annals of Thoracic Surgery*, 79(4), pp.1276-1283.
- Ahmad, R., Gillinov, A., McCarthy, P., Blackstone, E., Apperson-Hansen, C., Qin, J., Agler, D., Shiota, T. and Cosgrove, D. (2004). Annular Geometry and Motion in Human Ischemic Mitral Regurgitation: Novel Assessment with Three-Dimensional Echocardiography and Computer Reconstruction. *The Annals of Thoracic Surgery*, 78(6), pp.2063-2068.
- Akdemir, R., Ozhan, Y., Bulur, S., Unlu, Y., Gunduz, Y., Arinc, Y., Yildiz, A. and Uyan, C. (2005). Color M-Mode Regurgitant Flow Propagation Velocity: A New Echocardiographic Method for Grading of Mitral Regurgitation. *Echocardiography*, 22(9), pp.713-722.
- Al-Maisary, S., Engelhardt, S., Graser, B., Wolf, I., Karck, M. and De Simone, R. (2017). Computer-based comparison of different methods for selecting mitral annuloplasty ring size. *Journal of Cardiothoracic Surgery*, 12(1).
- Al Meslmani, B., Mahmoud, G., Sommer, F., Lohoff, M. and Bakowsky, U. (2015). Multifunctional network-structured film coating for woven and knitted polyethylene terephthalate against cardiovascular graft-associated infections. *International Journal of Pharmaceutics*, 485(1-2), pp.270-276.
- Andreassen, B., Veronesi, F., Gerard, O., Solberg, A. and Samset, E., 2020. Mitral Annulus Segmentation Using Deep Learning in 3-D Transesophageal Echocardiography. *IEEE Journal of Biomedical and Health Informatics*, 24(4), pp.994-1003.
- AZoM.com. (2002). Pyrolytic Carbon for Biomedical Applications. [online] Available at: <https://Jude.azom.com/article.aspx?ArticleID=1463> [Accessed 13 Sep. 2019].
- Baillargeon, B., Costa, I., Leach, J., Lee, L., Genet, M., Toutain, A., Wenk, J.,

- Rausch, M., Rebelo, N., Acevedo-Bolton, G., Kuhl, E., Navia, J. and Guccione, J. (2015). Human Cardiac Function Simulator for the Optimal Design of a Novel Annuloplasty Ring with a Sub-valvular Element for Correction of Ischemic Mitral Regurgitation. *Cardiovascular Engineering and Technology*, 6(2), pp.105-111
- Barras, C. and Myers, K. (2000). Nitinol – Its Use in Vascular Surgery and Other Applications. *European Journal of Vascular and Endovascular Surgery*, 19(6), pp.564-569.
- Biffi, B., 2019. A computational framework for mitral valve analysis combining multi-modality imaging, statistical shape modelling and fluid-structure simulations. Ph.D. University College London.
- Bogaert, Dymarkowski and Taylor, 2012. Clinical Cardiac Imaging. *Vasa*, 34(3), pp.213-213.
- Borghetti, V., 2000. Biological versus prosthetic ring in mitral-valve repair: enhancement of mitral annulus dynamics and left-ventricular function with pericardial annuloplasty at long term. *European Journal of Cardio-Thoracic Surgery*, 17(4), pp.431-439.
- Bothe, Y., Kvitting, J.-P. E., Swanson, J. C., Hartnett, S., Ingels, N. B. & Miller, D. C. (2010). Effects of different annuloplasty rings on anterior mitral leaflet dimensions. *The American Association for Thoracic Surgery. J Thorac Cardiovasc Surg*, 139, pp.1114–1122.
- Bothe, Y., Miller, D. and Doenst, T. (2013). Sizing for Mitral Annuloplasty: Where Does Science Stop and Voodoo Begin?. *The Annals of Thoracic Surgery*, 95(4), pp.1475-1483.
- Braunberger, E., Deloche, A., Berrebi, A., Fayssoil, A., Celestin, J., Meimoun, P., Chatellier, G., Chauvaud, S., Fabiani, J. and Carpentier, A. (2001). Very Long-Term Results (More Than 20 Years) of Valve Repair With Carpentier's Techniques in Nonrheumatic Mitral Valve Insufficiency. *Circulation*, 104(suppl 1), pp. I-8-I-11.
- Carpentier A. (1969) Reconstructive valvuloplasty. A new technique of mitral valvuloplasty. *Presse Med*, 77, pp.251-253.
- Carpentier, A., Lessana, A., Relland, J., Belli, E., Mihaileanu, S., Berrebi, A.,

- Palsky, E. and Loulmet, D. (1995). The “Physio-Ring”: an advanced concept in mitral valve annuloplasty. *The Annals of Thoracic Surgery*, 60(5), pp.1177-1186.
- Carpentier, A., Adams, D. and Filsoofi, F. (2010). *Carpentier's Reconstructive Valve Surgery*. London: Elsevier Health Sciences, pp.33.
- Castillo, J., Solís, J., González-Pinto, Á. and Adams, D. (2011). Surgical Echocardiography of the Mitral Valve. 64(12), pp.1169-1181.
- Chan, V., Elmistekawy, E., Ruel, M., Hynes, M. and Mesana, T. (2018). *How Does Mitral Valve Repair Fail in Patients with Prolapse? —Insights From Longitudinal Echocardiographic Follow-Up*.
- Chang, B., Youn, Y., Ha, J., Lim, S., Hong, Y. and Chung, N., 2007. Long-term clinical results of mitral valvuloplasty using flexible and rigid rings: A prospective and randomized study. *The Journal of Thoracic and Cardiovascular Surgery*, 133(4), pp.995-1003.
- Chang, C., Lin, P., Chang, J., Chu, J., Hsieh, M. and Chiang, C. (1994). Long-term results of polytetrafluoroethylene mitral annuloplasty. *The Annals of Thoracic Surgery*, 57(3), pp.644- 647.
- Chen, J., Manning, M., Frazier, A., Jeudy, J. and White, C., 2009. CT Angiography of the Cardiac Valves: Normal, Diseased, and Postoperative Appearances. *RadioGraphics*, 29(5), pp.1393-1412.
- Chiesa, R., Giavaresi, G., Fini, M., Sandrini, E., Giordano, C., Bianchi, A. and Giardino, R. (2007). In vitro and in vivo performance of a novel surface treatment to enhance osseointegration of endosseous implants. *Oral Surgery, Oral Medicine, Oral Pathology, Oral Radiology, and Endodontology*, 103(6), pp.745-756.
- Choi, A., McPherson, D. and Kim, Y. (2016). Computational virtual evaluation of the effect of annuloplasty ring shape. *International Journal for Numerical Methods in Biomedical Engineering*, 33(6), pp.2831.
- Ciobanu, A., Griffin, S., Bennett, S. and Vinereanu, D. (2013). Catastrophic mitral prosthesis dehiscence diagnosed by three-dimensional transesophageal echocardiography. *Journal of Clinical Ultrasound*, 42(4), pp.249-251.
- Cohn, L., Couper, G., Aranki, S., Rizzo, R., Kinchla, N. and Collins, J. (1994).

- Long-term results of mitral valve reconstruction for regurgitation of the myxomatous mitral valve. *Thorac Cardiovasc Surg*, 107, pp.143-151.
- Correale, M., Ieva, R., Manuppelli, V., Rinaldi, A., & Di Biase, M. (2009). Controversies in echocardiography: 2D vs 3D vs 4D. *Minerva cardioangiologica*, 57(4), pp.443–455.
- David, T., Ivanov, J., Armstrong, S., Christie, D. and Rakowski, Y. (2005). A comparison of outcomes of mitral valve repair for degenerative disease with posterior, anterior, and bileaflet prolapse. *The Journal of Thoracic and Cardiovascular Surgery*, 130(5), pp.1242-1249.
- Delgado, V., Tops, L., Schuijf, J., de Roos, A., Brugada, J., Schalij, M., Thomas, J. and Bax, J. (2009). Assessment of Mitral Valve Anatomy and Geometry With Multislice Computed Tomography. *JACC: Cardiovascular Imaging*, 2(5), pp.556-565.
- Díaz Lantada, A., Valle-Fernández, R., Morgado, P., Muñoz-García, J., Muñoz Sanz, J., Muñoz-Guijosa, J. and Otero, J. (2009). Development of Personalised Annuloplasty Rings: Combination of CT Images and CAD-CAM Tools. *Annals of Biomedical Engineering*, 38(2), pp.280-290.
- Dreyfus, G., Neto, O. and Aubert, S. (2006). Papillary muscle repositioning for repair of anterior leaflet prolapses caused by chordal elongation. *The Journal of Thoracic and Cardiovascular Surgery*, 132(3), pp.578-584.
- Dryden, I., Oxborrow, N. and Dickson, R., 2008. Familial relationships of normal spine shape. *Statistics in Medicine*, 27(11), pp.1993-2003.
- Dryden, I.L. and Mardia, K.V. (2016). Statistical Shape Analysis, with Applications in R. *Second Edition*. John Wiley and Sons, Chichester.
- Dumont, E., Gillinov, A., Blackstone, E., Sabik, J., Svensson, L., Mihaljevic, T., Houghtaling, P. and Lytle, B. (2007). Reoperation After Mitral Valve Repair for Degenerative Disease. *The Annals of Thoracic Surgery*, 84(2), pp.444-450.
- Duran, C. and Ubago, J. (1976). Clinical and Hemodynamic Performance of a Totally Flexible Prosthetic Ring for Atrioventricular Valve Reconstruction. *The Annals of Thoracic Surgery*, 22(5), pp.458-463.
- Eckert, C., Zubiate, B., Vergnat, M., Gorman, J., Gorman, R. and Sacks, M. (2009). In Vivo Dynamic Deformation of the Mitral Valve Annulus. *Annals of Biomedical Engineering*, 37(9), pp.1757-1771.

- Edelstein, S. and Yahalom, M. (2009) “Cardiac device-related endocarditis: Epidemiology, pathogenesis, diagnosis and treatment — a review,” *International Journal of Angiology*, 18(04), pp. 167–172. Available at: <https://doi.org/10.1055/s-0031-1278347>.
- European Society of Cardiology, 2021. *Comparison between 2D and 3D*. [image] Available at: <https://www.escardio.org/Education/Practice-Tools/EACVI-toolboxes/3D-Echo/comparison-between-2d-and-3d> [Accessed 26 September 2021].
- Faletta, F. and Narula, J. (2018). Chordae tendineae - an overview | ScienceDirect Topics. [online] Scimedirect.com. Available at: <https://www.sciencedirect.com/topics/neuroscience/chordae-tendineae> [Accessed 1 Oct. 2018].
- Fasol, R., Meinhart, J., Deutsch, M. and Binder, T. (2004). Mitral valve repair with the Colvin-Galloway future band. *The Annals of Thoracic Surgery*, 77(6), pp.1985-1988.
- Fattouch, K., Guccione, F., Sampognaro, R., Panzarella, G., Corrado, E., Navarra, E., Calvaruso, D. and Ruvolo, G. (2009). POINT: Efficacy of adding mitral valve restrictive annuloplasty to coronary artery bypass grafting in patients with moderate ischemic mitral valve regurgitation: A randomized trial. *The Journal of Thoracic and Cardiovascular Surgery*, 138(2), pp.278-285.
- Ferrao de Oliveira, J. (2006). Mitral valve repair: better than replacement. *Heart*, 92(2), pp.275-281.
- Flachskampf, F., Chandra, S., Gaddipatti, A., Levine, R., Weyman, A., Ameling, Y., Hanrath, P. and Thomas, J. (2000). Analysis of Shape and Motion of the Mitral Annulus in Subjects With and Without Cardiomyopathy by Echocardiographic 3-Dimensional Reconstruction. *Journal of the American Society of Echocardiography*, 13(4), pp.277-287.
- Fontes, M. and Glower, D. (2018). *Mitral Valve Replacement*. [online] Clinical Pain Advisor. Available at: <https://www.clinicalpainadvisor.com/anesthesiology/mitral-valve-replacement/article/580652/> [Accessed 5 Aug. 2018].
- Foster, G., Dunn, A., Abraham, S., Ahmadi, N. and Sarraf, G. (2009). Accurate Measurement of Mitral Annular Dimensions by Echocardiography: Importance of Correctly Aligned Imaging Planes and Anatomic

- Landmarks. *Journal of the American Society of Echocardiography*, 22(5), pp.458-463.
- Gaasch, Y. (2018). Patient education: Mitral regurgitation (Beyond the Basics). [online] UpToDate. Available at: <https://Y.uptodate.com/home/subscription-options> [Accessed 10 Oct. 2018].
- Gelfand, E., Hughes, S., Hauser, T., Yeon, S., Goepfert, L., Kissinger, K., Rofsky, N. and Manning, Y. (2006). Severity of Mitral and Aortic Regurgitation as Assessed by Cardiovascular Magnetic Resonance: Optimizing Correlation with Doppler Echocardiography. *Journal of Cardiovascular Magnetic Resonance*, 8(3), pp.503-507.
- Glasson, J., Komeda, M., Daughters, G., Niczyporuk, M., Bolger, A., Ingels, N. and Miller, D. (1996). Three-dimensional regional dynamics of the normal mitral annulus during left ventricular ejection. *The Journal of Thoracic and Cardiovascular Surgery*, 111(3), pp.574-585.
- Gotman, I. (1997). Characteristics of Metals Used in Implants. *Journal of Endourology*, 11(6), pp.383- 389.
- Gourlay, T. and Black, R. (2016). Biomaterials and devices for the circulatory system. 1st ed. Cambridge: Woodhead.
- Graser, B. et al., 2014. Computerunterstütztes „ring sizing“ für die Anuloplastie. *Zeitschrift für Herz-,Thorax- und Gefäßchirurgie*, 28(5), pp.347–351.
- Gunning, G. and Murphy, B. (2014). Determination of the tensile mechanical properties of the segmented mitral valve annulus. *Journal of Biomechanics*, 47(2), pp.334-340.
- Gutowski, K. (2007). Grabb & Smith's Plastic Surgery, 6th Edition. *Plastic and Reconstructive Surgery*, 120(2), p.570.
- Gupta, S., Li, Y., Keshavamurthy, J., Sharma, G. and Polimenakos, A. (2017). Case-based approach to demonstrate utility of cardiac magnetic resonance imaging (MRI) for planning biventricular repair with inconclusive echo: illustration of two cases. *Quantitative Imaging in Medicine and Surgery*, 7(6), pp.732-735.
- Ha, Y., Koo, Y., Huh, Y., Kim, G., Kweon, J., Kim, N., Kim, Y., Kang,

- J., Lim, T., Song, J., Lee, S. and Yang, D., 2018. Effect of pannus formation on the prosthetic heart valve: In vitro demonstration using particle image velocimetry. *PLOS ONE*, 13(6), p.e0199792.
- Hassan, M., Windsor, J., Salerno, T. and Ricci, M. (2014). Use of Pledged Sutures in Mitral Annuloplasty. *Innovations: Technology and Techniques in Cardiothoracic and Vascular Surgery*, 9(2), pp.148-149.
- Himbert, D., Descoutures, F., Brochet, E., Iung, B., D taint, D., Messika-Zeitoun, D., Alkholder, S., Mimoun, L., Sordi, M., Depoix, J., Ducrocq, G., Nataf, P. and Vahanian, A. (2018). *Transvenous Mitral Valve Replacement After Failure of Surgical Ring Annuloplasty*.
- Hossien, A., Nithiarasu, P., Cheriex, E., Maessen, J., Sardari Nia, P. and Ashraf, S. (2015). A multidimensional dynamic quantification tool for the mitral valve. *Interactive CardioVascular and Thoracic Surgery*, 21(4), pp.481-487.
- Ht.edwards.com. (2019). [online] Available at: <http://ht.edwards.com/resourcegallery/products/rings/pdfs/2190.pdf> [Accessed 28 June. 2019].
- Hu, X. and Zhao, Q. (2011). Systematic evaluation of the flexible and rigid annuloplasty ring after mitral valve repair for mitral regurgitation. *European Journal of Cardio-Thoracic Surgery*.
- Hueb, A., Jatene, F., Moreira, L., Pomerantzeff, P., Kall s, E. and de Oliveira, S. (2002). Ventricular remodelling and mitral valve modifications in dilated cardiomyopathy: New insights from anatomic study. *The Journal of Thoracic and Cardiovascular Surgery*, 124(6), pp.1216-1224.
- Human body anatomy system. (2017). [image] Available at: <https://anatomywiki101.com/papillary-muscle-blood-supply/> [Accessed 3 Oct. 2018].
- Ionasec, R., Voigt, I., Georgescu, B., Yang Wang, Houle, Y., Vega-Higuera, F., Navab, N. and Comaniciu, D., 2010. Patient-Specific Modelling and Quantification of the Aortic and Mitral Valves From 4-D Cardiac CT and TEE. *IEEE Transactions on Medical Imaging*, 29(9), pp.1636-1651.
- Iung, B. (2003). A prospective survey of patients with valvular heart disease in Europe: The Euro Heart Survey on Valvular Heart Disease. *European Heart Journal*, 24(13), pp.1231-1243.

- Jensen, M., Jensen, Y., Smerup, M., Levine, R., Yoganathan, A., Nygaard, Y., Hasenkam, J. and Nielsen, S. (2008). Saddle-Shaped Mitral Valve Annuloplasty Rings Experience Lower Forces Compared with Flat Rings. *Circulation*, 118(14_suppl_1), pp. S250-S255.
- Jensen, M., Jensen, Y., Levine, R., Yoganathan, A., Andersen, N., Nygaard, Y., Hasenkam, J. and Nielsen, S., 2011. Saddle-shaped mitral valve annuloplasty rings improve leaflet coaptation geometry. *The Journal of Thoracic and Cardiovascular Surgery*, 142(3), pp.697-703.
- Jiao, L. *et al.* (2018) “Femtosecond laser produced hydrophobic hierarchical structures on additive manufacturing parts,” *Nanomaterials*, 8(8), pp. 601.
- Jolliffe, I. and Cadima, J., 2016. Principal component analysis: a review and recent developments. *Philosophical Transactions of the Royal Society A: Mathematical, Physical and Engineering Sciences*, 374(2065), pp.20150202.
- Kaji, s., Nasu, M. and Yamamuro, A., Tanabe, K., Nagai, K., Tani, T., Tamita, K., Shiratori, K., Kinoshita, M., Senda, M., Okada, Y. and Morioka, S.(2005). Annular geometry in patients with chronic ischemic mitral regurgitation: three-dimensional magnetic resonance imaging study. *Circulation*, 112(409), pp.14.
- Kamp, D. and Valocik, G., 2005. Three-dimensional Echocardiography in Mitral Valve Disease. *European Cardiology Review*, 1(1), pp.1.
- Kanjanauthai, S. (2015). Mitral Valve Anatomy: Overview, Gross Anatomy, *Microscopic Anatomy*. [online] Emedicine.medscape.com. Available at: <https://emedicine.medscape.com/article/1878301-overview#a2> [Accessed 26 Sep. 2018].
- Kaplan, S. (1998). Three-dimensional Echocardiographic Assessment of Annular Dimension, Shape, and Dynamics in the Normal and Regurgitant Mitral Valve. *Journal of the American College of Cardiology*, 31(2), pp.284A.
- Kaplan, S. R., Bashein, G., Sheehan, F. Y., Legget, M. E., Munt, B., Li, X. N., et al. (2000). Three-dimensional echocardiographic assessment of annular shape changes in the normal and regurgitant mitral valve. *American Heart Journal*, 139(3), pp. 378-387.
- Karas,S. and Elkins, R.C. (1970). Mechanism of Functional of the Mitral Valve

- Leaflets, Chordae Tendineae and Left Ventricular Papillary Muscles in Dogs. *Circulation Research*, 26(6), pp.689-696.
- Kim, J., Kim, E., Jin, G. and Choi, J., 2017. A Review of the Use of Cardiac Computed Tomography for Evaluating the Mitral Valve before and after Mitral Valve Repair. *Korean Journal of Radiology*, 18(5), pp.773.
- Kottayil, B., Sunil, G., Kappanayil, M., Mohanty, S., Francis, E., Vaidyanathan, B., Balachandran, R., Nair, S. and Kumar, R. (2013). Two-ventricle repair for complex congenital heart defects palliated towards single-ventricle repair. *Interactive CardioVascular and Thoracic Surgery*, 18(3), pp.266-271.
- Kurosawa, Y., Nakano, M., Kawase, M., Kasegawa, Y., Nakano, K. and Eishi, K. (1999). Mitral valve repair by Carpentier-Edwards Physio annuloplasty ring. *The Japanese Journal of Thoracic and Cardiovascular Surgery*, 47(8), pp.355-360.
- Kwan, J., Jeon, M., Kim, D., Park, K. and Lee, Y. (2009). Does The Mitral Annulus Shrink or Enlarge During Systole? A Real-Time 3D Echocardiography Study. *Journal of Korean Medical Science*, 24(2), pp.203.
- Kwon, S. and Gopal, A., 2017. 3D and 4D Ultrasound: Current Progress and Future Perspectives. *Current Cardiovascular Imaging Reports*, 10(12).
- Lancellotti, P., Tribouilloy, C., Hagendorff, A., Popescu, B., Edvardsen, T., Pierard, L., Badano, L. and Zamorano, J. (2013). Recommendations for the echocardiographic assessment of native valvular regurgitation: an executive summary from the European Association of Cardiovascular Imaging. *European Heart Journal - Cardiovascular Imaging*, 14(7), pp.611-644.
- Lau, K., Diaz, V., Scambler, P. and Burriesci, G., 2010. Mitral valve dynamics in structural and fluid–structure interaction models. *Medical Engineering & Physics*, 32(9), pp.1057-1064.
- Liang, C., Hu, Y., Liu, N., Zou, X., Wang, Y., Zhang, X., Fu, Y. and Hu, J., 2020. Laser Polishing of Ti6Al4V Fabricated by Selective Laser Melting. *Metals*, 10(2), pp.191.
- Liao, J. and Vesely, I. (2003). A structural basis for the size-related mechanical properties of mitral valve chordae tendineae. *Journal of Biomechanics*, 36(8), pp.1125-1133.

- Lin, E. and Alessio, A. (2009) “What are the basic concepts of temporal, contrast, and spatial resolution in cardiac CT?,” *Journal of Cardiovascular Computed Tomography*, 3(6), pp. 403–408. Available at: <https://doi.org/10.1016/j.jcct.2009.07.003>.
- Lindner, M., Hoeges, S., Meiners, Y., Wissenbach, K., Smeets, R., Telle, R., Poprawe, R. and Fischer, Y., 2011. Manufacturing of individual biodegradable bone substitute implants using selective laser melting technique. *Journal of Biomedical Materials Research Part A*, 97A(4), pp.466-471.
- Lee, A., Hsiung, M., Salgo, I., Fang, F., Xie, J., Zhang, Y., Lin, Q., Looi, J., Wan, S., Wong, R., Underwood, M., Sun, J., Yin, Y., Wei, J., Tsai, S. and Yu, C., 2013. Quantitative Analysis of Mitral Valve Morphology in Mitral Valve Prolapse With Real-Time 3-Dimensional Echocardiography. *Circulation*, 127(7), pp.832-841.
- Lyczkowska, E., Szymczyk, P., Dybala, B. and Chlebus, E., 2014. Chemical polishing of scaffolds made of Ti–6Al–7Nb alloy by additive manufacturing. *Archives of Civil and Mechanical Engineering*, 14(4), pp.586-594.
- Macnab, A. (2004). Three-dimensional echocardiography is superior to multiplane transoesophageal echo in the assessment of regurgitant mitral valve morphology. *European Journal of Echocardiography*, 5(3), pp.212-222.
- Magne, J., Sénéchal, M., Mathieu, P., Dumesnil, J., Dagenais, F. and Pibarot, P. (2008). Restrictive Annuloplasty for Ischemic Mitral Regurgitation May Induce Functional Mitral Stenosis. *Journal of the American College of Cardiology*, 51(17), pp.1692-1701.
- Mahmood, F., Karthik, S., Subramaniam, B., Panzica, P., Mitchell, J., Lerner, A., Jervis, K. and Maslow, A. (2008). Intraoperative Application of Geometric Three-Dimensional Mitral Valve Assessment Package: A Feasibility Study. *Journal of Cardiothoracic and Vascular Anesthesia*, 22(2), pp.292-298.
- Mahmood, F. and Matyal, R. (2015). A Quantitative Approach to the Intraoperative Echocardiographic Assessment of the Mitral Valve for Repair. *Anesthesia & Analgesia*, 121(1), pp.34-58.
- Manfreda, E., Mitteroecker, P., Bookstein, F. and Schaefer, K., 2006. Functional

morphology of the first cervical vertebra in humans and nonhuman primates. *The Anatomical Record Part B: The New Anatomist*, 289B(5), pp.184-194.

- Manivasagam, V.K. *et al.* (2021) “Surface modification strategies to improve titanium hemocompatibility: A comprehensive review,” *Materials Advances*, 2(18), pp. 5824–5842. Available at: <https://doi.org/10.1039/d1ma00367d>.
- Marcu, C., Beek, A. and van Rossum, A., 2006. Clinical applications of cardiovascular magnetic resonance imaging. *Canadian Medical Association Journal*, 175(8), pp.911-917.
- McCarthy, K., Ring, L. and Rana, B. (2010). Anatomy of the mitral valve: understanding the mitral valve complex in mitral regurgitation. *European Journal of Echocardiography*, 11(10), pp.i3- i9.
- Medtronic.com. (2019). Medtronic Annuloplasty System for Reconstruction of *Pathological Mitral Valves*. [online] Available at: <https://Y.medtronic.com/us-en/healthcare-professionals/products/cardiovascular/heart-valves-surgical/cg-future-annuloplasty-system.html> [Accessed 19 Mar. 2019].
- Millington-Sanders, C., Meire, A., Lawrence, L. and Stolonski, C. (1998). *Structure of chordae tendineae in the left ventricle of the human heart*.192, pp.573-581
- Müller, R., Abke, J., Schnell, E., Macionczyk, F., Gbureck, U., Mehrl, R., Ruszczak, Z., Kujat, R., Englert, C., Nerlich, M. and Angele, P. (2005). Surface engineering of stainless steel materials by Covalent collagen immobilization to improve implant biocompatibility. *Biomaterials*, 26(34), pp.6962-6972.
- Myerson, S., d’Arcy, J., Christiansen, J., Dobson, L., Mohiaddin, R., Francis, J., Prendergast, B., Greenwood, J., Karamitsos, T. and Neubauer, S. (2016). Determination of Clinical Outcome in Mitral Regurgitation With Cardiovascular Magnetic Resonance Quantification CLINICAL PERSPECTIVE. *Circulation*, 133(23), pp.2287-2296.
- Naoum, C., Leipsic, J., Cheung, A., Ye, J., Bilbey, N., Mak, G., Berger, A., Dvir, D., Arepalli, C., Grewal, J., Muller, D., Murphy, D., Hague, C., Piazza, N., Webb, J. and Blanke, P. (2016). Mitral Annular Dimensions and Geometry in Patients With Functional Mitral Regurgitation and Mitral Valve Prolapse. *JACC: Cardiovascular Imaging*, 9(3), pp.269-280.
- Niczyporuk, M. and Miller, D. (1991). Automatic tracking and digitization of

- multiple radiopaque myocardial markers. *Computers and Biomedical Research*, 24(2), pp.129-142.
- Niu, J., Li, Z. and Salvendy, G., 2007. Mathematical Methods for Shape Analysis and form Comparison in 3D Anthropometry: A Literature Review. *Digital Human Modelling*, pp.161-170.
- Nkomo, V., Gardin, J., Skelton, T., Gottdiener, J., Scott, C. and Enriquez-Sarano, M. (2006). Burden of valvular heart diseases: a population-based study. *The Lancet*, 368(9540), pp.1005-1011.
- Oliveira, D. et al. (2020) “Geometric description for the anatomy of the mitral valve: A Review,” *Journal of Anatomy*, 237(2), pp. 209–224. Available at: <https://doi.org/10.1111/joa.13196>.
- Otto, C. (2003). Timing of surgery in mitral regurgitation. *Heart*, 89(1), pp.100-105.
- Ormiston, J., Shah, P., Tei, C. and Wong, M. (1981). Size and motion of the mitral valve annulus in man. I. A two- dimensional echocardiographic method and findings in normal subjects. *Circulation*, 64(1), pp.113-120.
- Owais, K. et al., 2014. Three-Dimensional Printing of the Mitral Annulus Using Echocardiographic Data: Science Fiction or in the Operating Room Next Door? *Journal of Cardiothoracic and Vascular Anesthesia*, 28(5), pp.1393–1396.
- Owida, A. et al., 2011. Artery vessel fabrication using the combined fused deposition modelling and electrospinning techniques. *Rapid Prototyping Journal*, 17(1), pp.37–44.
- Ozaki, S., Saito, A., Nakaminami, Y., Ono, M., Noguchi, N. and Motomura, N. (2013). Comprehensive evaluation of fibrin glue as a local drug-delivery system—efficacy and safety of sustained release of vancomycin by fibrin glue against local methicillin-resistant *Staphylococcus aureus* infection. *Journal of Artificial Organs*, 17(1), pp.42-49.
- Padsalgikar, A. (2015). Polyurethanes in cardiac device leads - Effect of morphology on performance. [ebook] Available at:[https://Y.researchgate.net/publication/275649249_Polyurethanes_in_cardiac_device_leads_-_Effect_of_morphology_on_performance/](https://Y.researchgate.net/publication/275649249_Polyurethanes_in_cardiac_device_leads_-_Effect_of_morphology_on_performance/references) references [Accessed 15 Sep. 2019].
- Pai, R., Tanimoto, M., Jintapakorn, Y., Azevedo, J., Pandian, N. and Shah, P.

- (1995). Volume-rendered three-dimensional dynamic anatomy of the mitral annulus using a transesophageal echocardiographic technique. 4(6), pp.623-627.
- Paquay, Y., de Ruijter, J., van der Waerden, J. and Jansen, J. (1996). Tissue reaction to Dacron® velour and titanium fibre mesh used for anchorage of percutaneous devices. *Biomaterials*, 17(12), pp.1251-1256.
- Pham, D., Xu, C. and Prince, J., 2000. Current Methods in Medical Image Segmentation. *Annual Review of Biomedical Engineering*, 2(1), pp.315-337.
- Pham, T., Sulejmani, F., Shin, E., Wang, D. and Sun, Y. (2017). Quantification and comparison of the mechanical properties of four human cardiac valves. *Acta Biomaterialia*, 54, pp.345-355.
- Pick, A. (2008). *Top view of mitral valve*. [image] Available at: <https://Y.heart-valve-surgery.com/heart-surgery-blog/2008/09/02/mitral-valve-annulus-definition-diagrams-prolapse-calcification-treatment/> [Accessed 1 Oct. 2018].
- Pierce, E., Bloodworth, C., Imai, A., Okamoto, K., Saito, Y., Gorman, R., Gorman, J. and Yoganathan, A. (2018). Mitral annuloplasty ring flexibility preferentially reduces posterior suture forces. *Journal of Biomechanics*, 75, pp.58-66.
- Pitsis, A. *et al.* (2019) ‘Mitral valve repair: Moving towards a personalised ring’, *Journal of Cardiothoracic Surgery*, 14(1). doi:10.1186/s13019-019-0926-7.
- Plomp, K., Viðarsdóttir, U., Weston, D., Dobney, K. and Collard, M., 2015. The ancestral shape hypothesis: an evolutionary explanation for the occurrence of intervertebral disc herniation in humans. *BMC Evolutionary Biology*, 15(1).
- Purser, M., Richards, A., Cook, R., Osborne, J., Cormier, D. and Buckner, G. (2009). Evaluation of a Shape Memory Alloy Reinforced Annuloplasty Band for Minimally Invasive Mitral Valve Repair. *The Annals of Thoracic Surgery*, 88(4), pp.1312-1316.
- Purser, M.F. *et al.*, 2010. A Novel Shape Memory Alloy Annuloplasty Ring for Minimally Invasive Surgery: Design, Fabrication, and Evaluation. *Annals of Biomedical Engineering*, 39(1), pp.367– 377.
- Ramot, Y., Rousselle, S., Yellin, N., Willenz, U., Sabag, I., Avner, A. and Nyska, A.

- (2016). Biocompatibility and Systemic Safety of a Novel Implantable Annuloplasty Ring for the Treatment of Mitral Regurgitation in a Minipig Model. *Toxicologic Pathology*, 44(5), pp.655-662.
- Rausch, M., Bothe, Y., Kvitting, J., Swanson, J., Ingels, N., Miller, D. and Kuhl, E. (2011). Characterization of Mitral Valve Annular Dynamics in the Beating Heart. *Annals of Biomedical Engineering*, 39(6), pp.1690-1702.
- Ryan, L., Jackson, B., Hamamoto, Y., Eperjesi, T., Plappert, T., St. John-Sutton, M., Gorman, R. and Gorman, J. (2008). The Influence of Annuloplasty Ring Geometry on Mitral Leaflet Curvature. *The Annals of Thoracic Surgery*, 86(3), pp.749-760.
- Sacks, M. and Yoganathan, A. (2007). Heart valve function: a biomechanical perspective. *Philosophical Transactions of the Royal Society B: Biological Sciences*, 362(1484), pp.1369-1391.
- Sacks, M. and Yoganathan, A. (2008). Heart valve function: a biomechanical perspective. *Philosophical Transactions of the Royal Society B: Biological Sciences*, 363(1502), pp.2481-2481.
- Salkeld, S., Patron, L., Lien, J., Cook, S. and Jones, D. (2016). Biological and functional evaluation of a novel pyrolytic carbon implant for the treatment of focal osteochondral defects in the medial femoral condyle: assessment in a canine model. *Journal of Orthopaedic Surgery and Research*, 11(1).
- Samuel, L. (2018). *The circulatory system*. [image] Available at: <http://Y.interactive-biology.com/75/show-me-a-diagram-of-the-human-heart-here-are-a-bunch/> [Accessed 22 Sep. 2018].
- Schneider, R., Perrin, D., Vasilyev, N., Marx, G., del Nido, P. and Howe, R., 2009. Mitral annulus segmentation from three-dimensional ultrasound. 2009 IEEE International Symposium on Biomedical Imaging: From Nano to Macro.
- Schneider, R., Perrin, D., Vasilyev, N., Marx, G., del Nido, P. and Howe, R. (2010). Mitral Annulus Segmentation From 3D Ultrasound Using Graph Cuts. *IEEE Transactions on Medical Imaging*, 29(9), pp.1676-1687.
- Sengupta, S. (2014). Three dimensional echocardiography in mitral valve disease, pp. 9- 20

- Shahin, G., Heijden, G., Bots, M., Cramer, M., Jaarsma, Y., Gadellaa, J., Riviere, A. and Swieten, Y. (2006). The Carpentier-Edwards Classic and Physio Mitral Annuloplasty Rings: A Randomized Trial. *The Heart Surgery Forum*, 8(5), pp.389.
- Sharony, R., Saunders, P., Nayar, A., McAleer, E., Galloway, A., Delianides, J., Schwartz, C., Applebaum, R., Kronzon, I., Colvin, S. and Grossi, E. (2004). Semirigid partial annuloplasty band allows dynamic mitral annular motion and minimizes valvular gradients: an echocardiographic study. *The Annals of Thoracic Surgery*, 77(2), pp.518-522.
- Shiota, Graser, B., Wald, D., Al-Maisary, S., Grossgasteiger, M., de Simone, R., Meinzer, Y. and Wolf, I. (2013). Using a shape prior for robust modelling of the mitral annulus on 4D ultrasound data. *International Journal of Computer Assisted Radiology and Surgery*.
- Shiota, M., Gillinov, A., Takasaki, K., Fukuda, S. and Shiota, T. (2011). Recurrent Mitral Regurgitation Late after Annuloplasty for Ischemic Mitral Regurgitation. *Echocardiography*, 28(2), pp.161-166.
- “SJM™ Rigid Saddle Ring” (2013). Available at: <https://Y.cardion.cz/file/21/sjm-rigid-saddle-ring.pdf> (Accessed: September 29, 2021).
- Skov, S., Røpcke, D., Tjørnild, M., Ilkjær, C., Rasmussen, J., Nygaard, Y., Jensen, M. and Nielsen, S., 2017. The effect of different mitral annuloplasty rings on valve geometry and annular stress distribution†. *Interactive CardioVascular and Thoracic Surgery*, 24(5), pp.683-690.
- Sonne, C., Sugeng, L., Watanabe, N., Weinert, L., Saito, K., Tsukiji, M., Yoshida, K., Takeuchi, M., Mor-Avi, V. and Lang, R. (2008). Age and body surface area dependency of mitral valve and papillary apparatus parameters: assessment by real-time three-dimensional echocardiography. *European Journal of Echocardiography*, 10(2), pp.287-294.
- Spiegelstein, D., Ghosh, P., Sternik, L., Tager, S., Shinfeld, A., & Raanani, E. (2007). Current strategies of mitral valve repair. *The Israel Medical Association Journal : IMAJ*, 9(4), pp. 303-309.
- Spence, P., Peniston, C., David, T., Mihic, N., Jabr, A., Narini, P. and Salerno, T. (1986). Toward a Better Understanding of the Etiology of Left Ventricular Dysfunction after Mitral Valve Replacement: An Experimental Study with

- Possible Clinical Implications. *The Annals of Thoracic Surgery*, 41(4), pp.363-371.
- Spratt, J.R., Spratt, J.A., Beachley, V., Kang, Q. (2012). [SEP]Strength comparison of mitral annuloplasty ring and suturing combinations: an in-vitro study. *Journal of Heart Valve Disease*, 21, pp. 286-292
- Srichai, M., Grimm, R., Stillman, A., Gillinov, A., Rodriguez, L., Lieber, M., Lara, A., Weaver, J., McCarthy, P. and White, R., 2005. Ischemic Mitral Regurgitation: Impact of the Left Ventricle and Mitral Valve in Patients with Left Ventricular Systolic Dysfunction. *The Annals of Thoracic Surgery*, 80(1), pp.170-178.
- St. Jude Medical™ (2018). *MITRAL ANNULOPLASTY RING*. [image] Available at: <http://Jude.medicalexpo.com/prod/st-jude-medical/product-70886-446932.html> [Accessed 10 Sep. 2018].
- Stanisławska, A. (2014). Biomaterials and Implants in Cardiac and Vascular Surgery Review. *Advances in Materials Science*, 14(3), pp.5-17.
- Stevanella, M., Maffessanti, F., Conti, C., Votta, E., Arnoldi, A., Lombardi, M., Parodi, O., Caiani, E. and Redaelli, A. (2011). Mitral Valve Patient-Specific Finite Element Modelling from Cardiac MRI: Application to an Annuloplasty Procedure. *Cardiovascular Engineering and Technology*, 2(2), pp.66-76.
- Sugeng, L., Spencer, K., Mor-Avi, V., DeCara, J., Bednarz, J., Weinert, L., Korcarz, C., Lammertin, G., Balasia, B., Jayakar, D., Jeevanandam, V. and Lang, R., 2003. Dynamic Three-Dimensional Color Flow Doppler: An Improved Technique for the Assessment of Mitral Regurgitation. *Echocardiography*, 20(3), pp.265-273.
- Sugimoto, T., Ogawa, K., Asada, T., Mukohara, N., Higami, T., Obo, Y., Gan, K. and Kawamura, T. (1995). Mitral Valve Repair Using an Annuloplasty Ring Made of Artificial Woven Dacron Graft. *Japanese Circulation Journal*, 59(3), pp.176-179.
- Sundermann, S., Gessat, M., Cesarovic, N., Frauenfelder, T., Biaggi, P., Bettex, D., Falk, V. and Jacobs, S. (2013). Implantation of personalised, biocompatible mitral annuloplasty rings: feasibility study in an animal model. *Interactive CardioVascular and Thoracic Surgery*, 16(4), pp.417- 422.
- Talonen, J., Hänninen, Y., Nenonen, P. and Pape, G. (2005). Effect of strain rate on

- the strain- induced $\gamma \rightarrow \alpha'$ -martensite transformation and mechanical properties of austenitic stainless steels. *Metallurgical and Materials Transactions A*, 36(2), pp.421-432.
- Timek, T., Lai, D., Dagum, P., Green, G., Glasson, J., Daughters, G., Ingels, N. and Miller, D. (2000). Atrial contraction airtal annular dynamics during rapid atrial pacing. *Surgery*, 128(2), pp.361-367.
- Tiwari, A. and Patwardhan, K., 2016. Mitral valve annulus localization in 3D echocardiography. 2016 38th Annual International Conference of the IEEE Engineering in Medicine and Biology Society (EMBC),.
- Topilsky, Y., Vaturi, O., Watanabe, N., Bichara, V., Nkomo, V., Michelena, Y., Le Tourneau, T., Mankad, S., Park, S., Capps, M., Suri, R., Pislaru, S., Maalouf, J., Yoshida, K. and Enriquez-Sarano, M. (2013). Real-Time 3-Dimensional Dynamics of Functional Mitral Regurgitation: A Prospective Quantitative and Mechanistic Study. *Journal of the American Heart Association*, 2(3), pp.e000039- e000039.
- Tsang, Y., Sugeng, L., Weinert, L., Chandra, S., Spencer, K., Jeevanandam, V., Raman, J. and Lang, R. (2011). *Value of Three-Dimensional Mitral Valve Parametric Models in the Assessment of Mitral Valve Disease*. [image] Available at: [https://Y.onlinejase.com/article/S0894-7317\(11\)00188-X/pdf](https://Y.onlinejase.com/article/S0894-7317(11)00188-X/pdf) [Accessed 8 Aug. 2018].
- Tsang, Y., Wu, G., Rozenberg, D., Mosko, J. and Leong-Poi, Y. (2009). Early Mitral Annuloplasty Ring Dehiscence with Migration to the Descending Aorta. *Journal of the American College of Cardiology*, 54(17), pp.1629.
- Van Bilsen, P., Popa, E., Brouwer, L., Vincent, J., Taylor, C., de Leij, L., Hendriks, M. and van Luyn, M. (2004). Ongoing foreign body reaction to subcutaneous implanted (heparin) modified Dacron in rats. *Journal of Biomedical Materials Research*, 68A (3), pp.423-427.
- Victor, S. and Nayak, V. (1994). Definition and function of commissures, slits and scallops of the mitral valve: Analysis in 100 hearts. *The Asia Pacific Journal of Thoracic & Cardiovascular Surgery*, 3(1), pp.10-16.
- Wang, Q., McGoron, A., Pinchuk, L. and Schoepfoerster, R. (2009). A novel small

- animal model for biocompatibility assessment of polymeric materials for use in prosthetic heart valves. *Journal of Biomedical Materials Research Part A*, 9999A, pp.442-453
- Wache, Y.M. et al., 2003. Development of a polymer stent with shape memory effect as a drug delivery system. *Journal of Materials Science: Materials in Medicine*, 14(2), pp.109–112.
- Watanabe, N., Ogasawara, Y., Yamamura, Y. and Wada, N. (2005). Mitral annulus flattens in ischemic mitral regurgitation: geometric differences between inferior and anterior myocardial infarction: a real-time 3-dimensional echocardiographic study. *Circulation*, 112, pp.458-462.
- Wei, Q. et al., 2015. Selective laser melting of stainless-steel/nano-hydroxyapatite composites for medical applications: Microstructure, element distribution, crack and mechanical properties. *Journal of Materials Processing Technology*, 222, pp.444–453.
- Weir-McCall, J., Blanke, P., Naoum, C., Delgado, V., Bax, J. and Leipsic, J., 2018. Mitral Valve Imaging with CT: Relationship with Transcatheter Mitral Valve Interventions. *Radiology*, 288(3), pp.638-655.
- Weyman, A. E. (1994). Principles and practices of echocardiography. Philadelphia, PA: Lea & Febiger.
- Zacà, V., Ballo, P. and Mondillo, S. (2007). Late mitral annuloplasty failure: The loss of the ring. *International Journal of Cardiology*, 114(1), pp.127-128.
- Xiong, Y., Zhang, D., Martyniuk, C., Trudeau, V. and Xia, X., 2008. Using Generalized Procrustes Analysis (GPA) for normalization of cDNA microarray data. *BMC Bioinformatics*, 9(1).
- Zigterman, B.G. et al. (2019) “Titanium surface modifications and their soft-tissue interface on nonkeratinized soft tissues—a systematic review (review),” *Biointerphases*, 14(4), pp. 040802. Available at: <https://doi.org/10.1116/1.5113607>.

Appendix

The R coding used in the method to complete the missing posterior annulus of the mitral annulus model is as followed.

```
library("readxl")

library(shapes)

multiplesheets <- function(fname) {

  # getting info about all excel sheets

  sheets <- readxl::excel_sheets(fname)

  tibble <- lapply(sheets, function(x) readxl::read_excel(fname, sheet = x))

  data_frame <- lapply(tibble, as.data.frame)

  # assigning names to data frames

  names(data_frame) <- sheets

  # print data frame

  data_frame

}

# specifying the path name

path <- "/Users/idryden/Dropbox/ FIU/Research/Annulus/MV-Coordinate-2.xlsx"

zz<- multiplesheets(path)

objs<-names(zz)

n<-length(objs)
```

```

z<-array(0,c(30,3,n))

y<-array(0,c(30,3,n))

for (i in 1:n){

objnm<-paste("zz$", "",objs[i],"",sep="")

datax <- eval(parse(text = objnm))

z[,i]<-as.matrix(datax[3:32,2:4])

y[,i]<-matrix(as.double(z[,i]),30)

}

#mean shape of all points

x <- y[,2:35]

ans <- procGPA(x,scale=FALSE)

### predict missing part using linear regression

out <- lm ( y[,1] ~ ans$mshape)

summary(out)

xnew <- predict( out, newdata=data.frame(ans$mshape))

filledin<- y[,1]

filledin[16:30,] <- xnew[16:30,]

# Note the missing part is now coloured red

plot(filledin,asp=1,col=2)

points(y[1:15,,1],col=1)

xfull <- array( 0, c(30,3,35))

xfull[,2:35] <- x

xfull[,1] <- filledin

```

```

out <- procGPA( xfull, scale=FALSE)

#the Procrustes rotated shapes of x-y coordinates only, with filled in shape in red
plotshapes( out$rotated[,1:2,2:35],joinline=1:30,col=4)
points( out$rotated[,1:2,1], col=2)
lines( out$rotated[,1:2,1], col=2)

#the Procrustes rotated shapes of x-z coordinates only, with filled in shape in red
plotshapes( out$rotated[,c(1,3),2:35],joinline=1:30,col=4)
points( out$rotated[,c(1,3),1], col=2)
lines( out$rotated[,c(1,3),1], col=2)

#the Procrustes rotated shapes of y-z coordinates only, with filled in shape in red
plotshapes( out$rotated[,c(2,3),2:35],joinline=1:30,col=4)
points( out$rotated[,c(2,3),1], col=2)
lines( out$rotated[,c(2,3),1], col=2)

#the registered object with missing part
newfill <- procOPA( out$mshape, xfull[,1])$Bhat
print(newfill)
print(out$percent)
plot(ans$percent,type="l")

#PC scores - two dimensional projection. No obvious outliers now.
plot( out$scores,asp=1,col=2)
text( out$scores, as.character(1:35))

```

```
#pairwise plots of first five PCS - no obvious outliers
pairs(out$scores[,1:5])

#3d plot of Procrustes rotated values - nearly flat.
shapes3d( out$rotated )
shapepca(out)
plot(centroid.size(xfull))
plotshapes(xfull[,24],joinline=1:30)
points(xfull[,16])
lines(xfull[,16],col=2)
points(xfull[,5])
lines(xfull[,5],col=3)
title("Objects 24 (black), 16 (red), 5 (green)")
```